

Tunable Narrow Bandpass
Sigma-Delta Analog-To-Digital Conversion
for
Mobile Communication Terminals

Sheng Ping Yang

March 1995



*A thesis submitted for the degree of Masters of Engineering
of The Victoria University of Technology*

Department of Electrical & Electronic Engineering
Faculty of Engineering
The Victoria University of Technology

FTS THESIS
621.39814 YAN
30001004467314
Yang, Sheng Ping
Tunable narrow bandpass
Sigma-Delta
analog-to-digital conversion

Declaration

My Masters studies were conducted under the guidance of Associate Professor, Dr. Michael Faulkner and Dr. Roman Malyniak as supervisors. Some of the research results reported in this thesis have been published as academic papers presented as conference papers. These papers are:

1. Shengping Yang and Michael Faulkner and Roman Malyniak, "A Tunable Bandpass Sigma-Delta A/D Conversion for Mobile Communication Receiver," Conference: *44th IEEE/VTS Vehicular Technology Conference*, Sweden, June, 1994, pp. 1346-1350.
2. Shengping Yang and Michael Faulkner and Roman Malyniak, "The Channel Selective Bandpass Sigma-Delta Analog-to-Digital Conversion for Mobile Communication Terminals " Conference: *IEEE International Conference on Universal Wireless Access*, Australia, April, 1994, pp. 157-161.

I hereby declare that the contents of this thesis are the results of original research except where appropriately referenced, and have not been submitted for a degree at any other university or educational institution.

Shengping Yang

Department of Electrical & Electronic Engineering,

Faculty of Engineering,

The Victoria University of Technology,

Victoria 3011, AUSTRALIA.

Acknowledgments

I sincerely appreciate Associate Professor, Dr. Michael Faulkner and Dr. Roman Malyniak for their constructive and detailed guidance. I thank Dr. Michael Faulkner for his spending of days and nights with me in guiding the research and for his financial support to my last semester. I thank Mr. Mark Briffa and Dr. Lige Xia for their valuable advice and interesting discussions.

I am grateful to Prof. E. Walker, Associate Professor, Dr. Len Herron, Ms. Ann Pleasant, Dr. Qiu Bin, Dr. Dirk Qiu and Dr. Wee-sit Lee for their extensively support to get the *Australia Development Cooperation Scheme Scholarship*.

To my wife Hong Zhang who managed to run the family while I spent countless hours doing this research. Without her love and support this work would have never been completed. I also dedicate this work to my parents with their tremendous support, and my daughter Xiuyi, who were deprived of my companionship on innumerable occasions.

Last but not least, I thank Mrs. Shirley Herrewyn, the administrative officer of the Department, for her special attention to our overseas students. I would like to thank Mr. Xue Feng Leng for his help on the Latex. I would like to thank Mr. Neil Larchin and all other friends who have been involved in one way or another during the course of my studies.

Abstract

A whole-of-band receiver structure is proposed. In this structure, the whole mobile band (125 channels for GSM) is digitized and channel selection is performed using DSP filters. The ADC is a critical component in this structure, requiring 13bits resolution at sampling rate of 50MHz. A modified $\Sigma\Delta$ ADC converter is proposed for this application. The $\Sigma\Delta$ ADC must be able to null the quantization noise at the frequency of the desired channel. The research considers the feasibility of varying this frequency for tuning different channels. This is a novel concept for $\Sigma\Delta$ systems and so the simplest form of $\Sigma\Delta$ structure was chosen for evaluation to reduce the degrees of freedom in the many variables involved.

A second order noise tunable bandpass $\Sigma\Delta$ ADC is studied using pole zero placement techniques in the z-plane. Tuning is performed by moving the zero positions around the unit circle. The optimized pole position is a compromise between noise performance and stability. The signal noise ratio is equivalent to 8bits, indicating a higher order $\Sigma\Delta$ ADC would be required for a practical radio receiver.

Sensitivity analysis showed that the quantization noise is sensitive to errors in the system's main tuning coefficient adjustment. Accuracy for this coefficient has to be better than 1%, indicating that some external precision components will be required for any VLSI implementation.

The effect of multichannel signals on the performance of the ADC is studied. It is shown that saturation of intermediate nodes dominated the intermodulation performance of the ADC. However, the loss of performance is not great (3dB to 6dB) and can be offset by over designing the ADC to give an appropriate safety margin. The successful implementation of noise4 tunable $\Sigma\Delta$ converter requires accurate setting of the adjustable coefficients. This is seen as the major design obstacle.

Contents

1	Background	2
1.1	Introduction	2
1.1.1	Single Channel and Whole-of-Band Receivers	3
1.1.2	Analog to Digital Converter for Whole-of-Band Receiver	4
1.2	Aim	5
1.2.1	General Aim	5
1.2.2	Specific Aim	5
1.3	Methodology and Scope	6
1.4	The Layout of the Thesis	6
2	Fundamentals of Receiver Design and ADC Conversion	8
2.1	Receiver architecture	9
2.1.1	Super Heterodyne Receiver	9
2.1.2	Direct Conversion Receiver	10
2.1.3	The motivation for proposing a new receiver	11
2.1.4	Proposed Receiver	12
2.2	Brief Overview of ADC Converter	15
2.2.1	Quantization error in ADC Conversion	15
2.2.2	The Necessity of Anti-aliasing Filter in ADC	16
2.2.3	Anti-aliasing with oversampling	17
2.2.4	Oversampling to Facilitate Quantization	18
2.2.5	The Criterion for Selecting ADC Converters	19
2.3	Delta Modulation and Circuit Structure	20
2.4	From Δ to $\Sigma\Delta$ Modulation	22
2.5	Conclusion	24

3	Sigma-Delta ($\Sigma\Delta$) Modulation for Lowpass Signals	25
3.1	Introduction	25
3.2	$\Sigma\Delta$ Modulation Structure and Principle	26
3.3	Basic Noise-Shaping Theory	28
3.3.1	The Noise Shaping Feature	28
3.4	Noise Shaping for First Order Systems	31
3.4.1	Quantization Noise	31
3.4.2	Signal to Quantization Noise Ratio	33
3.4.3	The Effect of Integrator Gain on $\Sigma\Delta$ Performance	34
3.5	Noise Shaping for High Order Systems	37
3.5.1	Quantization Noise	37
3.5.2	Signal to Quantization Noise for Second Order $\Sigma\Delta$ ADC	40
3.5.3	Alternative 2nd Order Transfer Function	41
3.6	Limit Cycles (Pattern Noise)	44
3.7	More Complex System	44
3.8	Conclusion	45
4	Design of Noise Tunable $\Sigma\Delta$ A/D Converter	47
4.1	Introduction	47
4.2	General Design of 2nd order tunable $\Sigma\Delta$ modulation	49
4.2.1	System Structure, Modeling and Transfer Function	50
4.2.2	Stability of the 2nd Order Bandpass $\Sigma\Delta$ A/D Converter	54
4.2.3	The Shape of the NTF	58
4.3	Quantization Noise and SNR	60
4.4	A Note on Sample Rate	62
4.5	Conclusion	62
5	Tuning Sensitivity Analysis	64
5.1	Coefficient Adjustment Range	64
5.2	Noise Tuning Sensitivity	66
5.3	A Note on Implementation	69
5.4	Conclusion	70
6	Intermodulation and Adjacent Channel Interference	71
6.1	Adjacent Channel Interference (ACI)	71
6.2	Intermodulation	73

6.3	Intermediate Stage Transfer Function	74
6.4	Conclsion	76
7	Conclusion	77
7.1	The Performance Summary	77
7.2	Novelty	79
7.3	Further Work	79
	References	80

Chapter 1

Background

1.1 Introduction

The world of mobile communication is dedicated to advancing the technological capability and understanding needed to bring people together. With each passing day, our society becomes more and more mobile and brings an increased demand for high quality voice communication service and convenient hand held terminals.

Recent developments of very large scale integration (VLSI) technology provide the means to achieve these goals. Now it is possible to make the terminals more attractive to customers. Carrying a miniature portable phone is no longer difficult and one no longer feels isolated from home and the business. This feature is very important in an emergency situation. Reduced energy consumption will also extend the battery life and , in a remote area, this is an important feature.

However, current portable phones and mobile terminals have not yet reached perfection in terms of miniaturization, lower costs, low energy consumption and flexibility. The future goal of personal communication system is to provide everybody with a convenient facility

using lower cost , smaller size terminals. Eventually it is hoped that the terminals will be the size of a wristwatch, a pen or a lighter with reasonable battery life.

With the continuous advancing in VLSI technology, the combination of digital signal processing (DSP) and VLSI provides the means to achieve these goals. DSP has an improved performance when compared with analog processing, since the problems of component temperature drift, aging and manufacturing tolerances are eliminated. Analog components are also bulky and in some cases expensive. DSP, on other hand, is eminently suitable for VLSI implementation. though its processing power has to be considered in some stage.

A few years ago, all the functions of a radio receiver were implemented using analog components. The only digital components were simple microprocessors which drove the display and performed other housekeeping operations in the radio. As VLSI technology improved, DSP function were included in the radio. This started off with the voice codec and progressed to include more and more new signal processing functions, such as channel coding, modulation, demodulation, frequency offset correction and timing recovery. Modern radio receivers use DSP for all the baseband processing requirements of the radio. Only the RF processing functions of channel selection (filtering) and down conversion use analog components.

This work seeks to further advance the evolution in radio circuit design by incorporating the channel selection filtering into the DSP. A by-product of this process is that the receiver changes from a single channel receiver to a whole-of-band receiver.

1.1.1 Single Channel and Whole-of-Band Receivers

Traditional radios are single channel receivers (see Fig. 1.1 (a)). They receive a band of channels, down convert them to a lower intermediate frequency (IF) for channel selection (filtering) using expensive and bulky crystal filters. After the channel is isolated it is further down converted to baseband and then converted into digital format using an analog to digital converter (ADC) for demodulation and further processing in a DSP unit.

On the other hand, whole-of-band receivers (see Fig. 1.1 (b)) down-convert a whole

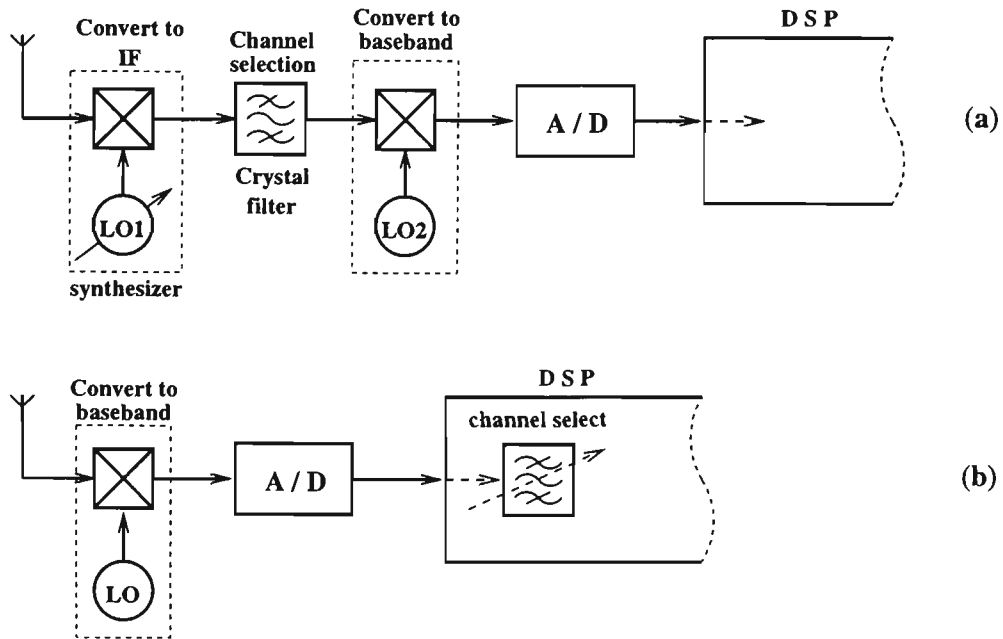


Figure 1.1: (a) a single band receiver structure, and (b) a whole-of-band receiver structure.

band of channels (mobile band) to baseband and then digitize the whole band by using a high speed ADC. DSP is used for channel selection (filtering) as well as demodulation. This allows the elimination of a number of traditional receiver functions, such as the need for a synthesizer for channel changing and a crystal filter for channel selection. These advantages are traded off against the need for a higher processing capability in the DSP unit and a much higher performance requirement on the ADCs. In fact, the ADCs became the most critical component in the whole receiving structure and these are the topic of this research.

1.1.2 Analog to Digital Converter for Whole-of-Band Receiver

ADCs in a whole-of-band receiver must have a very high sampling frequency to cover the total bandwidth of the incoming signal. They must also have a high dynamic range because the incoming waveform contains many active channels. The ADC specification for a receiver designed to operate on the Global System for Mobile (GSM) digital cellular standard must have a sample rate in the vicinity of 50MHz and a dynamic range equivalent to 13 bits (see chapter 2). This is a difficult specification to meet, even using current flash technology. The possible use of an alternative technology based on $\Sigma\Delta$ techniques is the topic of this research.

Traditional $\Sigma\Delta$ ADCs have high sampling rates and also can be designed to give very high resolution. They use noise shaping techniques to null the quantization noise at a given frequency. Most of these have been targeted at voice applications where the quantization noise is nulled at DC (zero frequency). They are not suitable for whole-of-band receivers because the desired channel does not usually occur at DC. However, it might be possible to modify the operation of the traditional lowpass ADC, to null the quantization noise at different frequencies. The feasibility of doing this is the goal of this research.

1.2 Aim

1.2.1 General Aim

- To study the feasibility of using $\Sigma\Delta$ ADCs in a whole-of-band receiver for mobile radio communication systems.
- To identify any problems that impinge on performance of the radio, or create an implementation difficulty.

1.2.2 Specific Aim

- Develop a suitable $\Sigma\Delta$ ADC structure that will minimize quantization noise in the received band.
- Investigate the practical problem of adjusting the quantization noise null frequency when the desired channel changes to a different frequency.
- Determine the suitability for VLSI implementation.
- Investigate the performance in a typical radio multichannel environment.

1.3 Methodology and Scope

In this work the proposed new $\Sigma\Delta$ structure is analyzed using pole zero placement techniques in the z-plane and the results are confirmed using time domain simulation. Time domain simulations are also used to study non-linear effects. The software tools used for this work include SPW Comdisco and Matlab.

Because the problem is very complex and open ended, it was necessary to reduce the scope of the analysis so that meaningful results could be obtained in the time available. In this work, the $\Sigma\Delta$ ADC was limited to a 2nd order structure to reduce the degrees of freedom in the simulation. In considering the practical implementation, the bandwidths and channel spacings were based on the GSM specification (125 channels; 200kHz channel spacing; 25MHz total mobile band).

1.4 The Layout of the Thesis

The first part of Chapter 2 introduces the conventional radio receiver and proposes the new receiver architecture. The second part overviews ADCs, the major concepts of quantization, anti-aliasing filtering, and oversampling. The chapter concludes with a discussion on Δ modulation and its extension to $\Sigma\Delta$ modulation.

Chapter 3 describes the design of the $\Sigma\Delta$ ADC for lowpass signals. This shows that the operational characteristics can be described from the pole/zero location in the z-plane. The concepts of noise transfer function (NTF) and signal transfer function (STF) are introduced. The performance is predicted by assuming the quantization error is uniformly distributed white noise. The effect of converter order and oversampling rate on the signal to noise ratio (SNR) is presented.

Chapter 4 describes the design of a noise tunable $\Sigma\Delta$ ADC for bandpass signals based on a lowpass $\Sigma\Delta$ ADC with a number of modifications. The noise tuning operation is realized by moving zeros of the system around the unit circle. The stability of the noise tunable

$\Sigma\Delta$ ADC converter is ensured by providing a contour boundary for the selection of system pole positions. The optimized pole position is shown to be a compromise between noise and stability. Finally the chapter shows that the simulation of SNR follows the calculations reasonably close (maximum error < 5dB). Quantization noise is assumed white in both operations.

Chapter 5 places the noise tunable $\Sigma\Delta$ ADC into the practical GSM environment. It discusses the coefficient adjustment for noise tuning and determines the sensitivity of the inband noise to adjustment error in these coefficients. The calculation shows the range and the accuracy requirements in manufacturing some of the coefficients.

Chapter 6 considers the intermodulation problem caused by the multichannel input. It discusses two non-linear phenomenon in the ADC. These are output saturation and saturation of internal nodes. Chapter 7, the last chapter, summarizes the research and suggests further areas of investigation.

Chapter 2

Fundamentals of Receiver Design and ADC Conversion

This chapter briefly reviews the conventional design of receivers. Then, the proposed receiver structure is presented which makes full use of DSP techniques. A high sampling rate ADC is needed to convert the whole of the mobile band which then allows channel selection and filtering to be done in the DSP unit. ADCs with high resolution and high sampling rates, as required by radio receivers, are very expensive and require large currents (poor power efficiency). To overcome this problem the proposed receiver suggests the use of a different ADC converter, called a noise tunable $\Sigma\Delta$ ADC. These have the potential for low power consumption and low cost implementation in VLSI. Section 2.2 reviews the major characteristics of ADC, such as quantization, aliasing and oversampling, [Clayton 1982] [Hoeschele 1986] [Sheingold 1978]. Finally section 2.3 develops the concept of $\Sigma\Delta$ modulation from the well-known delta modulator (ΔM).

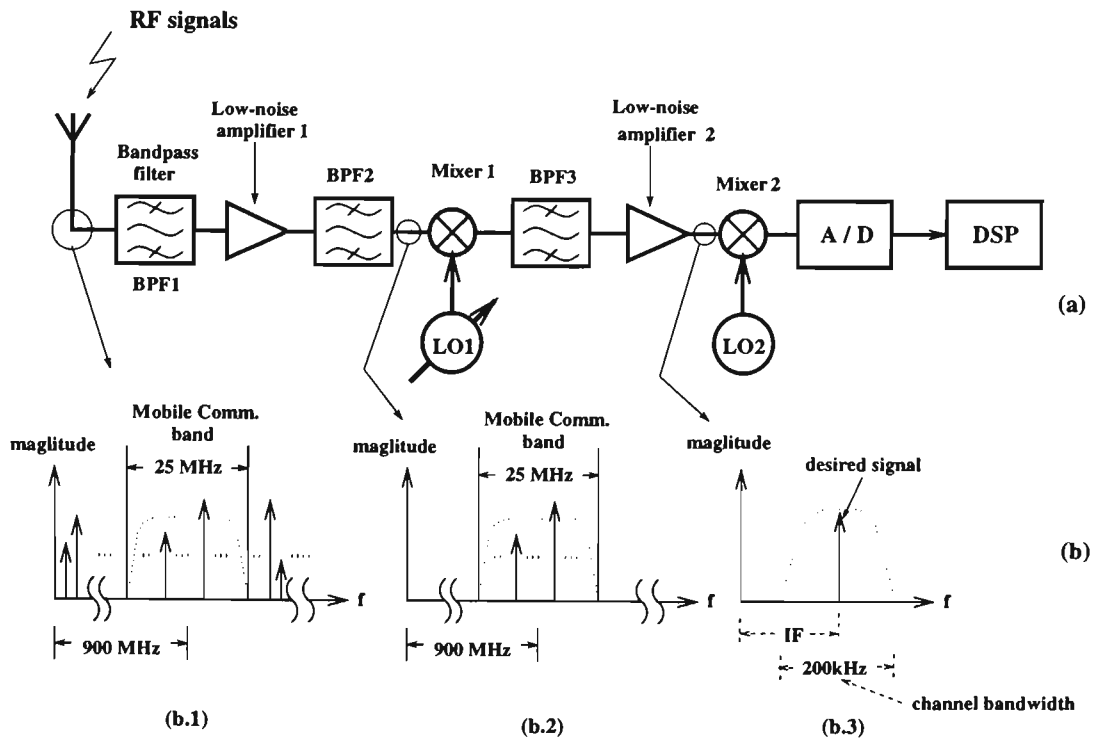


Figure 2.1: (a) A simplified example of a super heterodyne receiver architecture, (b) signals in the frequency domain at different stages.

2.1 Receiver architecture

The following two subsections review two traditional receiver structures [Lindquist 1993] [S.J.Erst 1984] and describe some of their limitations. The final subsection describes the new receiver design and shows how a potentially low cost $\Sigma\Delta$ ADC converter can be incorporated into the system.

2.1.1 Super Heterodyne Receiver

The super heterodyne receiver (see Fig. 2.1) operates by translating the incoming signal (RF signal) to a fixed intermediate frequency (IF) at which most of the filtering and amplification is done. Channel selection is performed by varying the frequency of the first local oscillator. There may be more than one stage of frequency conversion, and filtering is necessary in each step to avoid problems with the interfering image frequencies. The filtering is usually performed by crystal or ceramic filters which are difficult to integrate. Thus to make

a fully integrated receiver, the conventional heterodyne approaches is not suitable.

The super heterodyne receiver architecture is shown in Fig.2.1(a). The receiver's antenna receives the whole signal band shown in Fig. 2.1(b.1). The first bandpass filter (BPF1) immediately after the antenna, which is usually a ceramic filter, eliminates out of band components including the image frequency. This reduces the total inputs to the system and avoids saturation. The next filter (BPF2) before Mixer 1 does further filtering in order to attenuate possible noise introduced by the amplifier and further attenuates unwanted signals left over from BPF1. The signals left after BPF1 and BPF2 are all in the mobile band. The signals before Mixer 1 are shown in Fig. 2.1(b.2). Mixer 1 translates the input band to a lower intermediate frequency (IF). BPF3 filters the desired channel, which is selected by adjusting the frequency of the LO 1 shown in Fig. 2.1(b.3). The second local oscillator and Mixer 2 further reduce the signal frequency, so that ADC conversion is possible prior to demodulation within the DSP unit. The main selectivity in the radio is provided by BPF3, which, often is an expensive, bulky, crystal filter.

2.1.2 Direct Conversion Receiver

Figure 2.2 shows (below) the direct conversion [Lindquist 1993] architecture. The incoming RF signal is translated directly down to baseband, where all the filtering and most of the amplification is performed. The lowpass filters perform both channel selection and an anti-aliasing role prior to ADC conversion. The LO is tuned to the center of the desired channel frequency. Complex (inphase and quadrature) signals are required to stop the spectrum from folding onto itself about DC (i.e., the spectrum is not symmetrical about DC, which is the case for real signals) [Cavers and Liao 1991]. The use of I and Q signals requires two ADC converters, but the bandwidth of the input ADC signal is halved (100kHz instead of 200kHz), allowing the minimum Nyquist sample rate to be halved also (200kHz sampling/sec.). Quadrature demodulators do have errors (carrier leak, phase and gain imbalance) [Roome 1989], but these errors can be corrected by the subsequent DSP processing [Roome 1989]

Direct conversion has several advantages compared to the standard super heterodyne. The baseband filtering makes high selectivity easier to achieve, and integrable lowpass filters, using analog switched capacitor or active filter techniques, can be employed. Since there are

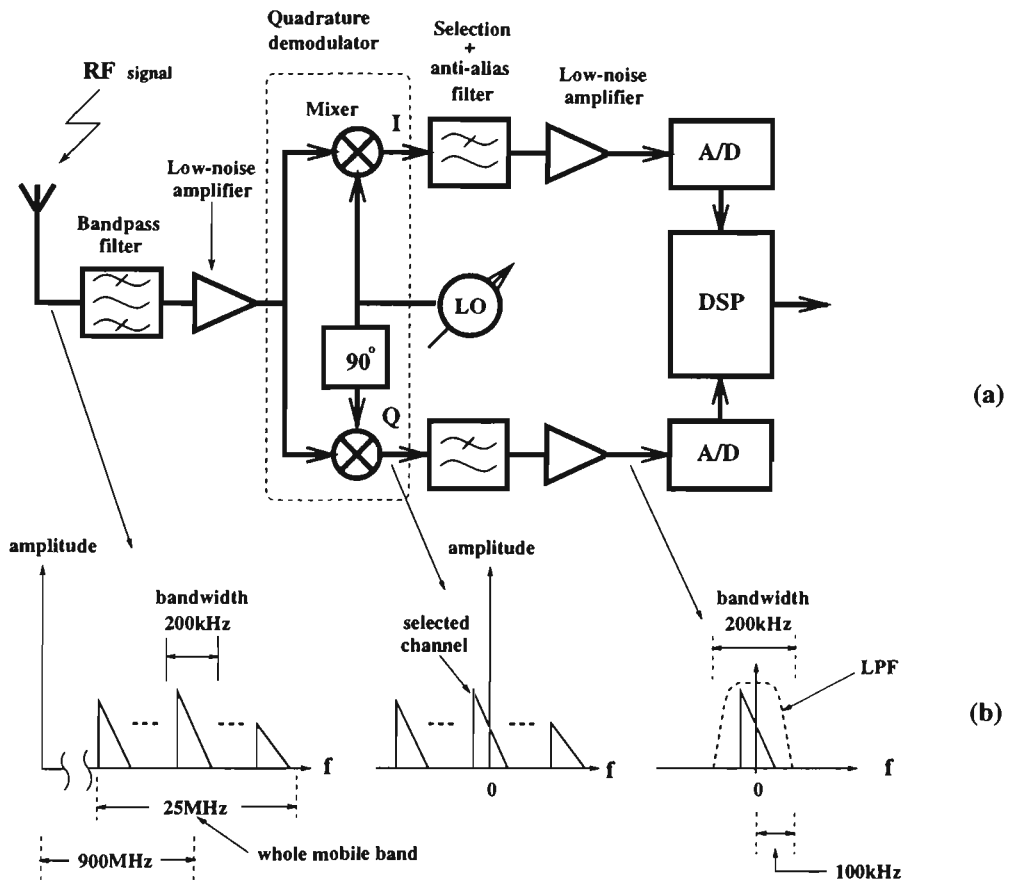


Figure 2.2: A direct receiver architecture.

no IF filters, the size of the receiver can be made smaller and power consumption reduced.

2.1.3 The motivation for proposing a new receiver

The majority of existing hand-held cellular phones are of the conventional super heterodyne type. These receivers suffer from high production costs because they require non-integrable, bulky, radio frequency (RF, 900MHz) and intermediate frequency (IF, about 100 MHz) components, such as filters.

The direct conversion architecture overcomes some major disadvantages encountered by conventional super heterodyne receivers. However, an adjustable local oscillator (synthesizer) is still required and the selectivity is provided by analog circuits. They have difficulty in

providing the preferred ideal filter characteristics of sharp cut-offs and linear phase.

The purpose of proposing a new receiver is to simplify the design of the conventional receiver by moving more functions into the DSP unit. In this case, the ADCs receive the whole of the band, so that digital filtering and signal processing are used for channel selection and final down conversion to baseband. The need for analog crystal filters is removed and the synthesizer can be replaced by a fixed frequency oscillator.

2.1.4 Proposed Receiver

The new receiver operates by translating the whole band of incoming multi-channel signals (125 channels, for the GSM system) to baseband by using a fixed frequency local oscillator and quadrature demodulator as indicated at point *a* in Fig.2.3. The double lines at point *b* indicate I and Q channels. The technique is similar to that used in Fig. 2.2 (next page) except the whole band is converted (25MHz) rather than one channel (200kHz). Quadrature demodulation means that two ADCs are required, however, the signal bandwidth on each of these is halved (12.5MHz). The minimum (Nyquist) sampling rate is 25M samples/sec. but a practical sampling frequency would be more like 50M samples/sec. After AD conversion the desired channel is selected using digital filtering techniques. The filtering can be incorporated as part of the decimation process, since a high sample rate is not required after the desired channel has been isolated. The signal at point *d* is the baseband signal and ready for demodulation.

The required ADC specifications for such a structure are quite stringent. Not only must they have a high sampling rate but they must have a wide dynamic range to cater for all the unwanted signals present across the band. The GSM specification states that:

$$\text{receiver sensitivity} = -102\text{dBm}$$

$$\text{receiver blocking level} > -23\text{dBm}$$

In addition, the quantization noise should be well below the received signal. A figure of -20dB is assumed here. Hence,

The New Receiver with $\Sigma\Delta$ A/D and DSP Tuning

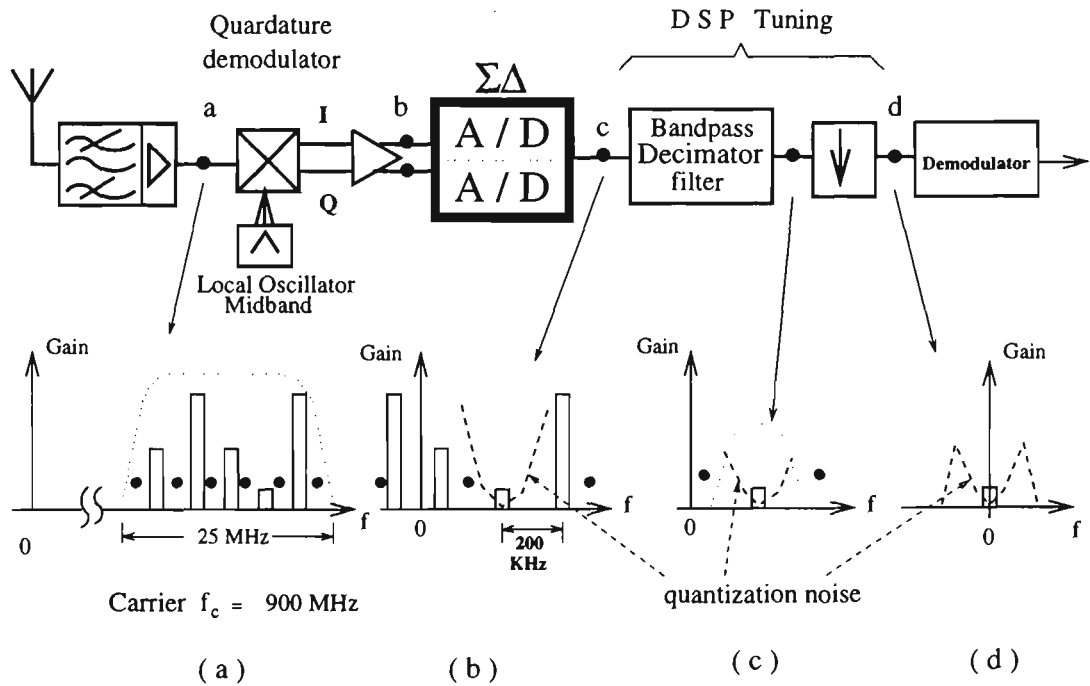


Figure 2.3: The proposed receiver with the noise tunable $\Sigma\Delta$ ADC converter

required dynamic range $> -23 + 102 + 20 = 99$ dB (17 bits)

Some of this dynamic range can be provided through the high oversampling rate (see section 2.2.4):

$$\text{Dynamic range} > 99 - 10\log((f_s / 2) / bwch) = 99 - 10\log(25 / 0.2) = 78.03\text{dB}$$

(13 bits)

This figure, with low power consumption and with a sample rate of 50MHz, is at the boundary of current technology using traditional flash techniques.

$\Sigma\Delta$ ADCs use high oversampling rates and noise shaping techniques to provide a large dynamic range. They have low power consumption and are suitable for integration on VLSI circuits. The noise shaping nulls the quantization noise at a desired frequency. If this frequency can be adjusted to fall on the channel to be received, then the dynamic range requirements can be met (see Fig. 2.3 b, c and d). The other channels experience much higher

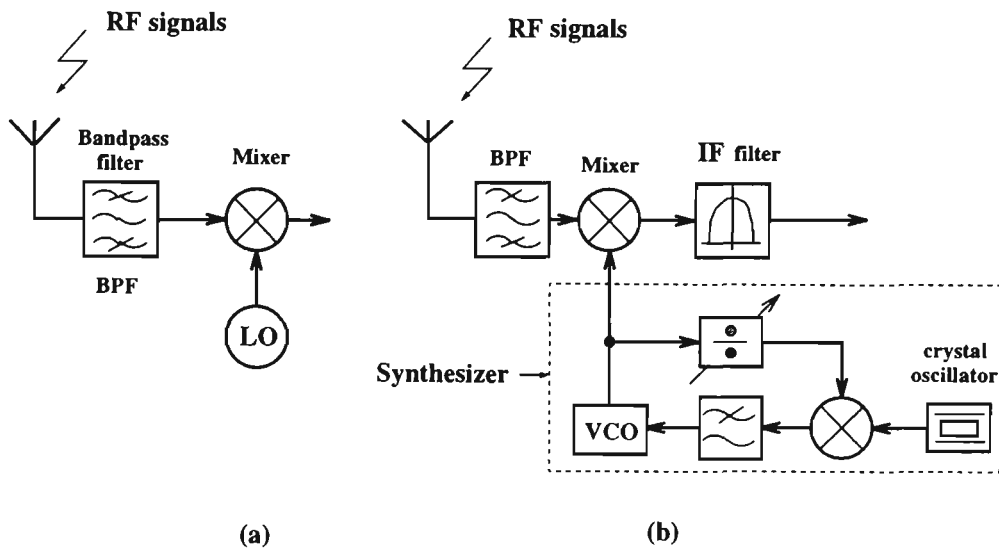


Figure 2.4: Local oscillators, (a) in the proposed receiver and, (b) in the conventional receiver.

levels of quantization noise, but, since they are not being used this does not matter. Selection of another channel requires the shifting of the quantization null frequency. The $\Sigma\Delta$ ADC must be (noise) tunable. This is a new concept for $\Sigma\Delta$ ADCs and the research in this thesis hopes to determine its practicality. The major advantages of performing channel selection in the DSP unit are:

- DSP filters can have near brick wall frequency responses (provided a certain amount of delay is tolerable) and linear phase characteristics.
- DSP filters are very stable can have exact matching (often necessary for the I and Q channels in the quadrature demodulator).
- The filter characteristics can be selected by software. The receiver becomes very flexible, modulation and filtering are software selectable.
- DSP is suitable for VLSI technology, with low cost, small size and reasonable power consumption.
- There is no need for a voltage control oscillator(VCO) / Synthesizer [S.J.Erst 1984], and a simple local oscillator(LO) circuitry is all that is necessary (see Fig. 2.4).
- Channel tuning is performed in the DSP unit by changing filter coefficients. Fast frequency hopping is possible, because there is no need for a synthesiser to settle after changing frequency.

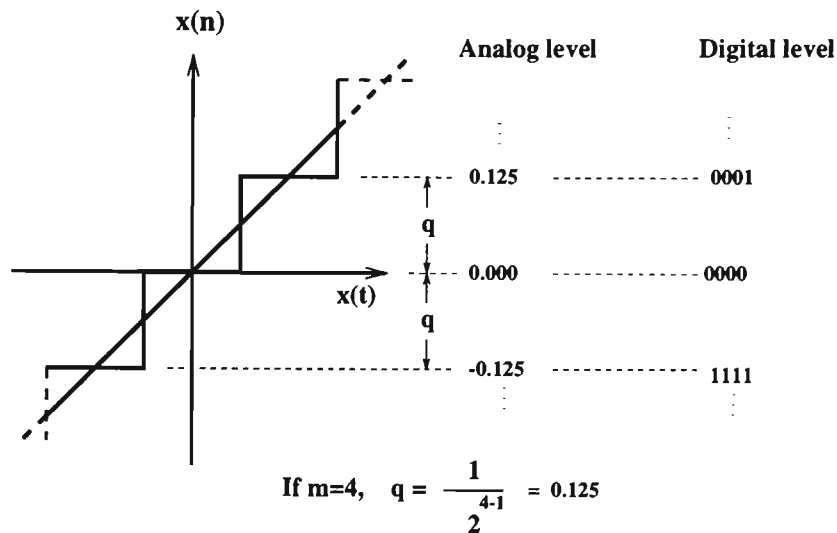


Figure 2.5: The quantization levels for a scaled sequence.

The next section overviews the major features of ADC converters.

2.2 Brief Overview of ADC Converter

This section provides a method for calculating quantization error and explains the necessity of an anti-aliasing filter in ADC conversion. Oversampling eases the requirements on the anti-aliasing filter and the quantizing process.

2.2.1 Quantization error in ADC Conversion

When the signal is sampled to obtain the sequence $x(n)$, each value is encoded by using finite word-length of m -bits including the sign bit. Assuming the sequence is scaled such that $|x(n)| \leq 1$ for fractional number representation, the pertinent dynamic range is 2. Since the encoder employs m -bits, shown in Fig. 2.5, the number of levels available for quantizing $x(t)$ is 2^m . The interval between successive levels, q , is given by:

$$q = \frac{1}{2^{m-1}} \quad (2.1)$$

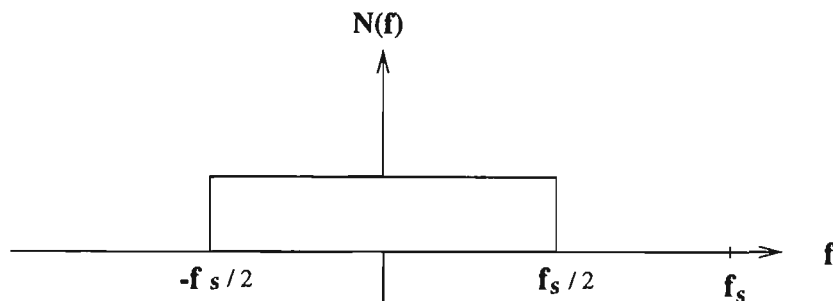


Figure 2.6: The quantization noise power density applicable to general ADC converters.

For an input signal which is large compared to an LSB step, the error term $e(n)$ is a random quantity in the interval with equal probability. Its mean square value (variance), e_{rms}^2 , can be found as [Candy and Temes 1992]:

$$e_{rms}^2 = \frac{1}{q} \int_{-q/2}^{q/2} e^2 de = \frac{q^2}{12} = \frac{2^{-2m}}{3} \quad (2.2)$$

and represents the steady state input quantization noise power. Fig. 2.6 shows the spectrum of the quantization noise.

In the following discussion, it is assumed that all the power is contained in the positive half of the spectrum. When a quantized signal is sampled at frequency $f_s = 1/T_s$, all of its noise power folds into the frequency band $0 \leq f < f_s/2$. If the noise is white, the spectral density of the sampled noise [Bennett 1948] is given by

$$E(f) = e_{rms} \sqrt{2/f_s} = e_{rms} \sqrt{2T_s} \quad (2.3)$$

The concepts discussed here apply, in general, to ADC converters.

2.2.2 The Necessity of Anti-aliasing Filter in ADC

By sampling an input signal $x(t)$ at a frequency f_s , the sampled signal $x(n)$ ($n = 0, 1, 2, \dots$) can be expressed in the frequency domain as the summation of the original signal component and images at integer multiples of the sampling frequency. Therefore input signals above

Nyquist frequency, f_N , can not be properly converted and they also produce new signals in the base-band, which did not exist in the original signal. This non-linear phenomena is a signal distortion called aliasing.

The distortion can be prevented by properly lowpass filtering the input signal up to the Nyquist frequency. This lowpass filter (called anti-aliasing filter) must have a flat frequency response over the signal band of interest and attenuate the frequencies, above the Nyquist frequency, enough to put them under the noise level. Also, the non-linear phase distortion caused by the anti-aliasing filter may create harmonic distortion and audible degradation. Since the analog anti-aliasing filter is the limiting factor in controlling the bandwidth and phase distortion of the input signal, a high performance anti-aliasing filter is required to obtain high resolution and minimum distortion. When the input signal is sampled at the frequency well above the Nyquist frequency, the requirements on anti-aliasing filter are greatly reduced. This will be discussed next.

2.2.3 Anti-aliasing with oversampling

The minimum required sampling rate for a signal with bandwidth f_N (Nyquist criterion) is shown in Fig. 2.7(a). In this case, the requirement for the anti-aliasing filter is very high because it needs a sharp cutoff frequency. Oversampling relieves the need for a sharp cutoff, continuous-time anti-aliasing filter by sampling the signal at an elevated rate Df_s , where D is an oversampling factor ($D \geq 1$), as shown in Fig.2.7(b).

The large difference between the desired signal bandwidth and the new anti-aliasing filter cutoff frequency $Df_s / 2$ means that the available transition bandwidth for the filter is now many times its passband width, and this makes it much easier to realize the anti-aliasing filter with cheap analog circuitry.

In order to accommodate the same final sampling rate f_s as before, the oversampling signal must be further filtered to suppress frequencies above $f_s / 2$. This further filtering can be done in a digital format, after the signal has been quantized. In practice, the digital filtering and the sampling rate reduction take place simultaneously in a DSP unit. The combination is called a decimator [Crochiere and Rabiner 1981] [Candy 1986] [Chu and Burrus 1984]

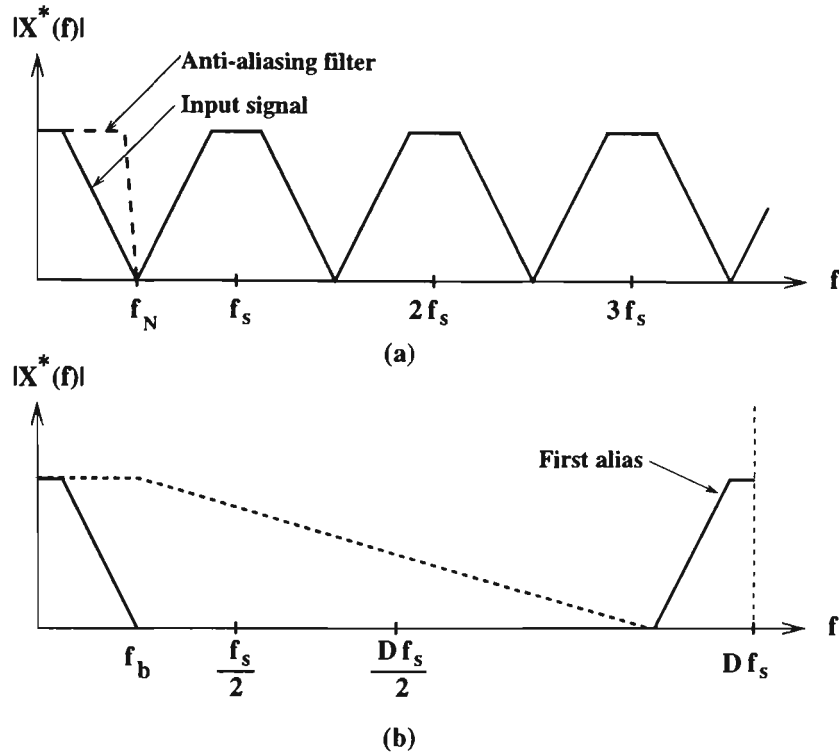


Figure 2.7: Oversampling for anti-aliasing, a high intermediate sampling rate Df_s permits the frequency response of anti-aliasing filter (dashed line) to roll off gradually.

[Dijkstra *et al.* 1988] [Goodman and Carey 1977]. The decimator therefore finally completes the sampling operation of signal acquisition to the target rate f_s .

2.2.4 Oversampling to Facilitate Quantization

When a full precision quantizer is used, the total noise power is constant, whatever the sample rate [Park 1993]. Therefore the average noise spectral density of $E(f)$ will be reduced when the sampling rate is increased to Df_s , as shown in Fig. 2.8. The noise power which lies in the bandwidth of interest, N_{inband} , is given by:

$$N_{inband}(Df_s) = \int_0^{f_b} E^2(f)df = \frac{2f_b e_{rms}^2}{Df_s} \quad (2.4)$$

which is much smaller than the noise power of a Nyquist sampler ($f_s = 2f_N$).

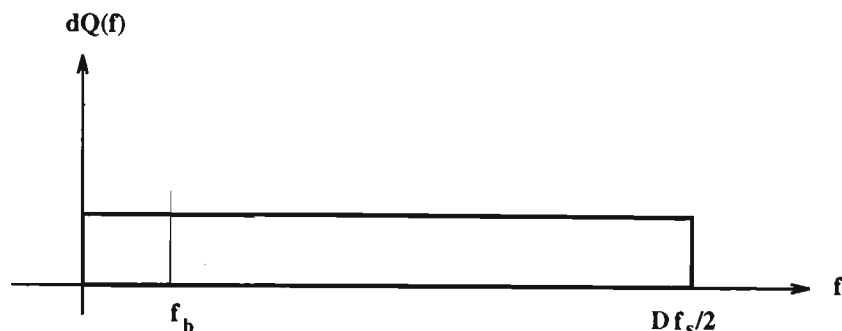


Figure 2.8: Oversampling for reducing the average level of quantization noise density, when $Df_s \gg f_b$, the baseband noise is much smaller than that of the conventional ADC converters.

Oversampling at a rate Df_s reduces noise power in the band of interest by $B(D)$ dB, where

$$B(D) = 10 \log \frac{N_b(Df_s)}{N_{inband}(f_s)} = -10 \log(D) \quad (2.5)$$

for $D \geq 1$. Doubling the sampling rate causes 3dB decrease in inband noise.

2.2.5 The Criterion for Selecting ADC Converters

There are several aspects to be considered in the selection of an appropriate ADC converter for the proposed receiver. These include speed, cost and accuracy. Speed limitations are inherent in the particular techniques but a range of speeds can be expected for different converter devices using the same conversion technique. Increased accuracy is obtained at the expense of a reduction in conversion speed. In general, cost is directly related to speed, number of bits used and accuracy, but the cost of a converter device (indeed of any device), is greatly influenced by market factors which might be quite unrelated to the performance of the device.

Only two types of AD converters can reach the required characteristics. These are the 'flash' and $\Sigma\Delta$ ADCs. The former costs more [Hoeschele 1986], because it has same accuracy all over the band limitation, and the later can only obtain the required accuracy over a small bandwidth [Hauser 1991]. In this application this limitation can be accepted since only one radio channel is needed at a time. This is why the noise tunable $\Sigma\Delta$ ADC is focused in

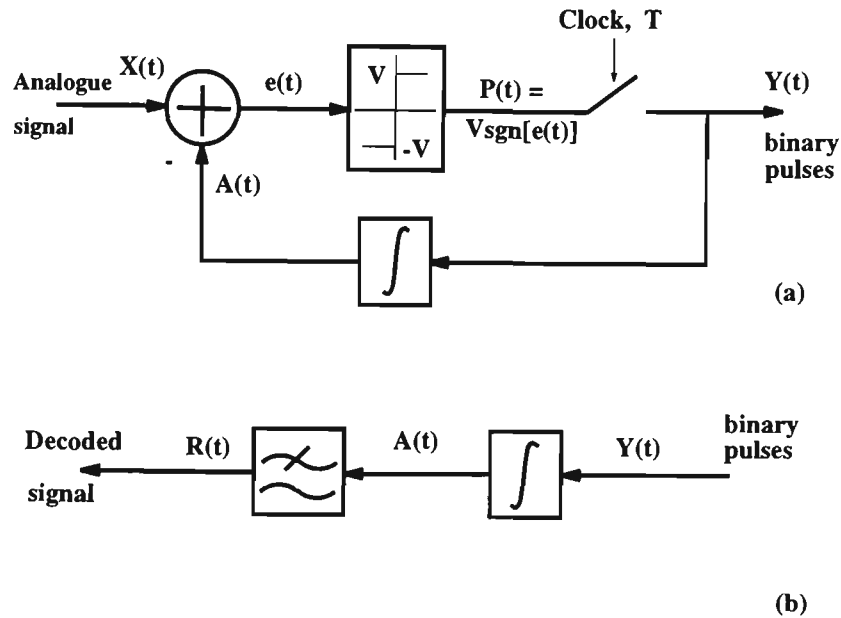


Figure 2.9: The basic structure of Δ modulator.

the research. General introductions to ADC conversion can be found in [Sheingold 1978] [Clayton 1982] [Garrett 1981] [Gray 1990a] [Gray 1990b] [Darling and Hawksford 1990] [Hauser 1991] [Jayant and Noll 1984] [Oppenheim and Schaffer 1989] [Widrow 1956].

2.3 Delta Modulation and Circuit Structure

It is helpful to introduce delta modulation (Δ) before considering the concept of $\Sigma\Delta$ modulation, because the concept of $\Sigma\Delta$ modulation was developed as an extension of the well established Δ modulation technique [Steele 1975]. This research on the noise tunable $\Sigma\Delta$ ADC converter is a further development of the Δ and $\Sigma\Delta$ modulation techniques discussed in [Inose *et al.* 1962] [Candy 1985] [Schreier and Snelgrove 1989] [S.Jantzi *et al.* 1991] [Lainey *et al.* 1983].

Fig.2.9(a) shows a delta modulator (ΔM). The principle of the ΔM can be described as follows: an analogue input signal $X(t)$ is encoded by the ΔM into binary (1 bit) pulses $Y(t)$ which are conveyed to the terminals for transmission. These pulses are also locally decoded back to an analogue waveform $A(t)$ by an integration process in the feedback loop, then subtracted from the input signal to form an error signal $e(t)$, which, is quantized to one of two

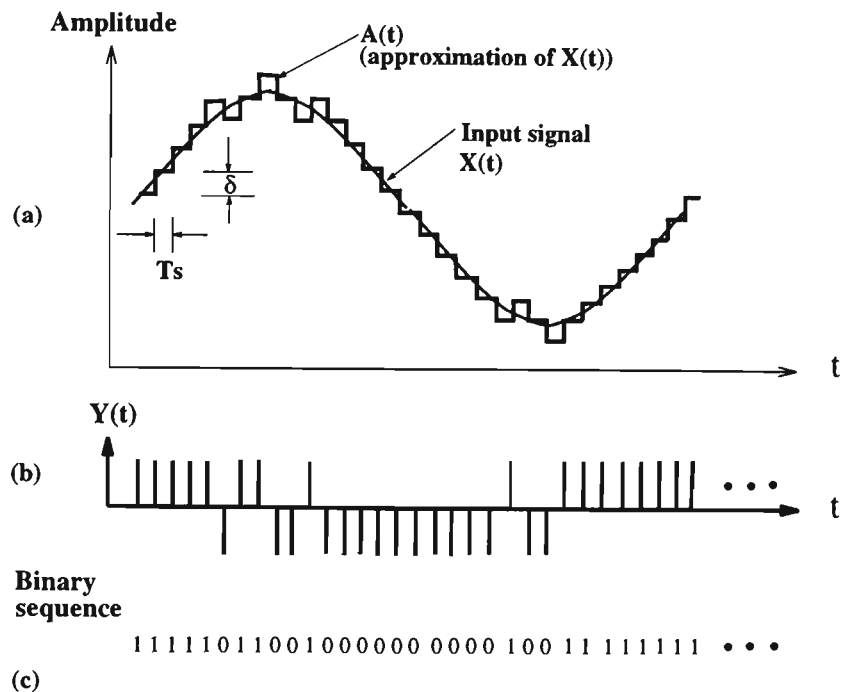


Figure 2.10: The waveforms at each point, (a) the input signal $X(t)$ and the approximation of $X(t)$, (b) the binary pulses at the output of the encoder, (c) binary sequence of (b).

possible levels depending on its polarity.

The output of the quantizer, $P(t)$, is sampled periodically to produce the output binary pulses. The feedback loop arrangement of the ΔM ensures that the polarity of the pulses are adjusted by the sign of the error signal $e(t)$ which causes the local decoded waveform $A(t)$ to track the input signal $X(t)$.

Put another way, the ΔM produces binary pulses at its output which represent the sign of the difference between the input and feedback signal, hence the prefix ' Δ ' is given to the system.

After transmission the binary pulses are recovered, as shown in Fig.2.9(b). They are passed through a local decoder, an integrator, to produce a waveform which differs from the original signal by the error signal $e(t)$ in the encoder. The final decoded signal $R(t)$ is obtained by low-pass filtering the waveform at the output to remove any quantization noise which lies outside the band of interest. As Delta modulation is conceptually simple, it is therefore all the more surprising to find that the system is difficult to analyze. The encoder prohibits simple analysis – there are the quantizer, which is of course a non-linear device, the system sampler

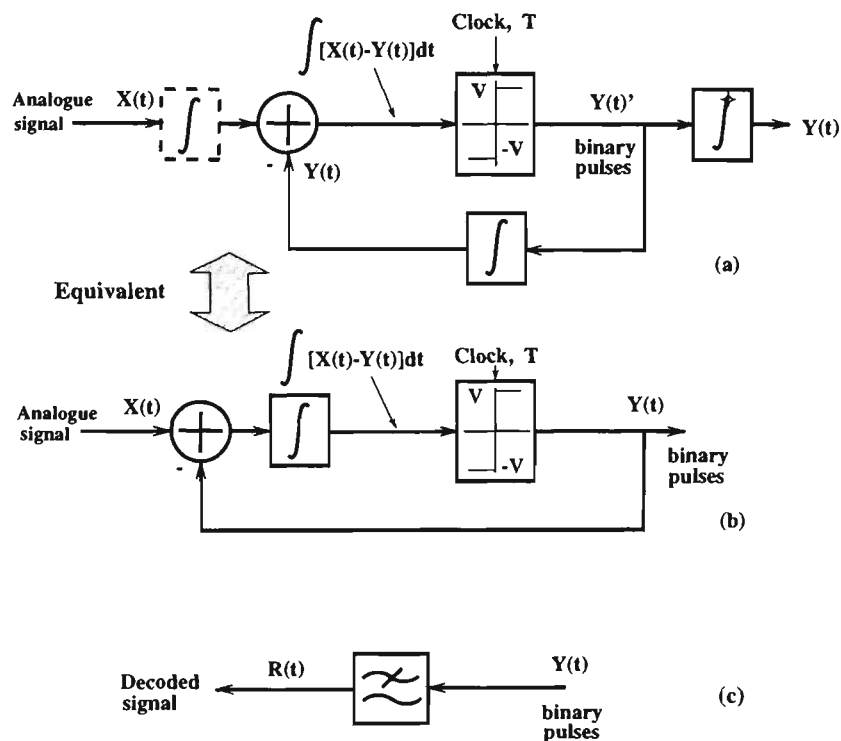


Figure 2.11: The extend development from Δ modulation to $\Sigma\Delta$ Modulation.

which causes the output pulses to be both time and amplitude quantized, and the feedback loop.

2.4 From Δ to $\Sigma\Delta$ Modulation

Δ Modulation technique requires two integrators for the modulation and demodulation processes, as shown in Fig. 2.9. Since integration is a linear operation, the second integrator in the demodulation side can be moved before the modulator without changing overall input and output relationship. The structure in the Fig.2.11 (a) shows a basic model of the $\Sigma\Delta$ modulator in which the error signal before the quantizer is $\int [X(t) - Y(t)]dt$. The integrator in Fig.2.11 (a) can be put either after the loop or before the loop. The two integrators can be rearranged into a single integrator, as shown in Fig. 2.11 (b), while keeping the error signal before the quantizer the same. The name Sigma-Delta modulation probably comes from putting the integrator (sigma) in front of the Delta modulator. The conversion proceeds in two steps: First, an error signal is obtained between desired analog input signal and the

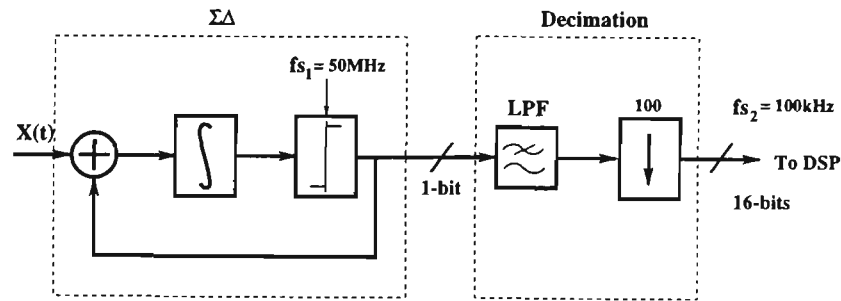


Figure 2.12: A complete $\Sigma\Delta$ ADC system .

sampled, digitized output signal. The error signal is integrated and the output of the integrator is sampled (usually with a 1-bit quantizer). A high oversampling rate is used. The output signal $Y(t)$ can be considered as a pulse density signal and it can be reconstructed into analog form by lowpass filters. However, it is more usual to use the 1 bit sampled output as the input to subsequent digital signal processing system. Digital filtering is used to suppress the out-of-band quantization noise and this is combined with a decimation process to reduce the sample rate, as shown in Fig. 2.12. The final output is a tradition pulse code modulation (PCM) signal sampled close to the Nyquist limit.

Large decimation ratios are normally required (between 50 and 500) [Candy and Temes 1992] [Candy 1986] [Crochiere and Rabiner 1981] and, in practice, these are achieved using two or more decimation stages (e.g. a decimation by 10 followed by another decimation by 10 in frequency).

A detailed development history of $\Sigma\Delta$ ADC converter can be found in [Candy and Temes 1992]. Nowadays, a number of oversampling converters have been designed and manufactured. In fact, 20 bit resolution, oversampling $\Sigma\Delta$ ADC converters as discussed above have been available on the market for audio system [Karema *et al.* 1990]. As confidence has grown in oversampling methods, there is a willingness to accept more complex analog circuits and considerably more complex digital circuits in order to lower the oversampling ratio. Modern oversampled ADC converters have been found to include fifth-order filters [Adams *et al.* 1991], and cascaded modulators [Das and Chatterjee 1967] [Hayashi *et al.* 1986]. The trend is to extend the application of oversampling methods to higher signal frequencies. Whatever the applications, oversampling methods provide a wide range of trade-offs involving factors such as oversampling ratio, filter order, number of quantization levels, number of stages, and the complexity of the decimation filters.

2.5 Conclusion

The conventional receiver structure, including direct conversion, takes one channel at a time before the next tuning is made. Therefore the processing of incoming signals is concentrated on one signal and its filtering, detection and demodulation. The new proposed receiver structure digitizes the whole mobile band (125 channels for GSM system) and uses DSP techniques for decimation, filtering and channel selection. DSP is used to replace expensive and bulky crystal filters used in channel selection. Also the need for a complex frequency synthesizer is reduced or eliminated. The use of DSP gives greater flexibility (software selection) in the choice of bandwidth, modulation scheme and other operational functions. One of the disadvantages of the scheme is that a high speed, high resolution (13 bits) ADCs are required. Traditional flash techniques are expensive in both cost and power. A new type of $\Sigma\Delta$ ADC is proposed to solve this problem. It is shown that the $\Sigma\Delta$ ADC must tune its quantization noise null to the desired received channel if the required dynamic range is to be obtained.

Several important issues regarding AD converters were reviewed. These included Δ modulation, the extension from Δ modulation to $\Sigma\Delta$ modulation, anti-aliasing filtering and oversampling. Oversampling greatly relieves the requirements on the anti-aliasing filter (e.g. roll-off rate) and reduces the average spectrum density of the quantization noise by approximately 3dB/octave. But it is not adequate enough to rely totally on oversampling to improve the resolution of ADC converters. Therefore $\Sigma\Delta$ ADC converters with noise shaping characteristics are needed to further reduce the quantization noise level within a particular frequency band.

The majority of previous work on $\Sigma\Delta$ ADCs has concentrated on the conversion of lowpass signals for audio applications. All the important design and analysis techniques have been developed for these lowpass $\Sigma\Delta$ ADCs. It was decided to review and repeat some of this work to obtain a better understanding of the $\Sigma\Delta$ concept and this is presented in the next chapter.

Chapter 3

Sigma-Delta ($\Sigma\Delta$) Modulation for Lowpass Signals

3.1 Introduction

Previous chapters have introduced the possibility of using a $\Sigma\Delta$ ADC in the design of the proposed radio receiver. This chapter introduces $\Sigma\Delta$ ADCs. It describes the design, operation and major properties. Their performance is evaluated using analysis and simulations.

The advantages in implementation of such $\Sigma\Delta$ ADCs are that the circuits do not require any component trimming to achieve high resolution in the conversion process, reduced anti-aliasing filter requirements, and a system architecture that lends itself to switched-capacitor implementation [Lainey *et al.* 1983] [Norsworthy *et al.* 1989] [Hurst and Levinson 1989] [Bishop *et al.* 1990].

Although the sigma-delta modulator was first introduced by Inose and Yasuda in 1962

[Inose *et al.* 1962], it did not gain importance until recent developments in digital VLSI technologies, which provides the practical means to implement the large digital signal processing circuitry. The increasing use of digital techniques in communication and audio application has also contributed to the recent interest in cost effective high precision ADCs. The popularity of $\Sigma\Delta$ ADCs is due to their compatibility with present-day CMOS VLSI technology; almost 90% of the die is implemented in digital circuitry which enhances the prospect of compatibility.

The advantages of implementing $\Sigma\Delta$ ADC with VLSI techniques include higher reliability, increased functionality, and reduced chip cost. Those characteristics are commonly required in the digital signal processing implementation. Consequently, the development of DSP technology, in general, has been an important force in the development of high precision ADCs which can be integrated on the same die as the digital signal processor itself.

This chapter only considers lowpass (audio) $\Sigma\Delta$ ADCs. The novel bandpass $\Sigma\Delta$ ADC required for the new receiver architecture will be presented in chapter 4. Section 3.2 and 3.3 introduce the basic structure and principle of $\Sigma\Delta$ modulation and the noise-shaping theory on which the research is based. Section 3.4 investigates the performance of a first order system and section 3.5 considers second and higher order systems. Section 3.6 and 3.7 discuss the problems of limit cycles associated with $\Sigma\Delta$ ADC, and presents a brief literature summary on complex systems.

3.2 $\Sigma\Delta$ Modulation Structure and Principle

Conventional high resolution ADCs (i.e. successive approximation and flash type) operate near the Nyquist rate. These Nyquist samplers require a complicated analog lowpass filter(anti-aliasing filter) to limit the maximum frequency input to the ADC and sample-and-hold circuitry. On the other hand, the $\Sigma\Delta$ ADCs use a low resolution ADC (1-bit quantizer), noise shaping and a very high oversampling rate. Moreover, since precise component matching (or laser trimming) is not needed for the high resolution $\Sigma\Delta$ ADCs, they have very attractive implementation properties. They are suitable for integration on to VLSI digital circuits.

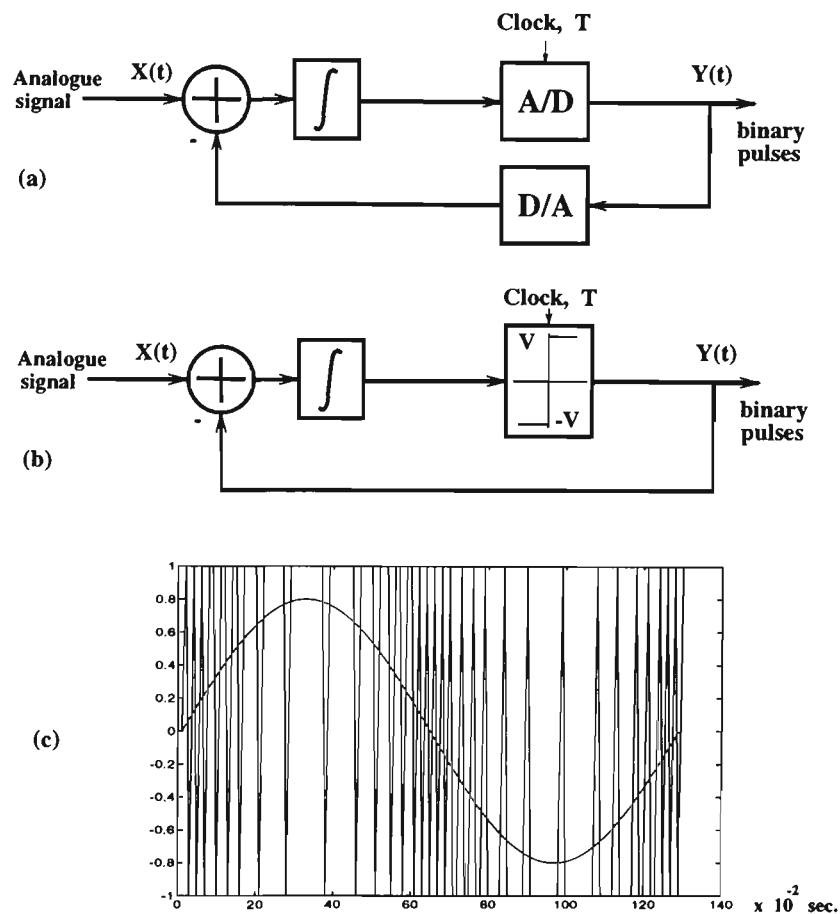


Figure 3.1: (a) The first order $\Sigma\Delta$ ADC structure, (b) with one bit quantizer in forward loop and one bit D/A in the feedback loop. (c) The input signal (sine-wave) and the binary pulsed output signal (MATLAB simulation), where $V = 1$ volt.

Fig. 3.1(a) shows the structure of a first order $\Sigma\Delta$ modulator with a 1-bit DAC in the feedback loop. The difference signal, between the desired input and the quantized feedback signal is fed to the quantizer via an integrator. The feedback forces the average value of the quantized signal to track the input signal. Any difference between them accumulates in the integrator and eventually corrects itself.

Fig. 3.1(c) shows the response (output) of the circuit to a sine-wave input. It illustrates how the quantized signal oscillates between two levels (± 1) in such manner that its local average equals the input signal amplitude [Candy 1974]. The output bit-stream contains the input signal and quantization noise. The quantization noise has strong high frequency components that can be removed by lowpass filtering. This is performed by a filter/decimation process which reduces the sample rate in conjunction with increasing the signal resolution (number of bits). High resolution performance can be obtained for both ADCs and DACs

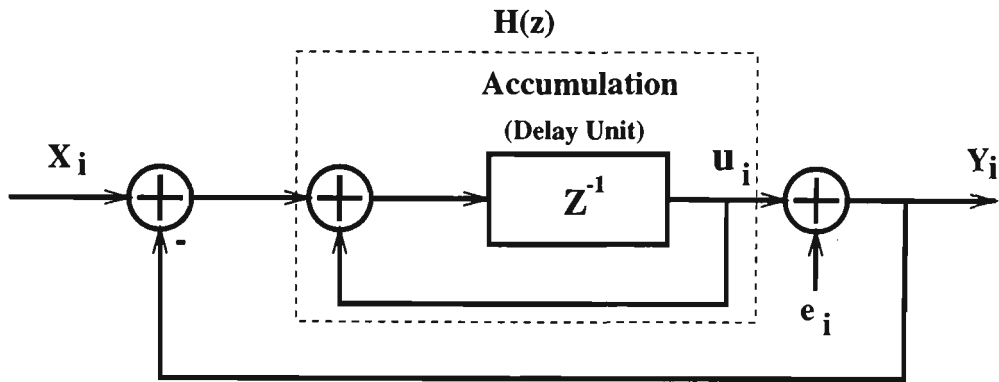


Figure 3.2: System model using a discrete time integrator to replace the analog integrator of Fig. 3.1.

using this technique, as has been described in [Welland *et al.* 1989] [Brandt *et al.* 1991] for compact disc sound system.

3.3 Basic Noise-Shaping Theory

$\Sigma\Delta$ ADCs use noise shaping techniques to remove (null) quantization noise from the part of the spectrum occupied by the desired signal. The design of the noise shaping functions is important, and it determines the performance of the $\Sigma\Delta$ ADC.

3.3.1 The Noise Shaping Feature

To analyze the $\Sigma\Delta$ ADC, the circuit shown in Fig. 3.1 (a) is transformed to its sampled-data equivalent, with the quantization error modeled as an added error e_i , as shown in Fig. 3.2 [Candy and Temes 1992]. The model assumes that the quantization noise is uncorrelated with the input signal and that it can be treated as white noise [Gray 1987] [Gray *et al.* 1989] [Gray 1990a]. The system can be analyzed using linear techniques.

As a $\Sigma\Delta$ ADC usually employs two-level (1 and -1) quantization, there is no need to place an actual D/A converter (Fig.3.1(b)) in the feedback loop. It is assumed that the sampling frequency is much greater than the input signal bandwidth, that is to say the input signal

remains unchanged during one sampling time period, so the system can be described in z -domain (if this is not the case, then a sample and hold device is required prior to the $\Sigma\Delta$ ADC).

From the z -domain model in Fig. 3.2, the system's transfer functions can be determined. It can accurately predict the error spectrum and general behavior of the $\Sigma\Delta$ modulation process.

The z transform of output $Y(z)$, obtained from Fig. 3.2, is :

$$Y(z) = \frac{H(z)}{1 + H(z)}X(z) + \frac{1}{1 + H(z)}E(z) \quad (3.1)$$

From Eq. (3.1), the signal transfer function (STF) becomes :

$$STF(z) = \frac{Y(z)}{X(z)} = \frac{H(z)}{1 + H(z)} \quad (3.2)$$

when $E(z) = 0$. The noise transfer function (NTF) becomes:

$$NTF(z) = \frac{Y(z)}{E(z)} = \frac{1}{1 + H(z)} \quad (3.3)$$

when $X(z) = 0$. These two transfer functions link the output to the input signal and to the source of quantization noise. The qualitative frequency responses of these two functions are shown in Fig. 3.3. In general, $|NTF|$ can always be made less than 1 (i.e. $|NTF| < 1$) around the baseband frequency ($z = 1$). Therefore, the $\Sigma\Delta$ ADC noise will be always smaller than ordinary quantization noise. Fig. 3.4 shows the spectral density of the noise from $\Sigma\Delta$ quantization compared with that of ordinary quantization [Candy and Temes 1992]. The grey and dark areas represent quantization noise power for a conventional ADC (e.g successive approximation / flash) and a noise tunable bandpass $\Sigma\Delta$ ADC respectively. It is clear that quantization noise in the $\Sigma\Delta$ ADC is much smaller within a narrow bandwidth around the null position. The result indicates that, with the same number of bits used in A/D conversion, $\Sigma\Delta$ ADC has much lower quantization noise power compared with that of conventional ADC . This is the reason that $\Sigma\Delta$ ADCs are so popular.

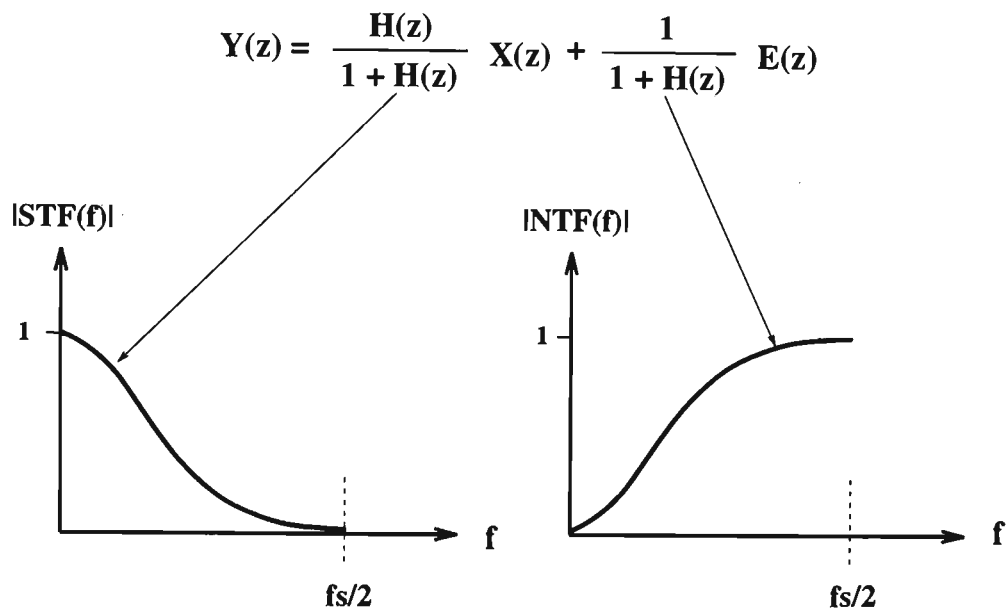


Figure 3.3: The noise shaping concept. Typical frequency responses of the system transfer function (*STF*) and the noise transfer function (*NTF*).

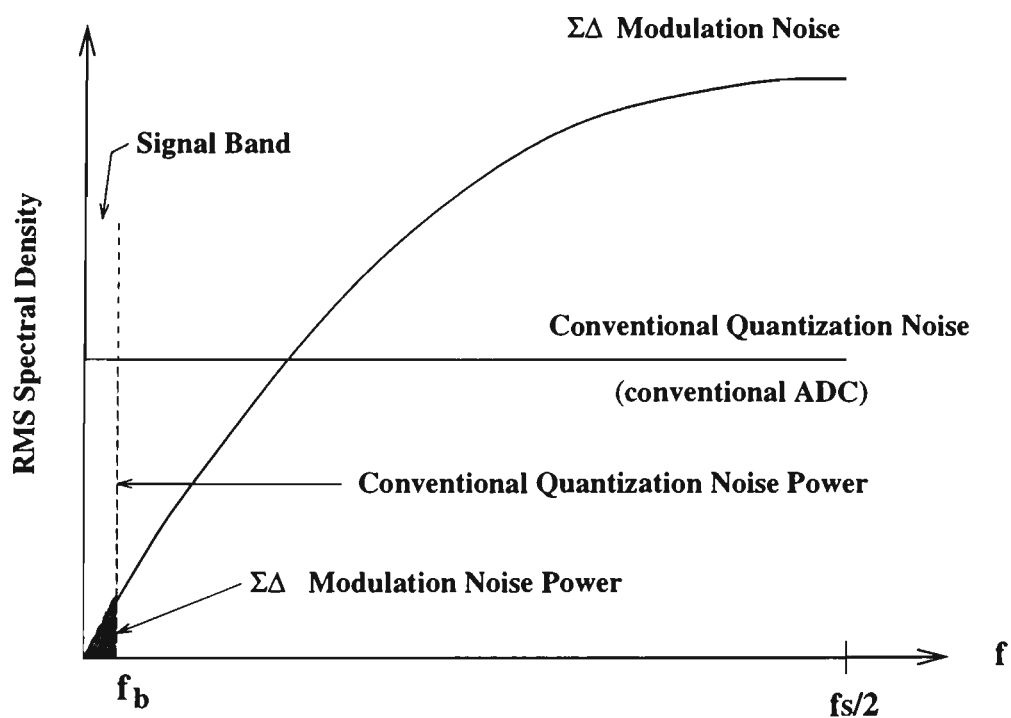


Figure 3.4: The comparison of quantization noise between a $\Sigma\Delta$ ADC and a conventional (flash etc.) ADC.

It is important to point out that there is no constraints put on $H(z)$ when Eq. (3.1) was derived. This means that $H(z)$ can be any structural function (not just only an integrator unit) and is universal. As such, the *NTF* can be made to target the need of reducing noise, from which the name of noise shaping comes. Much research [Candy and Temes 1992] [Brandt *et al.* 1991] [Carley 1989] [Hayashi *et al.* 1986] [Li 1993] [Matsuya *et al.* 1987] [Norsworthy *et al.* 1989] [Ritoniemi *et al.* 1990] (just name a few) into $\Sigma\Delta$ ADCs, is focused on improving the noise shaping function (*NTF*).

3.4 Noise Shaping for First Order Systems

This section investigates the improvement of a first order $\Sigma\Delta$ ADC system, in terms of quantization noise, signal to quantization noise ratio (S/N), and dynamic range. The investigation is extended by introducing a coefficient, g , into the integrator structure, $H(z)$. It is shown that this coefficient can adjust the pole position of the *NTF* and *STF* which affect the noise performance of the system.

3.4.1 Quantization Noise

The first order $\Sigma\Delta$ ADC described in Fig. 3.2 has $H(z) = z^{-1} / (1 - z^{-1})$, hence, *STF*(z) and *NTF*(z) become

$$STF(z) = \frac{Y(z)}{X(z)} = z^{-1} = \frac{1}{z} \quad (3.4)$$

and

$$NTF(z) = \frac{Y(z)}{E(z)} = 1 - z^{-1} = \frac{z - 1}{z} \quad (3.5)$$

Eq. (3.5) shows that the *NTF* has one zero at frequency $\omega = 0$ ($z = 1$) which reduces

the quantization noise at low frequencies and a pole at the origin which has no effect. The magnitude response of the STF is equal to 1 for all frequencies.

NTF equals zero at DC (zero frequency) has the effect of nulling the noise at $\omega = 0$. However, the magnitude of the NTF ($|NTF|$) increases at high frequencies. In this example $|NTF| = 2$ when $f = f_s / 2$. At high frequencies the quantization noise increases. This behavior is described as noise-shaping. Therefore, if the analog input signal to the modulator $x(t)$, is oversampled, the high-frequency quantization noise can be removed by digital lowpass filters without affecting the input signal characteristics' at baseband frequencies. This lowpass filtering is part of the subsequent decimation process.

To calculate the effective resolution of the $\Sigma\Delta$ ADC, it is assumed that the input signal is sufficiently busy so that the quantization error can be treated as white noise, which is uncorrelated with the signal. With the first order noise shaping function, Eq. (3.5), the spectral density of the modulation noise may then be described as [Candy and Temes 1992]:

$$|N(f)| = |E(f)| \cdot |1 - z^{-1}| = |E(f)| |1 - e^{-j\omega T_s}| = 2e_{rms} \sqrt{2T_s} \sin\left(\frac{\omega T_s}{2}\right) \quad (3.6)$$

where the $|E(f)|$ is obtained from equation (2.3). Clearly, the system reduces the noise at low frequencies, but increases it at high frequencies. The noise power in the signal band is :

$$N_{inband-1} = \int_0^{f_b} |N(f)|^2 df = \int_0^{f_b} |2e_{rms} \sqrt{2T_s} \sin\left(\frac{\omega T_s}{2}\right)|^2 df \approx e_{rms}^2 \frac{\pi^2}{3} (2f_b T_s)^3 \quad (3.7)$$

where $f_s \gg f_b$. Each doubling of the oversampling ratio thus reduces this noise by 9dB and provides 1.5 bits of extra resolution. This improvement in the resolution requires that the modulated signal be decimated to the Nyquist rate with a sharply selective digital filter.

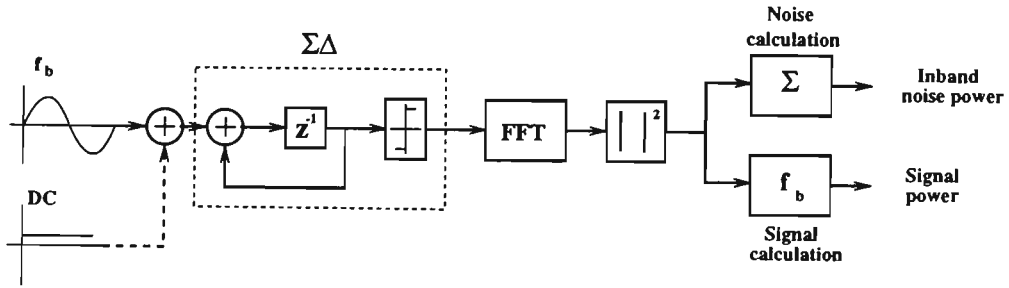


Figure 3.5: Simulation Model

3.4.2 Signal to Quantization Noise Ratio

The performance of $\Sigma\Delta$ ADC is normally evaluated using the signal to quantization noise ratio (S/N) and the dynamic range. The S/N ratio is defined as the input signal power divided by quantization noise power in the desired channel. Dynamic range is defined as the difference between the input signal level when input signal power equals the quantization noise power in the desired channel and the input signal level just before system saturation.

The signal to noise ratio for an input sinusoid with amplitude V (power, $S = V^2 / 2$) is

$$S / N = \frac{V^2}{2} / \left(\frac{e_{rms}^2 \pi^2}{3} (2f_b T_s)^3 \right) \quad (3.8)$$

The largest sine wave that the $\Sigma\Delta$ modulator will accommodate without saturating has a peak value 1.0 and a power value of $1 / 2$. The quantization noise power is given by Eq. (3.8), and therefore the maximum S/N can be expressed as :

$$S / N_{max} = \frac{3}{2e_{rms}^2 \pi^2} (2f_b T_s)^{-3} \quad (3.9)$$

These theoretical equations were checked using simulation. A signal with amplitude, V , and frequency f_b was used as an input to the first order $\Sigma\Delta$ ADC with MATLAB. The output signal was processed through a FFT. All inband noise components (bins) were summed together to obtain the noise power, from which the S/N ratio can be calculated. This is illustrated in Fig. 3.5.

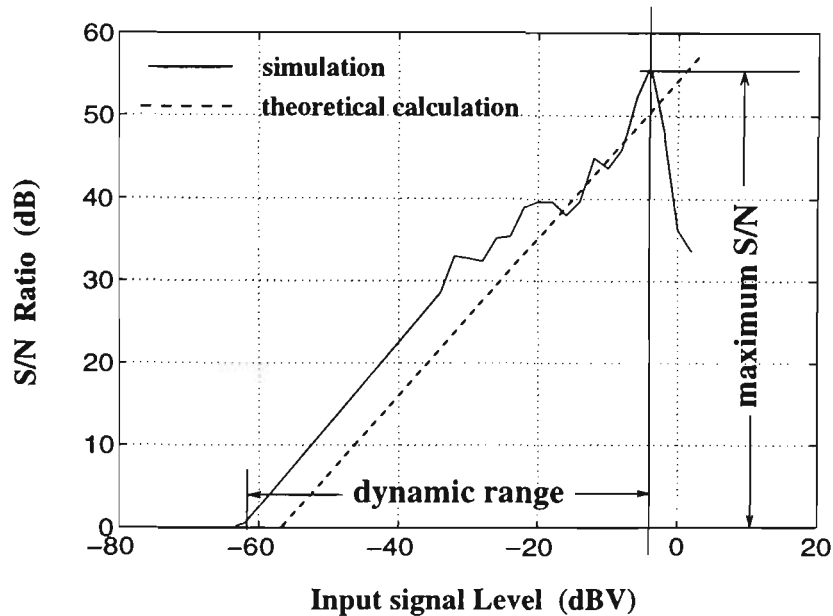


Figure 3.6: Signal to quantization noise ratio versus the amplitude of applied sine waves for the first order $\Sigma\Delta$ circuit, 0dB corresponds to an amplitude of 1 volt. The dotted-line is calculated using equation (3.9), the solid-line represents simulation from MATLAB. The turning point indicates onset saturation effects.

The model in Fig. 3.2 is simulated using MATLAB. The solid-line Fig. 3.6 is the plot of the signal to quantization noise versus the amplitude of the input signal. The dotted-line shows the theoretical calculated result using Eq.(3.9). A comparison of the plot shows that the theoretical equation provides the low bound values of the signal to noise ratio in the dynamic range (assuming the noise is white). The MATLAB model, uses a limiter as the quantizer, and makes no assumption about the quantization noise. Therefore a difference between the two results should be expected. Zero-dB input corresponds to a peak amplitude equal to 1 volt. The maximum S/N is about 56dB at full scale input (1 volt), and the maximum dynamic range is about 62dB. Simulations were conducted by setting the input signal frequency, $f_b = 0.05\pi$, bandwidth, $bw = 0.05\pi$, the sampling frequency, $f_s = 2\pi$ (normalized frequency), and using 4096 points for the FFT.

3.4.3 The Effect of Integrator Gain on $\Sigma\Delta$ Performance

To further investigate the behavior of the first order circuit, a coefficient g is placed in the forward loop. The modified circuit (based on Fig. 3.2) is shown in Fig. 3.7. The z-domain

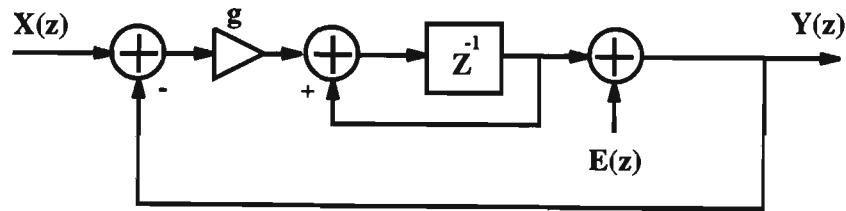


Figure 3.7: An analysis model (modified from Fig. 3.2) for investigating the behavior of the first order circuit with a coefficient g in the forward loop.

system transfer function of the system is :

$$Y(z) = \frac{gz^{-1}}{1 - (1 - g)z^{-1}}X(z) + \frac{1 - z^{-1}}{1 - (1 - g)z^{-1}}E(z). \quad (3.10)$$

Similarly, the signal transfer function STF is :

$$STF(z) = \frac{gz^{-1}}{1 - (1 - g)z^{-1}} \quad (3.11)$$

and the noise transfer function NTF is :

$$NTF(z) = \frac{1 - z^{-1}}{1 - (1 - g)z^{-1}} \quad (3.12)$$

It is clear the NTF has a pole at $z = 1 - g$ and a zero at $z = 1$ ($\omega = 0$). The NTF can still null the quantization noise at $\omega = 0$, as shown in Fig. 3.8. It shows the simulation of the output with the sine-wave input (0.8 volts). The Fast Fourier Transform Algorithm is applied to the output (bit-stream) of the system to gain the output spectrum. Fig. 3.8(a) is the baseband part of 3.8(b) and shows the noise power density in the vicinity of the applied signal.

The coefficient g determines the pole position which affects both the NTF and the STF. In this case the quantization noise power spectral density becomes:

$$|N(f)| = |E| \cdot \left| \frac{1 - e^{j\omega T_s}}{1 - (1 - g)e^{j\omega T_s}} \right| \quad (3.13)$$

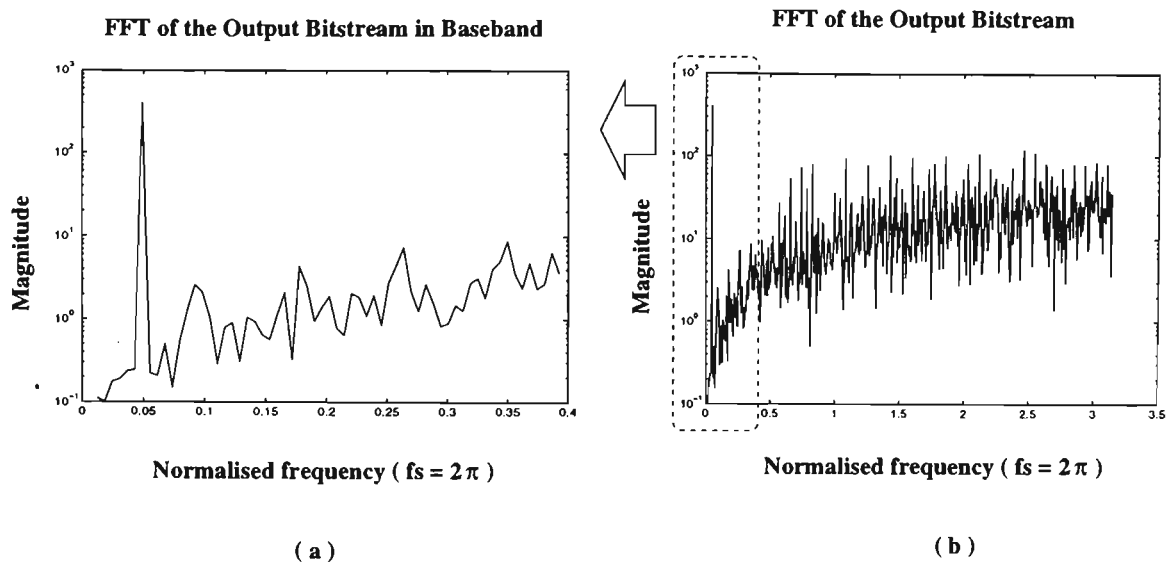


Figure 3.8: (b) Simulation spectrum of the first-order system with a coefficient g in the forward path. Sine input with amplitude = 0.8 volts, DC offset = 0.005, and frequency = 800Hz. The sampling frequency / clock frequency is 102.4kHz, points for calculating FFT is 4096, (a) The baseband enlargement of (b). [MATLAB simulation]

and the quantization noise power in the band from 0 to f_b becomes :

$$N_{inband}(f_b) = \int_0^{f_b} |N(f)|^2 df \quad (3.14)$$

Fig. 3.9 (next page) shows the calculated frequency response of the STF and NTF from Eq. (3.11) and (3.12) with three pole positions, corresponding to $g = 1(z = p_1)$, $g < 1(z = p_2)$ and $g > 1(z = p_3)$. The latter position (p_3) results in the lowest quantization noise within the signal band, but produces more out of band noise. If the NTF has too much gain then instability can result. Stability in this instance means that the error signal is bounded [Schreier and Snelgrove 1991]. If this is not the case, the error power will increase and dominate the operation of the $\Sigma\Delta$ modulator reducing its noise shaping effectiveness. To the best of the author's knowledge there is no complete theory that describes a stability boundary for $\Sigma\Delta$ ADCs. In this thesis, a commonly used 'rule of thumb' criteria will be employed. The criteria requires that $|NTF| < 2$ for all frequencies to avoid instability [Chao *et al.* 1990] [Schreier and Snelgrove 1989]. Therefore g can be set to give an optimum trade off between performance and stability. The STF is also effected by the different pole positions, but within the desired signal band there is little change if the oversampling rate is high; this is normally true for $\Sigma\Delta$ systems.

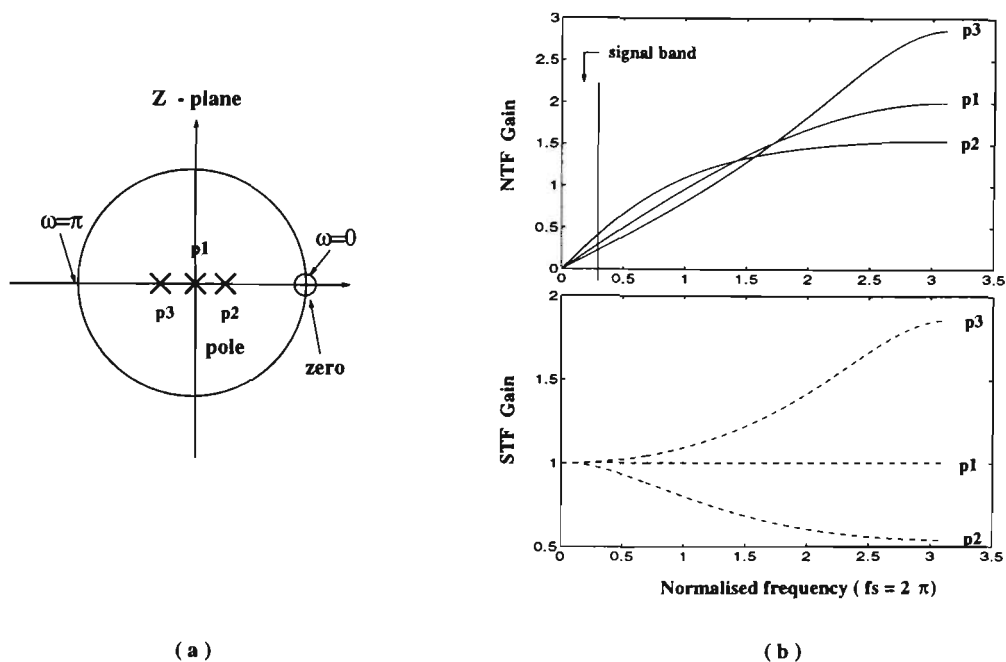


Figure 3.9: (a) The pole-zero position of 1st order system, pole can take the value of p_1, p_2 and p_3 separately, (b) calculated frequency response of the system for different pole position, $p_1 = 0, p_2 = 0.3$, and $p_3 = -0.3$. (simulated on MATLAB).

In brief, g can be adjusted to obtain the desired performance within the stability boundary, $|NTF| < 2$.

3.5 Noise Shaping for High Order Systems

This section discusses the improvement in noise shaping of a second order $\Sigma\Delta$ ADC system. The discussion is extended by introducing coefficients, g_1, g_2, b_1, b_2 and A_1 , into the system structure. It is shown that these coefficients can adjust the pole positions of the NTF and STF which affect the noise performance of the system.

3.5.1 Quantization Noise

High order noise shaping systems can further reduce the inband quantization noise. A second order $\Sigma\Delta$ ADC structure, based on [Agrawal and Shenoi 1983] and [Candy 1985], is

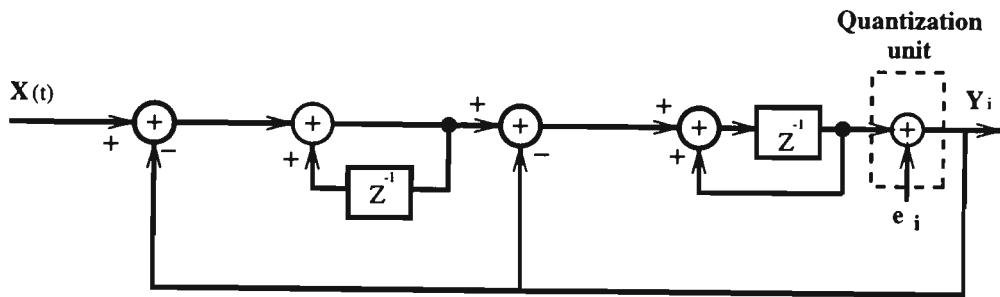


Figure 3.10: Double loop (the second order) digital $\Sigma\Delta$ modulator without any coefficients.

shown in Fig. 3.10. The system can be analyzed using its *NTF* and *STF* in a similar way as the previous first order system. The system transfer function of the double loop system becomes :

$$Y(z) = z^{-1}X(z) + (1 - z^{-1})^2E(z) \quad (3.15)$$

and the *STF*(z) and *NTF*(z) become:

$$STF_2(z) = z^{-1} \quad (3.16)$$

and

$$NTF_2(z) = (1 - z^{-1})^2 \quad (3.17)$$

Eq. (3.17) shows that the *NTF* has two zeros at frequency $\omega = 0$ ($z = 1$), which can further reduce the quantization noise at low frequencies, and two poles at the origin. The frequency response of the *STF* is flat across the band while the *NTF* has a similar shape to that shown in Fig. 3.3, except for a wider null at DC. The spectral density of the quantization noise can be derived from the *NTF* [Candy and Temes 1992], as in section 3.4.1:

$$N_2(f) = |E(f)| \cdot |(1 - e^{-j\omega T_s})^2| = 4e_{rms}\sqrt{2T_s} \sin^2\left(\frac{\omega T_s}{2}\right) \quad (3.18)$$

As before, feedback around the quantizer reduces the noise at low frequencies, but increases it at high frequencies. The quantization noise power in the signal band is :

$$N_{inband-2} = \int_0^{f_b} |N_2(f)|^2 df \approx e_{rms}^2 \frac{\pi^4}{5} (2f_b T_s)^5 \quad (3.19)$$

where $f_s \gg f_b$. This noise falls by 15dB/octave and provides 2.5 extra bits of resolution for every doubling of the sampling frequency [Brandt *et al.* 1991] [Candy 1985]. The technique can be extended to higher-order systems, by adding more feedback loops to the circuit [Ritoniemi *et al.* 1990].

When there are L loops and the system is stable, the power spectral density of the output quantization noise is [Candy and Temes 1992]:

$$|N_L|^2 = e_{rms}^2 2T_s \left(2 \sin \left(\frac{\omega T_s}{2} \right) \right)^{2L}, \quad (3.20)$$

and for oversampling ratios greater than 2, the noise in the signal band is given approximately by :

$$e_{inband-L} = e_{rms}^2 \frac{\pi^{2L}}{2L+1} (2f_b T_s)^{2L+1}. \quad (3.21)$$

This noise falls $3(2L+1)$ dB for every doubling of the sampling rate and provides $L+0.5$ extra bits. Fig. 3.11 shows the inband noise plotted against the oversampling ratio for examples of a conventional 1 bit ADC ($L = 0$), a single loop $\Sigma\Delta$ ADC ($L = 1$) and multiple loop $\Sigma\Delta$ ADC structure ($L = m$). These diagrams are derived from Eq. (3.21), which assumes white uncorrelated noise.

When $L > 2$, the system becomes complicated and there are difficulties in implementing the circuits. Different structures are usually used for these higher order systems [Rebeschini *et al.* 1989].

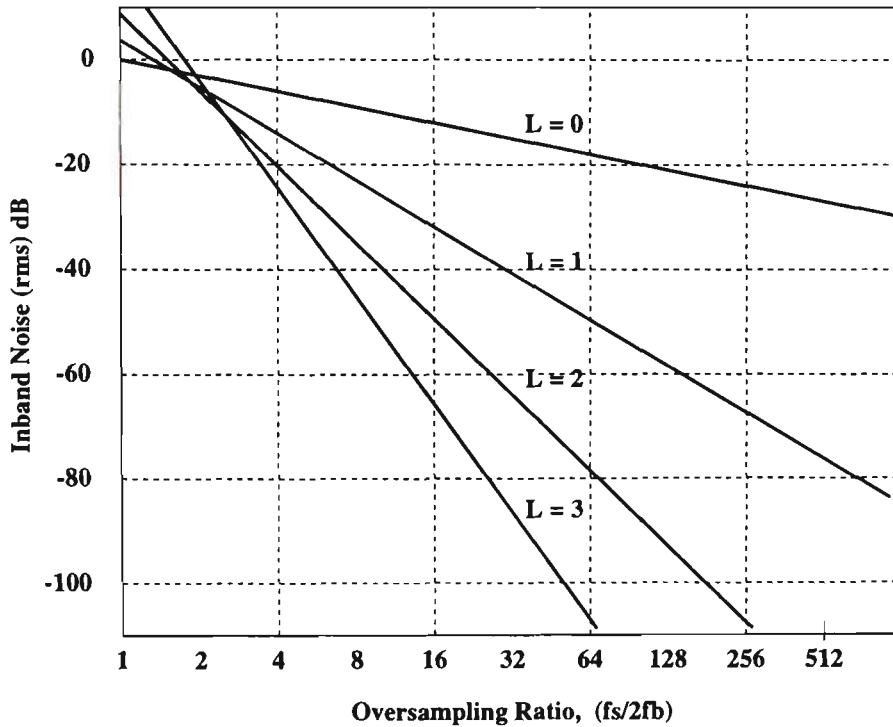


Figure 3.11: The rms noise versus oversampling ratio. $L = 0$ for the conventional ADC, and first, second, and third order $\Sigma\Delta$ quantization. Zero dB of noise corresponds to that of PCM sampled at the Nyquist rate.

3.5.2 Signal to Quantization Noise for Second Order $\Sigma\Delta$ ADC

The S/N ratio for 2nd order $\Sigma\Delta$ ADCs can be obtained using a similar process to that used for the 1st order systems (section 3.4.2). The S/N ratio for an input sine wave of input level V is:

$$S/N = \frac{V^2}{2} / \left(e_{rms}^2 \frac{\pi^4}{5} (2f_b T_s)^5 \right) \quad (3.22)$$

This reaches a maximum just prior to saturation when $V = 1$,

$$(S/N)_{max} = \frac{2.5}{e_{rms}^2 \pi^4} (2f_b T_s)^{-5} \quad (3.23)$$

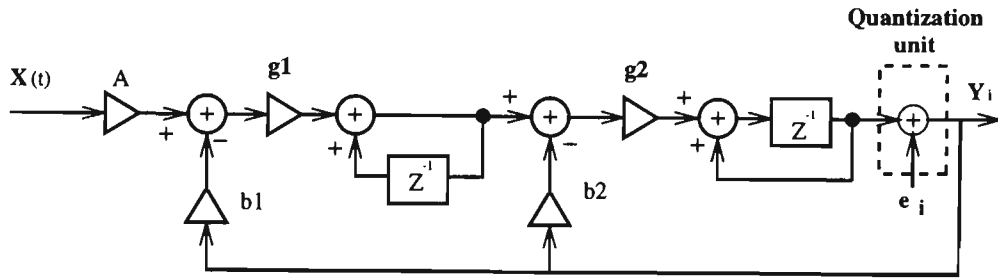


Figure 3.12: The second order digital $\Sigma\Delta$ ADC circuit with scaling coefficients.

3.5.3 Alternative 2nd Order Transfer Function

Coefficients can be added to the 2nd structure of Fig. 3.10 to control the NTF and STF. Five coefficients are shown in Fig.3.12. These coefficients can scale signals at different stages in the structure to improve the performance and control instability.

The principle of operation is similar to that of the first order $\Sigma\Delta$ ADC. The second feedback loop (through b_2) tries to track the output from the first integrator and so minimize the error signal into the second integrator. The z-domain system transfer function is derived from Fig.3.12 as:

$$Y(z) = \frac{g_1 g_2 A z^{-1}}{1 + (g_1 g_2 b_1 + g_2 b_2 - 2)z^{-1} + (1 - g_2 b_2)z^{-2}} X(z) + \frac{1 - 2z^{-1} + z^{-2}}{1 + (g_1 g_2 b_1 + g_2 b_2 - 2)z^{-1} + (1 - g_2 b_2)z^{-2}} E(z) \quad (3.24)$$

The STF is :

$$STF(z) = \frac{g_1 g_2 A z^{-1}}{1 + (g_1 g_2 b_1 + g_2 b_2 - 2)z^{-1} + (1 - g_2 b_2)z^{-2}} \quad (3.25)$$

The NTF is :

$$NTF(z) = \frac{1 - 2z^{-1} + z^{-2}}{1 + (g_1 g_2 b_1 + g_2 b_2 - 2)z^{-1} + (1 - g_2 b_2)z^{-2}} \quad (3.26)$$

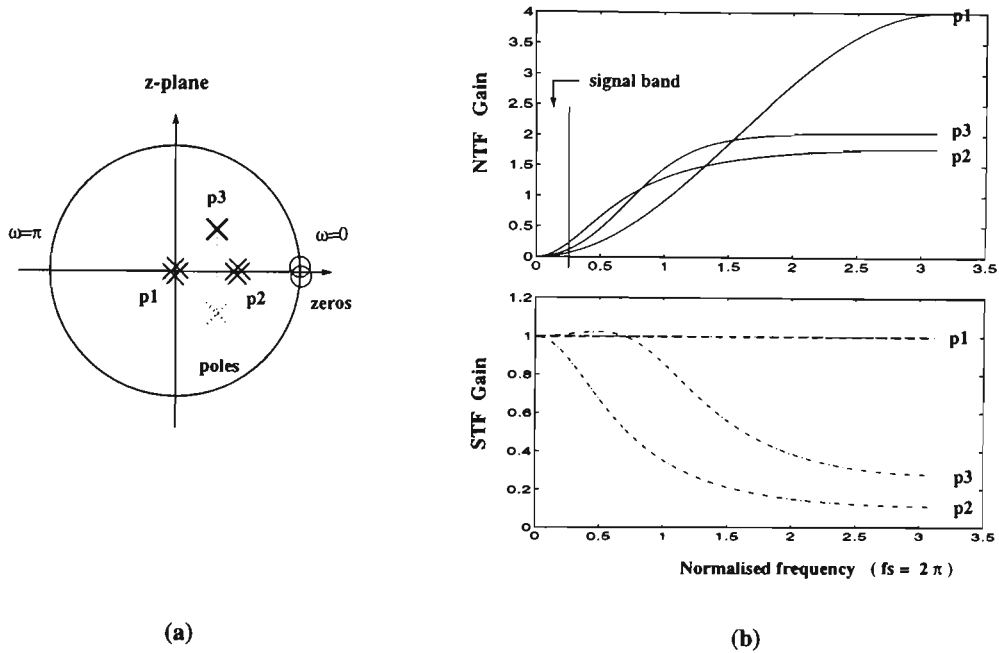


Figure 3.13: (a) The second order system description in z-plane, pole can take the value of p_1, p_2 and p_3 separately, (b) the calculated frequency response for different pole positions. (Simulated on MATLAB).

The NTF has two zeros at $z = 1$ and two poles at :

$$z_{1,2} = \frac{-v \pm \sqrt{v^2 - 4a}}{2a} \quad (3.27)$$

where $a = 1 - g_2 b_2$, and $v = g_1 g_2 b_1 + g_2 b_2 - 2$. All poles should be within the unit circle, or $|z| < 1$, for stability, otherwise they can be placed any where providing a good performance results. Fig. 3.13(b) shows the frequency response for the pole and zero positions, $p_1 = 0, p_2 = 0.5$, both with the zero angles, and $p_3 = 0.4$ with the angle of $\pi / 4$, shown in Fig. 3.13(a).

When all coefficients are equal to one, the system is the same as Fig. 3.10 and has two poles at the origin (p_1 of Fig.3.13(a)). There are many possible pole locations, but, generally speaking, the inband noise improves as the poles move further away from the zeros; however, the $|NTF|_{max}$ also increases and this can lead to instability causing noise to increase in the output. Making the $|NTF| \leq 2$ (for all frequencies) avoids instability, but this rules out the poles being positioned at the origin (p_1).

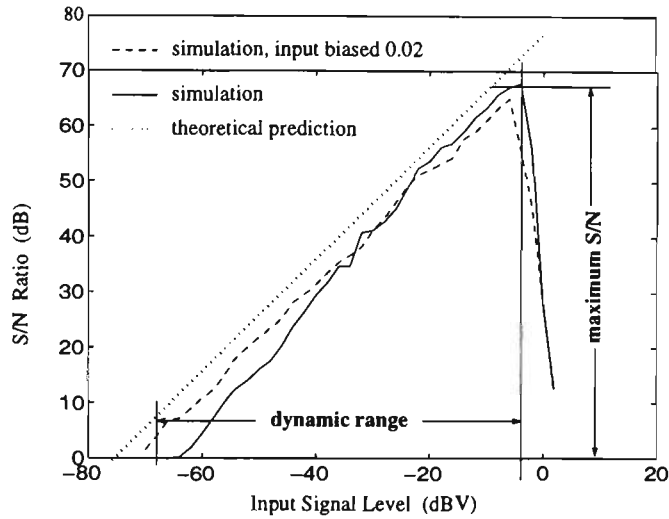


Figure 3.14: Signal to quantization noise ratio against the amplitude of applied sine waves for the second order $\Sigma\Delta$ circuit of the Fig. 3.12 ($A = 1, b_1 = 1, b_2 = 2, g_1 = 0.42$, and $g_2 = 0.83$ corresponding to pole positions being at p_2 in Fig.3.13(b)), 0 dB corresponds to an amplitude of 1 volt. Solid-line is for input signal without DC bias (based on the circuit in Fig.3.12). Dashed-line is for DC bias at 0.02 volt (based on the same circuit). The dotted-line is the theoretical prediction from Eq.(3.22). [MATLAB simulation]

Fig. 3.14 shows the S/N ratio plotted against amplitude for an input sine wave signal. The solid-line shows the simulation result. The dashed-line shows the effect of adding a 0.02V DC bias to the input signal. The dotted-line represents the theoretical result obtained from Eq.(3.22). The zero dB input level corresponds to a peak amplitude equal to 1 volt. The maximum of S/N ratio of 66dB occurs just before the saturation of the system. The dynamic range is about 64dB.

There are two reasons which may cause the difference between theoretical prediction of equation (3.22) and the simulation results. Firstly Eq.(3.22) is based on the assumption that the quantization error is equally distributed over one quantization step which is, generally true, for conventional ADCs, but it is not well suited to single bit $\Sigma\Delta$ ADC. Secondly the performance of the $\Sigma\Delta$ ADC is degraded at small input signal levels; this was probably due to limit cycles in the output. To a certain extent the problem was overcome by the addition of a DC bias signal, but this was at the expense of a slightly reduced performance at large input signal levels.

3.6 Limit Cycles (Pattern Noise)

The simulations conducted in this research showed that, low-order $\Sigma\Delta$ systems, and especially first-order systems, with 1-bit noise-shaping loops are prone to output quantization error that is deterministic or oscillatory rather than white noise-like. This manifests clearly the non-additive independent white noise character of 1-bit quantization. Under certain small amplitude signal input, the binary idling sequence at the output of $\Sigma\Delta$ modulator will exhibit a long and often complex, but repetitive, pattern. If the period of this pattern is long enough, its fundamental frequency component will lie in the audio baseband and pass through the decimator unattenuated, yielding a limit-cycle tone in the output of decimator. To relieve this, some form of dither signal can be added to the analog input. The dither tends to disrupt the long deterministic idling pattern in the $\Sigma\Delta$ output and hence prevents narrow band error power from appearing in the output [Hauser and Brodersen 1986] [Carley 1987].

The addition of a DC bias signal to the input was also found to be beneficial for many of the simulations performed in this thesis. The reason for this is not quite explainable, and needs investigation in the future.

3.7 More Complex System

Various approaches of $\Sigma\Delta$ modulator have been developed to give better noise-shaping. The following is a brief catalog:

- Single-stage with single-loop [Inose and Yasuda 1963] [Gray 1987] [Bishop *et al.* 1990] [Candy and Temes 1992] which are first order system.
- Single-stage with multi-loop [Li 1993] [Matsuya *et al.* 1987] [Chao *et al.* 1990] [Walden *et al.* 1990].
- Multi-stage with single loop [Matsuya *et al.* 1987] [Robert and Deval 1988] [Candy and Temes 1992] with a order $N \geq 2$.
- Multi-stage with multi-loop [Karema *et al.* 1990] [Candy and Temes 1992].

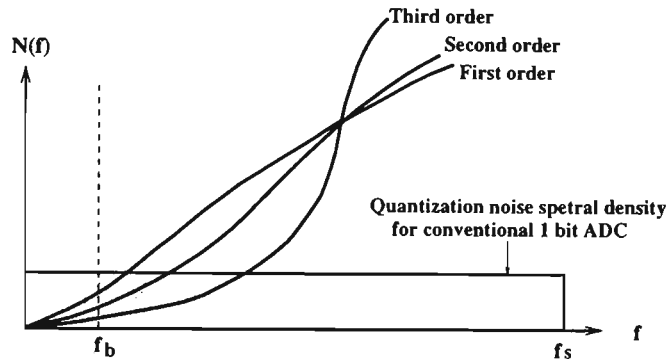


Figure 3.15: Basic concept of noise-shaping and performance of $\Sigma\Delta$ ADC for different order.

Among the above structures, some use feedback technique and others use feed forward, both with either 1-bit quantizer or a multi-bit quantizer. Researchers are continuing to look for better structures which will give improved noise shaping and reduced complexity.

3.8 Conclusion

$\Sigma\Delta$ modulators produce a pulse density output waveform. In a $\Sigma\Delta$ ADC, the quantization noise from the output waveform has a spectral null at zero frequency (in the signal band). The quantization noise outside this band can be removed by subsequent filtering. The higher the oversampling rate the more noise can be removed. The performance of $\Sigma\Delta$ ADCs can be analyzed through the pole and zero positions of the *STF* and *NTF*. The predicted results (the dotted-line in Fig.3.14) from this analysis differ from the simulation results (dashed-line in Fig.3.14) by about 6dB, which is reasonably close.

The shape of the *NTF* is determined by its order and its pole locations. Higher order systems have wider bandwidth nulls and hence better performance (Fig.3.15). The *NTF* and the oversampling rate determines the performance of the $\Sigma\Delta$ ADC (Fig.3.16). To obtain a 100dB dynamic range, a second order $\Sigma\Delta$ ADC will require an oversampling rate of about 180.

The next Chapter considers a noise tunable $\Sigma\Delta$ ADC which has the capability of nulling the quantization noise at frequencies other than DC.

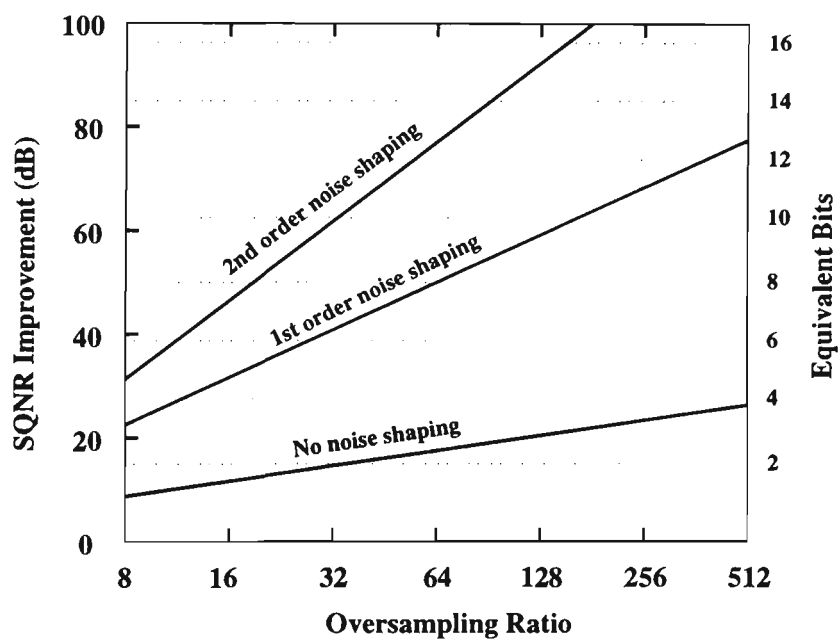


Figure 3.16: The calculated improvements in signal to quantization noise ratio through oversampling and decimating processing for single bit $\Sigma\Delta$ ADC.

Chapter 4

Design of Noise Tunable $\Sigma\Delta$ A/D Converter

Chapter 3 discussed the design of $\Sigma\Delta$ ADCs for lowpass signals and presented their performance in terms of S/N ratio and dynamic range.

This chapter discusses the design of $\Sigma\Delta$ ADCs for bandpass signals. It shows how the NTF can be modified to notch the quantization noise at different frequencies. A noise tunable $\Sigma\Delta$ ADC structure is proposed that can realize the new NTF, and its performance is investigated by pole/zero analysis.

4.1 Introduction

Oversampled $\Sigma\Delta$ ADCs have a number of benefits, these include inherent linearity, high tolerance to circuit imperfection, and only a small amount of analog circuitry is needed. The

bandpass variant of $\Sigma\Delta$ conversion should retain these advantages and offers a promising technique for the use in the developing area of digital radio as has been explained in chapter 1.

The $\Sigma\Delta$ noise shaping concept was extended to bandpass signals by [Schreier and Snelgrove 1989]. The advantage of the bandpass design is that, with a narrow-band signal, the sampling rate need only be much greater than that of the bandwidth of the signal rather than the carrier frequency. The oversampling ratio, R_b , is defined as one-half the sampling rate divided by the width of the band of interest, $R_b = f_s / (2 \cdot bw)$, where bw is the channel bandwidth. Table 4.1 compares the oversampling rate for lowpass and bandpass $\Sigma\Delta$ converters in a GSM environment. For the lowpass case, when the signal frequency increases, the oversampling ratio decreases (for fixed sampling frequency). For the bandpass case, the bandwidth of a channel is fixed, so the oversampling ratio R_b is constant. The R_b can be made quite large if $f_s \gg bw$. Fig. 4.1 shows the required performance of the new tunable bandpass $\Sigma\Delta$ ADC. It converts the whole signal band (125 channels) to digital format, but only the desired channel has the minimum quantization noise. The unwanted signals will be filtered in the following DSP unit as part of the decimation routine.

Sampling frequency f_s	Channel spacing f_{bw}	Center frequency f_c	Oversampling ratio $R_{lowpass}$	Oversampling ratio $R_{bandpass}$
52 MHz	200 kHz	200 kHz	130	130
		400 kHz	65	
		
		1000 kHz	26	
		1200 kHz	21.67	
		
		2.4 MHz	10.83	
...	...			

Table 4.1: Oversampling ratio comparison for lowpass and bandpass systems. The data is based on the GSM specification: 200kHz channel spacing and 25MHz total bandwidth.

For multichannel input signals the $\Sigma\Delta$ ADC minimizes the quantization noise at the frequency of the desired channel by appropriately adjusting the circuit parameters of the $\Sigma\Delta$ process. Channel selection is then performed in DSP unit as part of the subsequent decimation

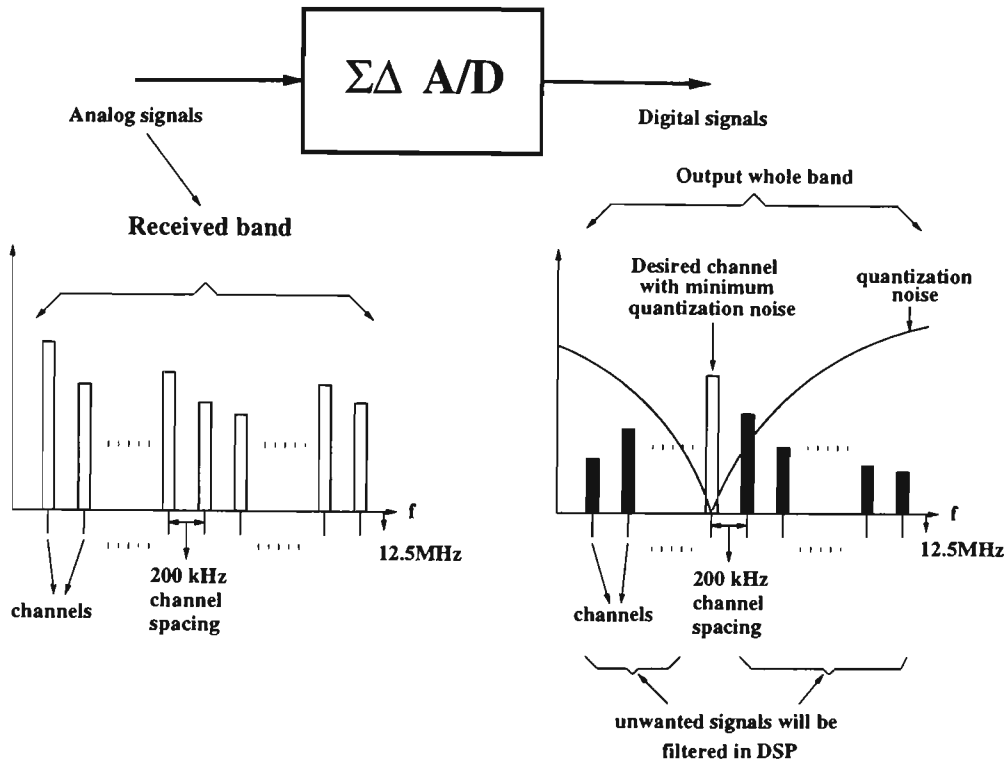


Figure 4.1: The required performance of the new tunable bandpass $\Sigma\Delta$ ADC in a GSM receiver.

process. The channel selection processes will not be considered in this thesis.

Section 4.2 discusses the design procedures including system structure, transfer function and the selection of pole positions which are linked to system stability and performance. Section 4.3 does the theoretical calculation and simulation of S/N ratios and section 4.4 discusses the feasibility of the choice of sampling frequency. Finally, section 4.5 summaries the design aspects of noise tunable $\Sigma\Delta$ A/D converters.

4.2 General Design of 2nd order tunable $\Sigma\Delta$ modulation

The key issue in the design of $\Sigma\Delta$ ADCs is the selection of the noise transfer function, since quantization noise is the most sensitive parameter. This design starts with the investigation of the NTF and STF of a bandpass $\Sigma\Delta$ modulator using pole-zero analysis. Conventional low-pass $\Sigma\Delta$ converters place the zeros of the noise transfer function at $\omega_c = 0$, as shown

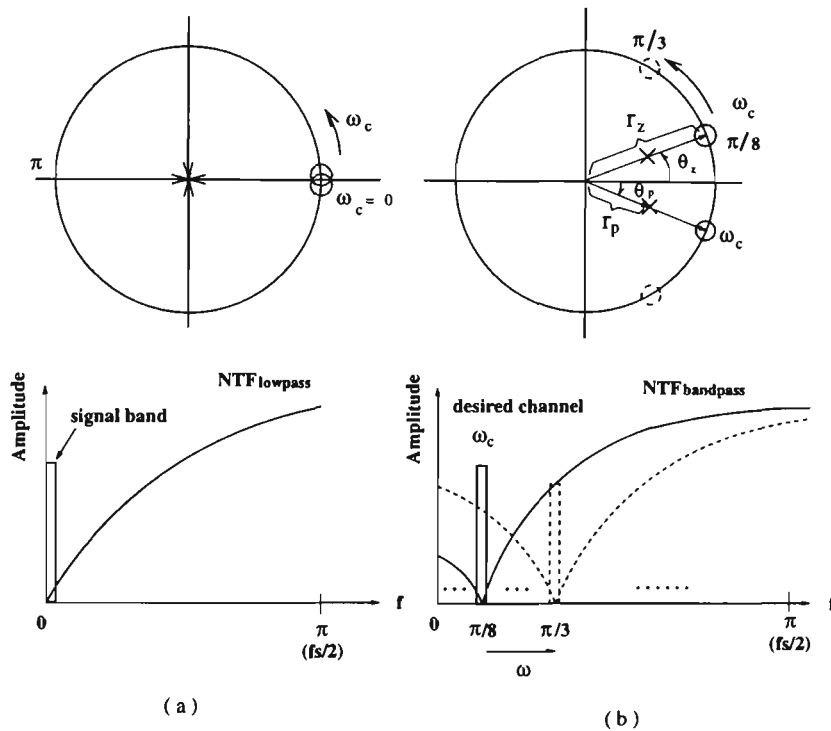


Figure 4.2: (a) NTF pole and zero placements for a 2nd order lowpass $\Sigma\Delta$ converter and (b) 2nd order bandpass $\Sigma\Delta$ converter tuned for minimum quantization noise at $\omega_c = \pi / 8$. The zero positions for channels at $\pi / 8$ and $\pi / 3$, are shown in solid-line and dashed-line respectively. In this case $\theta_p = \theta_z$ but this need not always be so.

in Fig.4.2(a). This nulls the quantization noise at DC and greatly reduces the noise level at low frequencies. Unfortunately, the quantization noise at higher frequencies increases. The bandpass $\Sigma\Delta$ modulator nulls quantization noise at a nonzero frequency, ω_c shown in Fig.4.2(b), and this gives a high signal-to-noise ratio for signals with a narrow bandwidth centered on ω_c . The placement of NTF zeros at $e^{\pm j\omega_c T_s}$, where $\omega_c T_s = \pi/8$, nulls the quantization noise at the desired channel (Fig. 4.2). Other channels can be selected by changing the $\omega_c T_s$ value (e.g $\omega_c T_s = \pi / 3$ as illustrated). The position of the poles effect the shape of the STF, the shape of the NTF null, and the stability of the system.

4.2.1 System Structure, Modeling and Transfer Function

It is a basic requirement for the bandpass $\Sigma\Delta$ modulator to null the quantization noise at the channel of interest. To do this a number of modifications to the basic lowpass structure, Fig. 3.10, were considered. The structure shown in Fig. 4.3 was eventually chosen since it

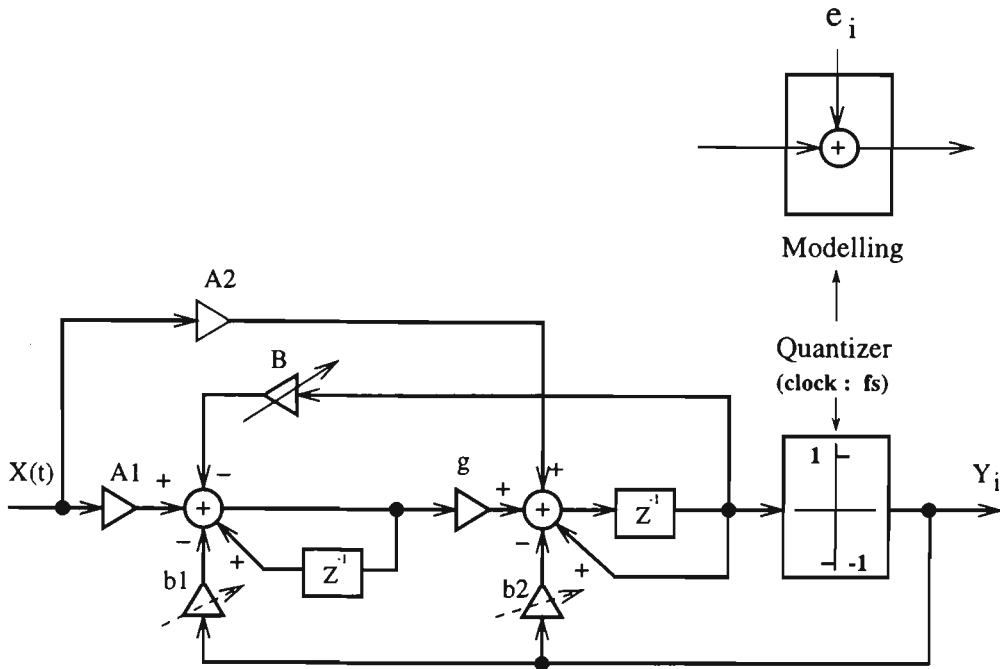


Figure 4.3: The structure of the second-order noise tunable bandpass $\Sigma\Delta$ quantizer

had the desired NTF characteristics of complex zeros on the unit circle. The STF has zeros at the origin and on the real axis. The poles for both STF and NTF are the same.

The method used to analyze the $\Sigma\Delta$ converter is to model the quantizer as an additive noise source. It is assumed that the quantization noise sequence $\{e_i\}$ in Fig.4.3 is white and uncorrelated with the quantizer input [Candy and Temes 1992], and that the input signal $x(t)$ is bandpass and oversampled. The linearized system transfer function can be obtained from the z transform-model as follows:

$$Y(z) = STF_{2b}(z) \cdot X(z) + NTF_{2b}(z) \cdot E(z) \quad (4.1)$$

where $STF_{2b}(z)$ is the signal transfer function:

$$STF_{2b}(z) = \frac{vz^{-1}(1 - \alpha z^{-1})}{1 - \phi_{d1}z^{-1} + \phi_{d2}z^{-2}} \quad (4.2)$$

and, $NTF_{2b}(z)$ is the noise transfer function:

$$NTF_{2b}(z) = \frac{1 - 2 \cos \theta_z z^{-1} + z^{-2}}{1 - \phi_{d1} z^{-1} + \phi_{d2} z^{-2}}. \quad (4.3)$$

θ_z is the angle of the zeros; the poles can be either both real or a complex conjugate pair. The following equations relate the pole-zero diagram (Fig. 4.2) to the developed structure (Fig.4.3):

$$v = gA_1 + A_2 \quad (4.4)$$

$$\alpha = \frac{A_2}{gA_1 + A_2} \quad (4.5)$$

$$2 - gB = 2 \cos \theta_z \quad (4.6)$$

$$\phi_{d1} = 2 - g(b_1 + B) - b_2 = \begin{cases} 2r_p \cos \theta_p & \text{if poles are complex} \\ -(\gamma + \eta) & \text{if poles are real} \end{cases} \quad (4.7)$$

$$\phi_{d2} = 1 - b_2 = \begin{cases} r_p^2 & \text{if poles are complex} \\ \gamma \cdot \eta & \text{if poles are real} \end{cases} \quad (4.8)$$

θ_p is the angle of the pole, r_p is the radius of the poles, and γ and η are pole positions on real axis, shown in Fig.4.4.

Equations (4.3) and (4.6) show that the coefficients, B , and g can be adjusted to make the

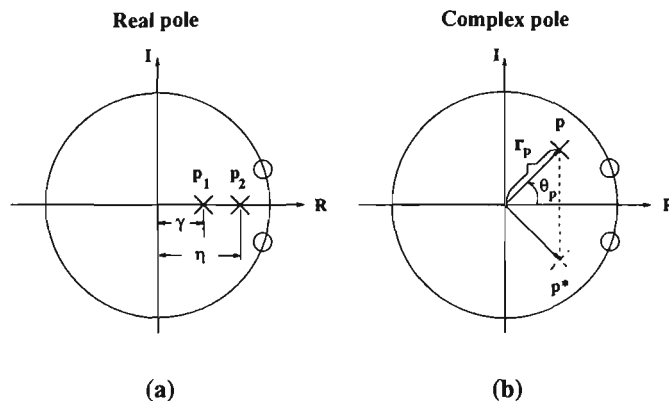


Figure 4.4: Illustration for real and complex pole positions.

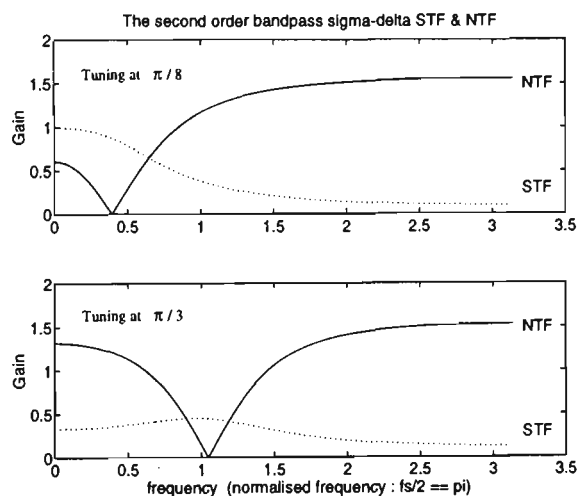


Figure 4.5: Frequency response of $STF(e^{j\omega_c T_s})$ and $NTF(e^{j\omega_c T_s})$ evaluated from equations (4.2) and (4.3), with pole and zero positions as in Fig. 4.2. The notch position are set at $\omega_c T_s = \pi/8$ and $\pi/3$.

$\Sigma\Delta$ ADC tune to the desired frequency (channel) at which the response of $NTF_{2b}(z)$ is equal to zero as shown in Fig. 4.5. The signal transfer function, $STF_{2b}(z)$, shares the same poles with the noise transfer function, $NTF_{2b}(z)$, but has zeros located on the real axis (one is at the origin). As such, this limits the amount of bandpass shaping of the $STF_{2b}(z)$'s frequency response for low-order converters. The criteria of the design is to choose a signal transfer function $STF_{2b}(z)$ which has a nearly constant gain and linear phase in the band of interest, and, if possible, a high attenuation in the out-of-band section.

Fig.4.6 shows simulation results for the bandpass $\Sigma\Delta$ converter based on the circuit of Fig.4.3 and the pole/zero location of Fig. 4.2. The simulations are for an input tone at a frequency, ω_c , the frequency where the noise is nulled. The value of the coefficient A_1 and g ,

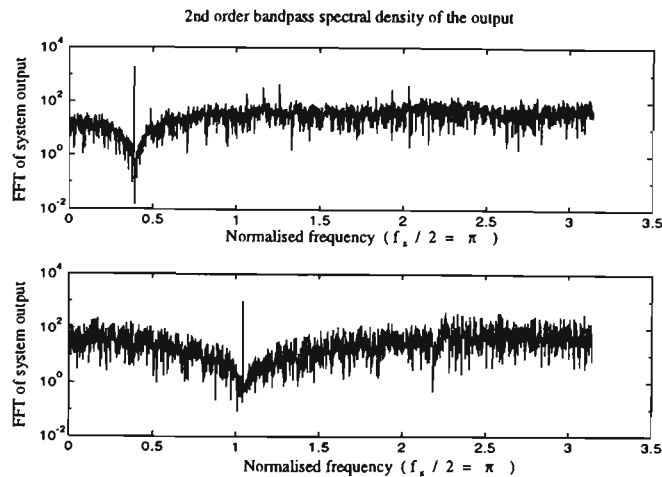


Figure 4.6: FFT of the simulated time domain output from circuit Fig. 4.3. In the MATLAB simulation, the coefficients are set to give the response of Fig. 4.5 ($A_1 = 0.5, A_2 = 0.3, g = 0.5, b_2 = 0.75, b_2 = 0.3478, B = 0.3045$ for notch position at $\pi/8$, and $b_2 = -0.5, B = 2.0$ notch position at $\pi/3$). [MATLAB simulation]

for the simulation, are both equal to 0.5, and r_p equals to 0.5, and the b_1, b_2 and B are to be calculated from Eq. (4.6), (4.7) and (4.8) for a noise null at $\omega_c = \pi/8$ and $\pi/3$ respectively.

The primary design criteria is to minimize the quantization noise energy in the bandpass signal, but this can have an adverse effect on stability. A stable system requires the quantization noise response to be less than 2 at all frequencies [Schreier and Snelgrove 1991] and all poles to lie inside the unit circle. The design method can be extended to N^{th} order ($N \geq 2$) system. The next subsection will discuss this in more detail.

4.2.2 Stability of the 2nd Order Bandpass $\Sigma\Delta$ A/D Converter

The coefficients can be designed to have arbitrary values, hence the poles can be placed anywhere on the z-plane. The location of the poles will allow, not only the design of a stable system, but also the optimization of the loop response for maximum effective resolution.

For a sampled-data system, the stability requirement dictates that the poles be placed within the unit circle. Another mechanism for instability is due to the limited dynamic input range of the quantizer, which places further constraints on the design of the noise transfer function [Ardalan and Paulos 1986] [Ardalan and Paulos 1987]. A signal at the input of

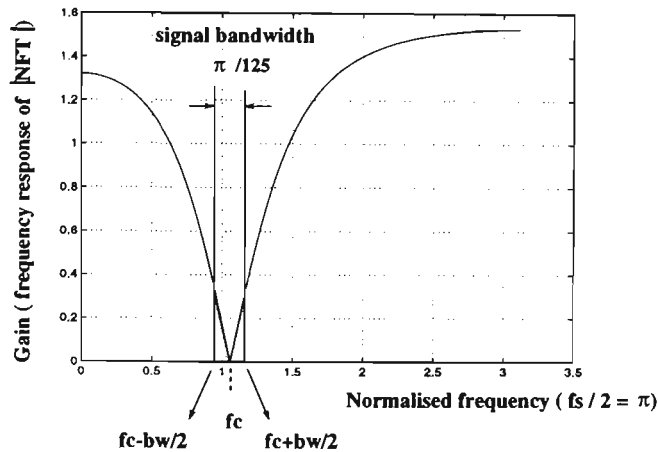


Figure 4.7: The integration region for calculating inband noise power over one channel bandwidth at the tuning point $\pi / 3$.

the quantizer, which exceeds the quantizer limits, will result in an increase in the amount of quantization noise. This excess noise circulates through the loop and can cause an even larger signal to appear at the quantizer input, eventually causing instability. Lee [Schreier and Snelgrove 1991] claimed that $|NTF_{2b}| < 2$, for all frequencies ($\omega_c T = 0$ to π) is a necessary condition for stable operation with zero input. Applying an input to the system raises signal level in the loop, hence $|NTF_{2b}|$ must actually be less than 2 for the $\Sigma\Delta$ ADC to remain stable. For the second order system, $|NTF_{2b}|$ is defined as:

$$\left| NTF_{2b} \right|_{\omega_c T_s = \{0, \pi\}} = \frac{(|z - e^{j\theta_z}|)(|z - e^{-j\theta_z}|)}{(|z - p_1|)(|z - p_2|)} < 2 \quad (4.9)$$

where $\theta_z = \omega_c T_s$. In this work the maximum value of $|NTF_{2b}|$ was limited to ≤ 1.6 to give an appropriate safety margin, as suggested by [S.Jantzi *et al.* 1991]. Eq. (4.9) was evaluated over all possible pole positions to obtain the stability boundaries $|NTF_{2b}| < 2$ and $|NTF_{2b}| \leq 1.6$ for notch frequencies of $\theta_z = \pi / 3$ and $\theta_z = \pi / 8$. Within the stability boundaries, the question of where the optimized pole positions is important to obtain the minimum inband quantization noise. Eq. (4.10) was evaluated over all possible pole positions to abstract the relative inband quantization noise trends (Fig. 4.7 is used to show the region on which the integration is performed by using Eq.(4.10)).

$$Pr_{inband_noise} = \int_{f_c - bw/2}^{f_c + bw/2} |NTF_{2b}(f)|^2 df \quad (4.10)$$

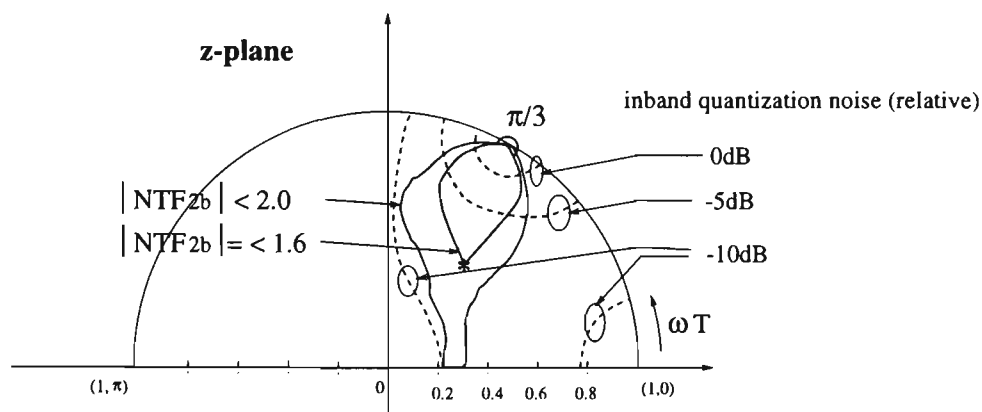


Figure 4.8: The safe zones described in z -plane for complex pole positions for $|NTF_{2b}| < 2$ and $|NTF_{2b}| \leq 1.6$. The poles are assumed complex conjugate and the noise notch point is at $\pi/3$. The lower half of the z -plane is not shown. '*' shows the optimum pole position.

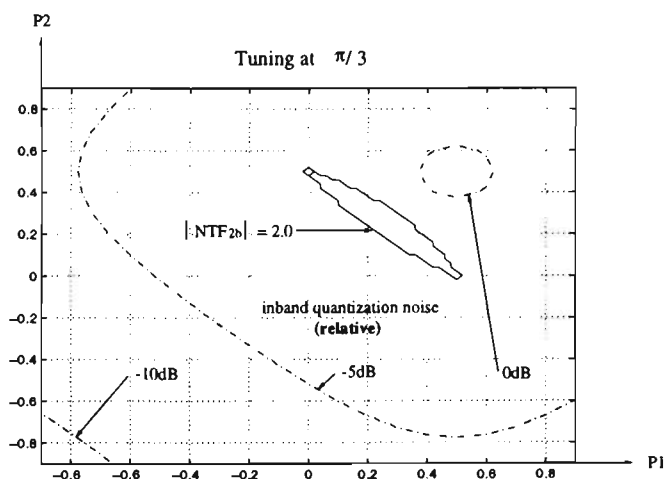


Figure 4.9: The safe zones for real pole positions of $|NTF_{2b}| \leq 2$. The poles on the real axis are located at p_1 and p_2 , shown in Fig. 4.4. The noise notch point is located at $\pi/3$. There is no safe selection of pole positions which satisfies the $|NTF_{2b}| \leq 1.6$ condition.

Figs. 4.8 and 4.9 show the regions of stability for complex and real poles, respectively, when the noise notch frequency is $\pi/3$. The shaded region, $|NTF_{2b}| \leq 1.6$, in Fig. 4.8 indicates the acceptable pole positions. In this case, real poles are not acceptable (Fig. 4.9). The dashed-lines in both Fig. 4.8 and Fig. 4.10 show the relative inband quantization noise contours for $f_s = 52\text{MHz}$ and GSM channel bandwidth, $bw = 200\text{kHz}$, for different selections of pole positions. The inband noise rapidly increases as the pole position moves closer to the zero. The optimum pole position within the stability region ($|NTF_{2b}| < 1.6$) can be obtained and is marked with an '*'.

Fig. 4.10 and Fig. 4.11 show the acceptable stability region and noise contours for a notch

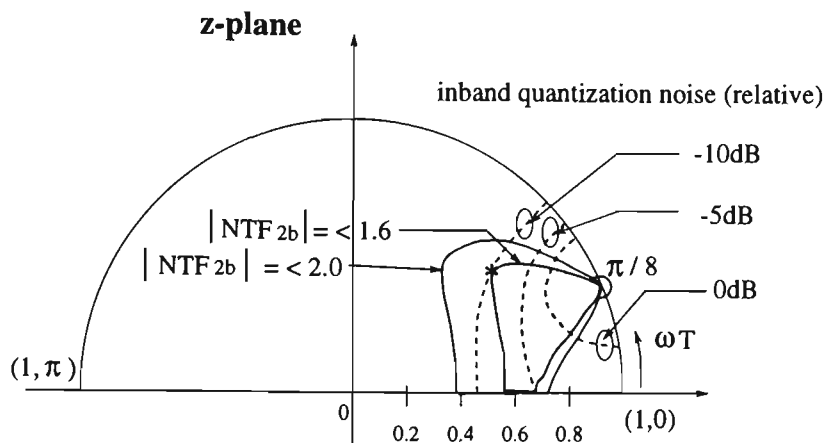


Figure 4.10: The safe zones for complex pole positions of $|NTF_{2b}| < 2$ and $|NTF_{2b}| \leq 1.6$. The poles are complex conjugates and the noise notch point is located at $\pi/8$. '*' shows the optimum pole position.

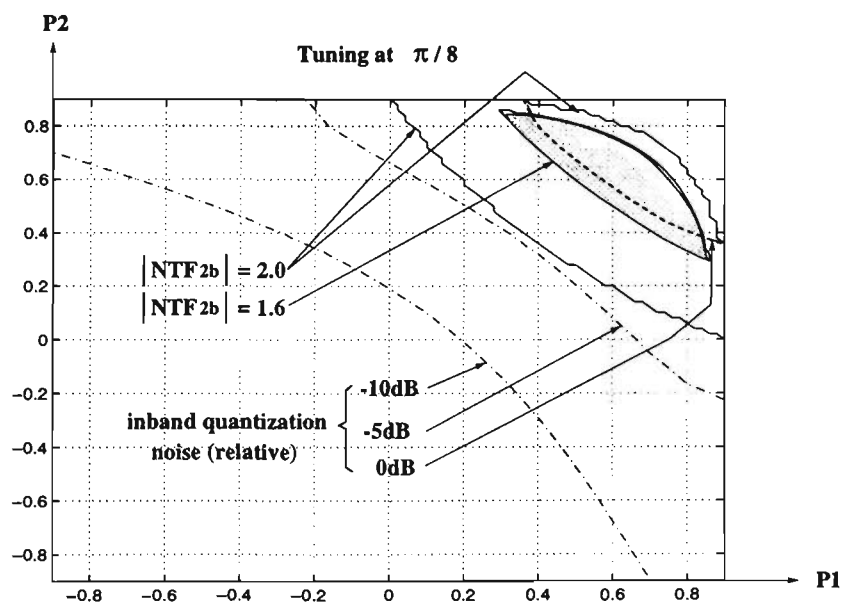


Figure 4.11: The safe zones for real pole positions of $|NTF_{2b}| \leq 2$ and $|NTF_{2b}| \leq 1.6$. The poles on the real axis are located at p_1 and p_2 , shown in Fig. 4.4. The noise notch point is located at $\pi/8$.

frequency of $\pi/8$. In this case the poles can be either complex or real, however, complex poles still produce the lowest inband noise. The range of possible pole positions can be extended if a small increase in inband noise can be tolerated. This allows the coefficients to take on a range of values, reducing the implementation problem. In this chapter the r_p was fixed at 0.6 and θ_p was set equal to θ_z , this gave a noise performance near optimum for both cases.

The next section discusses the effect of the pole positions on the shape of the NTF_{2b} .

4.2.3 The Shape of the NTF

The previous section showed that the pole positions affected the quantization noise as illustrated by the noise contours from Figs. 4.8 to 4.11. This is caused by changing shape of the NTF_{2b} and is illustrated in the next three diagrams where NTF_{2b} curves are plotted for different pole radii, r_p , and for three values of θ_p , these being $\theta_p = \theta_z$, $\theta_p > \theta_z$, and $\theta_p < \theta_z$ (Fig. 4.14).

For the case of $\theta_p = \theta_z$ (Fig. 4.12), the NTF_{2b} is almost symmetrical close to the noise null. As r_p reduces in magnitude, the 'V' opens out (reducing inband noise) but the peak noise power increases and so causes problems with stability. The choice of $r_p = 0.6$ corresponds closely to optimum of inband noise performance and system stability.

Similar effects occur when $\theta_p > \theta_z$ (Fig. 4.13) but the 'V' is no longer symmetrical and peaking occurs close to θ_p , for large pole radii. The peaking can cause the stability bound to be violated. In this case, no value of r_p is acceptable. In addition to this, peaking close to the wanted band can increase the requirements on the following decimation filters.

Finally, the condition $\theta_p < \theta_z$ (Fig. 4.14) produces peaking on the other side of the noise null. The peaking occurs at large r_p values which is similar to the previous case. Peaking can be avoided by keeping the poles away from the unit circle boundary and hidden behind the zeros ($\theta_p \doteq \theta_z$). The choice of $r_p = 0.6$ and $\theta_p = \theta_z$ is close to optimum of inband noise performance and system stability, and agrees with Fig. 4.8.

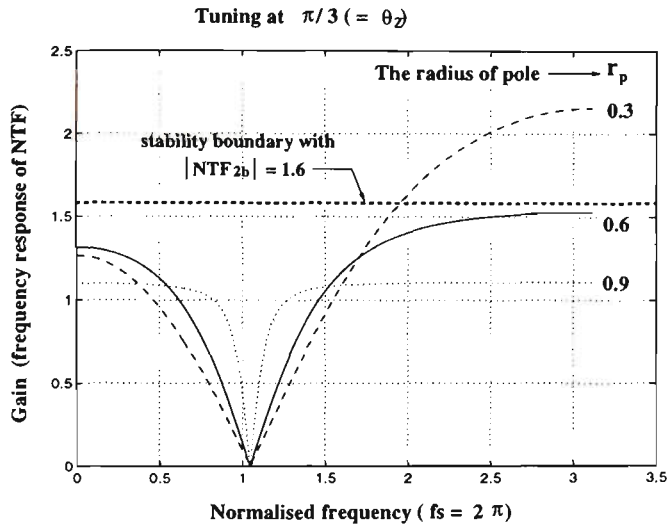


Figure 4.12: The effect of varying r_p in the NTF, while keeping the tuning point (desired channel) at $\pi/3$ and the $\theta_p = \theta_z$.

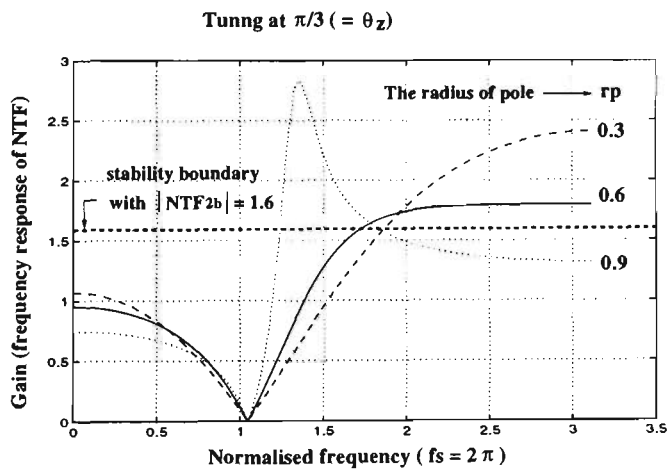


Figure 4.13: The effect of varying r_p in the NTF with $\theta_p > \theta_z$. ($\theta_p = \theta_z + \pi/12$).

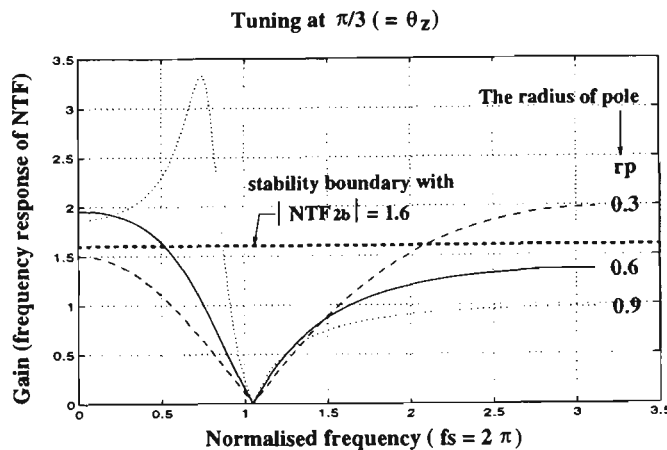


Figure 4.14: The effect of varying r_p in the NTF with $\theta_p < \theta_z$. ($\theta_p = \theta_z - \pi/12$)

4.3 Quantization Noise and SNR

The NTF_{2b} of the previous sections describes the noise gain of the system. To obtain the SNR some assumptions must be made about the quantizer error. Following [Candy and Temes 1992], the error is assumed white and uniformly distributed across the ± 1 amplitude range. Hence, the mean noise power, $e_{rms}^2 = 1/3$ and the noise power spectral density $E(f_s) = 2T_s e_{rms}^2 = (1/3)/(f_s/2)$, giving

$$SNR = \frac{a^2/2 \left| STF_{2b}(f_c) \right|^2}{\int_{f_c-bw/2}^{f_c+bw/2} \left| NTF_{2b}(f) \right|^2 E(f_s) df} \quad (4.11)$$

where a is the magnitude of the input signal. Eq. (4.11) produces the straight line plotted in Fig. 4.15 (next page) for the same conditions as in Fig. 4.7 (notch frequency at $\theta_z = \pi/3$, the sampling rate $f_s = 52MHz$ and a 200kHz channel bandwidth).

Time domain simulations were performed to verify the predicted SNR performance of the bandpass $\Sigma\Delta$ A/D. Fig. 4.16 shows a FFT plot of the output for two different input signal levels. Only the part of the frequency axis close to the signal frequency is shown (zoom view). The noise floor is significantly higher for the smaller signal due to weaker noise shaping effectiveness. This is a common phenomena in $\Sigma\Delta$ modulators and occurs when the input signal is low. It is called the *pattern noise* [Candy and Temes 1992]. The problem was overcome in the lowpass $\Sigma\Delta$ case by adding a high frequency dither signal to the input [Candy and Temes 1992]. In the bandpass $\Sigma\Delta$ case, a DC signal was found to be sufficient to counter the problem.

The plot of SNR vs input signal level for the simulated system follows the predicted performance line reasonably well (Fig. 4.15). The abrupt reduction in SNR for input signal above 1 V is caused by output saturation of the quantizer.

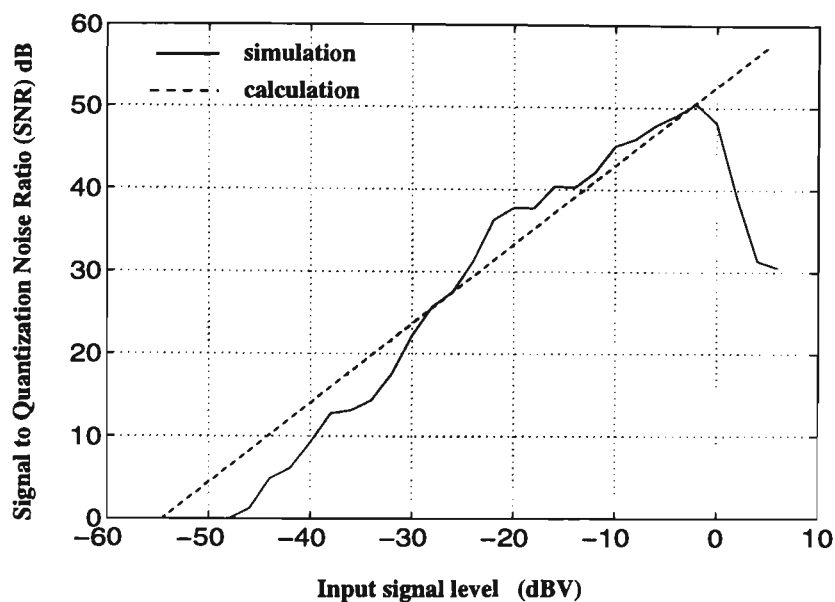


Figure 4.15: A graph of SNR plotted against the amplitude of the input signal sine wave; 0dB corresponds to an amplitude of 1 unit (1 V = 1 unit). The model in Fig. 4.3 is used in simulation and parameters are : $A_1 = 0.6, A_2 = 0.2, r_p = 0.6, g = 0.5, b_1 = -0.48, b_2 = 0.64$ and $B = 2.0$, with tuning point at frequency of $\pi / 3$. The dashed-line shows the graph of Eq. (4.11) and solid-line is for the simulation (based on the circuit in Fig.4.3). DC offset for simulation is 0.16 V. [MATLAB simulation]

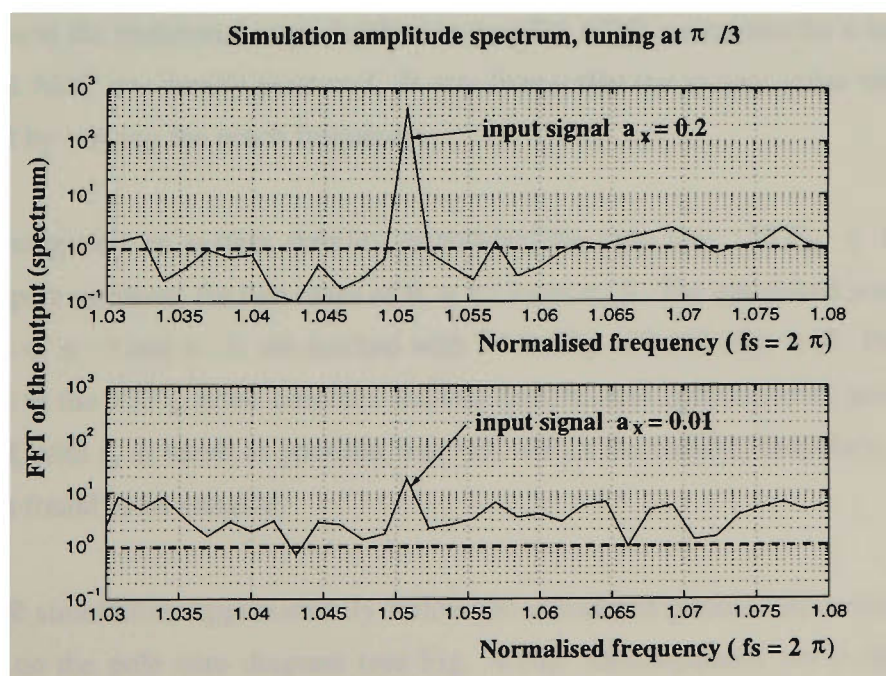


Figure 4.16: The output spectrum of the tunable bandpass $\Sigma\Delta$ converter tuning at $\pi / 3$, with the sine wave input signal amplitudes a_x of, (a) 0.2 and (b) 0.01. [MATLAB simulation]

4.4 A Note on Sample Rate

In the above simulations the sample rate was chosen as 52MHz in order to accommodate, with a reasonable safety margin, the 12.5MHz baseband bandwidth of the GSM system. (the GSM RF bandwidth is 25MHz but this reduces by half after quadrature down-conversion). From an implementation viewpoint, 52MHz might be considered a bit high, with many of the early implementations specifying frequencies in the range 1.024MHz to 15MHz [Friedman 1989], [Carley 1989], [Koch *et al.* 1986]. More recently $\Sigma\Delta$ DACs used in CD players have sampling rates of between 33MHz and 45MHz [Curtis 1991] and research trends indicate even higher sample rates through simulation studies (52.224MHz by Aziz [P. M. Aziz and Spiegel 1994]). In conclusion, sample rates of this frequency should be possible, if not now, then in the very near future, with the steady improvement in VLSI technology.

4.5 Conclusion

This chapter discussed the design of noise tunable bandpass $\Sigma\Delta$ ADC. After a number of modifications to the traditional second order lowpass $\Sigma\Delta$ ADC, a structure for a noise tunable bandpass $\Sigma\Delta$ ADC was finally produced. It was shown that the system noise null positions can be tuned by varying the notch frequency.

The investigation on system stability established the safe zone ($NTF_{2b} \leq 1.6$) for the selection of pole positions for two cases of $\theta_z = \pi/3$ and $\pi/8$. The optimized pole positions, for the cases of $\pi/3$ and $\pi/8$, are marked with '*' in Fig. 4.8 and Fig. 4.10. Further study on the shape of the NTF_{2b} noise contours showed that the near optimum pole positions were when $\theta_p = \theta_z$ with r_p as small as possible, but, still within the stability boundary. A value of $r_p = 0.6$ was found to be suitable.

The SNR simulations approximately follow the calculated prediction (maximum error < 6dB) based on the pole zero diagram (see Fig. 4.10). Discrepancies are probably due to the wrong assumption of a uniform distribution of the error signal in the prediction equation. For a second order noise tunable $\Sigma\Delta$ ADC, SNR was about 50dB (equivalent to 8 bits). It is

believed that the performance of the system can be improved by extending the system to a N^{th} order ($N > 2$).

52 MHz sample rate is assumed in the simulations to meet the GSM bandwidth requirement. The author believes that current development in silicon technology will allow a sample rate of more than 50 MHz sample rate to be achieved in the near future, if not now.

The next chapter will consider some implementation issues associated with the coefficients.

Chapter 5

Tuning Sensitivity Analysis

In the first section of this chapter, the values of the coefficients are calculated for the full A/D tuning range (0 to π). This will give an indication of the required spread in coefficient values needed for implementation. Only the range between 0 and $\pi / 2$ is needed to fulfill the GSM specification. In section 5.2, the sensitivity of the inband quantization noise to adjustment tolerance of the coefficients is evaluated for a channel at either end of the required tuning range ($\pi / 32$ and $\pi / 2$). It is shown that one of the coefficients (B) is particularly sensitive to adjustment error at the higher channel frequencies. This could cause a problem in VLSI implementation (section 5.3).

5.1 Coefficient Adjustment Range

Section (4.2.1) indicated that the coefficients g and B control the positions of the zeros and hence the frequency at which the noise is nulled. In this analysis g will be assumed to be fixed and the angle of the poles set to the angle of the zeros (see Fig. 4.2). B, b_1 and b_2 are

calculated from the following equations which were derived from (4.6) to (4.8).

$$b_1 = \frac{1 - r_p}{g}(2 \cos \theta_p - 1 - r_p) \quad (5.1)$$

$$b_2 = 1 - r_p^2 \quad (5.2)$$

$$B = \frac{2}{g}(1 - \cos \theta_z) \quad (5.3)$$

$\theta_z (= \theta_p)$ is evaluated with a step size of $\pi / 128$, which is the required channel bandwidth, and g is set to a value of 0.5 (Fig. 5.1). When tuning is between 0 to $\pi / 2$, the range of the coefficient B is from 0 to 4, b_1 is from 0.32 to -1.28, and b_2 is constant at 0.64. The pole radius is 0.6, as suggested in the previous chapter. The required change in coefficient to move the noise null frequency by one channel, $\partial(\text{coefficient}) / \partial \text{channel}$, varies from 0.0012 to 0.0967 for B and -0.0005 to -0.0387 for b_2 . Expressing these figures as a percentage of the maximum coefficient value gives:

$$\begin{aligned} \frac{\partial B}{\partial \text{channel}} &= 0.12\% \text{ to } 9.67\% \\ \frac{\partial b_1}{\partial \text{channel}} &= -0.05\% \text{ to } -3.87\% \end{aligned}$$

Fig. 5.1 shows that channels, with numbers under 20 or above 110, are likely to be more sensitive to coefficient accuracy than the channels in the 20 to 110 range. At first sight, the implementation of adjustments that are this fine (0.12 % for B) could be difficult in VLSI. However, some relaxation might be possible, if some increase in inband noise is acceptable. The next section will look at the sensitivity of the inband noise to the adjustment error in the coefficients.

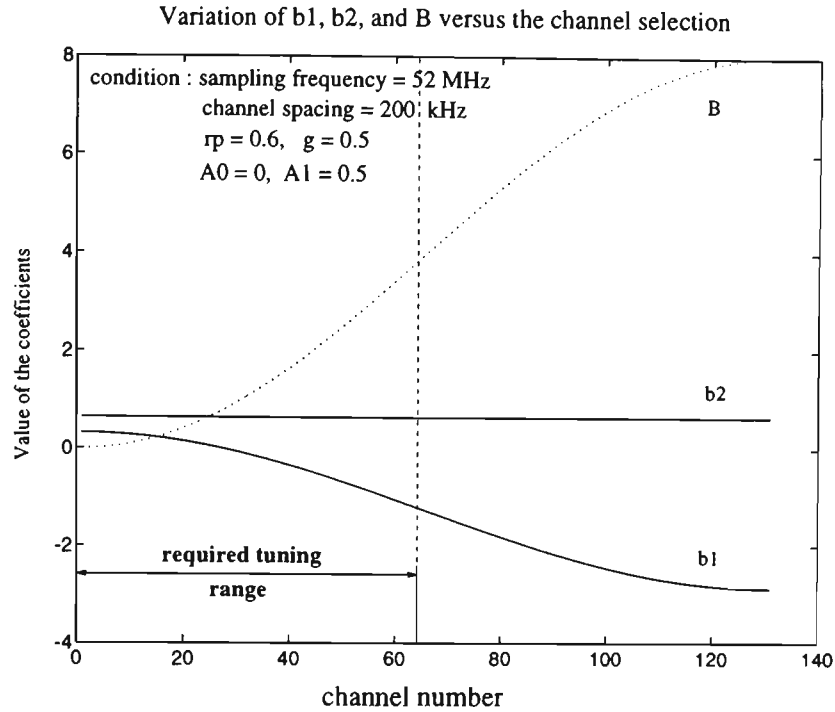


Figure 5.1: Coefficient value versus channel selection for a 2nd order noise tunable bandpass $\Sigma\Delta$ converter.

5.2 Noise Tuning Sensitivity

Because of the inaccuracy of the coefficients b_1 , b_2 and B , shown in Fig. 4.3, noise tuning can not be done exactly. It is expected, this will cause an increase in inband noise as shown in Fig. 5.2. The question of noise sensitivity to coefficient inaccuracy is important. The increase in noise will give some indication to the amount of over-design necessary to meet the system sensitivity requirement. The influence of each individual coefficient on the NTF is shown in Fig. 5.3. It is shown that B affects both the tuning point and the shape of the NTF_{2b} , while b_1 and b_2 only affect the shape of the NTF_{2b} . The inband noise, $N_{inband-2b}$, can be calculated from the NTF_{2b} (the denominator of Eq. (4.11)) by:

$$N_{inband-2b} = \int_{f_c - bw/2}^{f_c + bw/2} |NTF_{2b}(e^{j\omega T_s})|^2 \cdot E(f) \cdot df \quad (5.4)$$

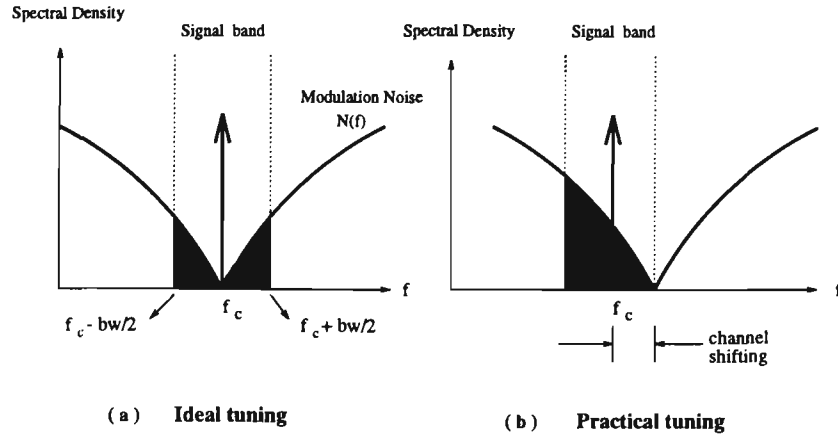


Figure 5.2: The shadowed areas represent noise power, (a) ideal tuning (tone sitting in the null position), (b) practical tuning, where coefficient errors produce a null offset.

$E(f)$ is the noise power spectral density. Assuming the quantization noise from the ADC is white [Bennett 1948] and making $E(f) = 2e_{rms}^2 / f_s$ a constant, Eq. 5.4 becomes

$$N_{inband_2b} = \frac{2e_{rms}^2}{f_s} \int_{f_c - bw/2}^{f_c + bw/2} |NTF'_{2b}(e^{j\omega T_s})|^2 \cdot df \quad (5.5)$$

Because of the inaccuracy in the circuit parameters, in-band noise power will be increased to N'_{inband_2b} , due to change in the noise shaping function of $NTF'_{2b}(e^{j\omega T_s})$:

$$N'_{inband_2b} = \frac{2e_{rms}^2}{f_s} \int_{f_c - bw/2}^{f_c + bw/2} |NTF'_{2b}(e^{j\omega T_s})|^2 \cdot df \quad (5.6)$$

To examine the influence of each b_1 , b_2 and B on the in-band noise power of the second-order bandpass $\Sigma\Delta$ converter, the following four equations, derived from Eqn.(5.5), are used:

$$\frac{\partial N_{inband_2b}}{\partial b_1} = \frac{2e_{rms}^2}{f_s} \int_{f_c - bw/2}^{f_c + bw/2} \frac{\partial(|NTF'_{2b}(e^{j\omega T_s})|^2)}{\partial b_1} \cdot df \quad (5.7)$$

$$\frac{\partial N_{inband_2b}}{\partial b_2} = \frac{2e_{rms}^2}{f_s} \int_{f_c - bw/2}^{f_c + bw/2} \frac{\partial(|NTF'_{2b}(e^{j\omega T_s})|^2)}{\partial b_2} \cdot df \quad (5.8)$$

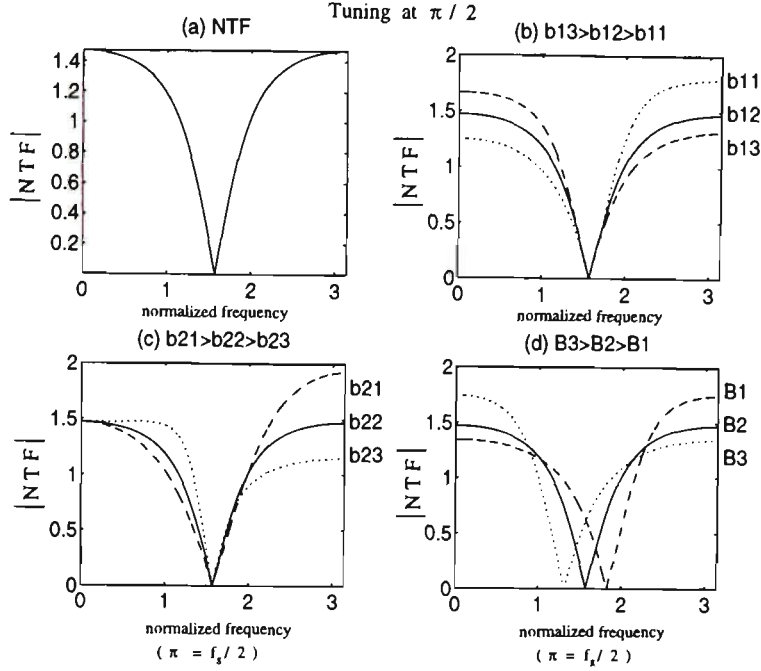


Figure 5.3: Normalized frequency on the X axes ($\pi = 26\text{MHz}$), the gain of NTF is on the Y axes. (a) tuning at $\pi / 2$, (b) the effect of changing b_1 , (c) b_2 and (d) B .

$$\frac{\partial N_{inband_2b}}{\partial B} = \frac{2e_{rms}^2}{f_s} \int_{f_c - bw/2}^{f_c + bw/2} \frac{\partial (|NTF_{2b}(e^{j\omega T_s})|^2)}{\partial B} \cdot df \quad (5.9)$$

To simplify the calculation, Fig. 5.2 can be used. The shadow area in Fig.5.2 (a) represents the noise power in an ideal tuning case and Fig. 5.2 (b) represents tuning in a practical situation. The ratio of in-band quantization noise power (shadowed area) in (b), P_{inc} , over that in (a), P_{org} , can be used to describe the sensitivity of channel selection to the tolerance of the coefficients.

Two examples, tuning at $\pi / 32$ and $\pi / 2$, are shown in Fig. 5.4. In-band noise is less sensitive to coefficients b_1 and b_2 than to B . The higher the tuned frequency, the more in-band noise power is generated for the same amount of error in coefficients B and b_2 . One separate example, shown in Fig. 5.4(d), has shown that with 10 % inaccuracy in B , there will be about 22 dB in-band noise increase for a channel at $\pi / 2$, and 2dB increase for a channel at $\pi / 32$. The increase in sensitivity at higher channel frequencies can be offset by over-designing the system, using a more complex (higher order) converter to give a large noise tolerance or by accurately controlling the coefficient value. This could involve some optimization feedback circuit. It is interesting to note that increasing b_1 and b_2 reduces the

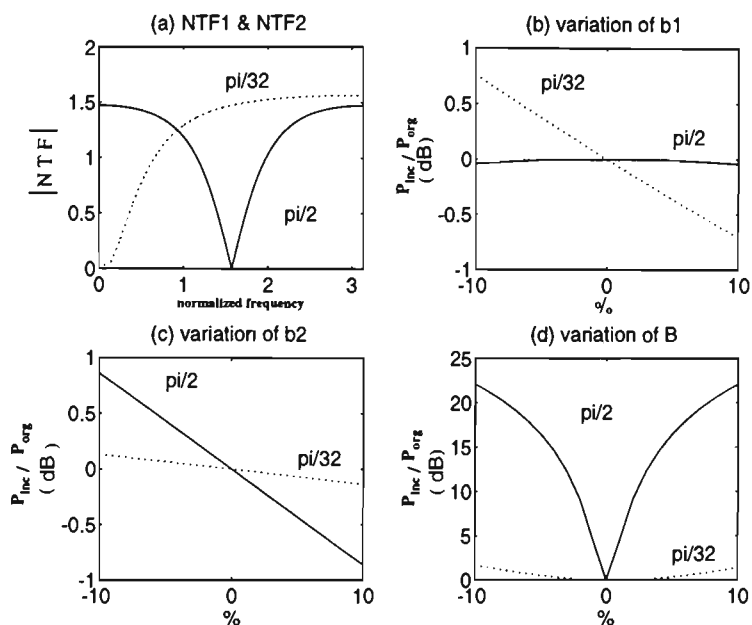


Figure 5.4: The inaccuracy of each coefficients, b_1 , b_2 and B , causes tuning off-set and the increase of in-band noise, (a) NTF for tuning at $\pi/32$ (dotted line) and $\pi/2$ (solid line) vs normalized frequency ($2\pi = 52$ MHz on the X axes, the gain of NTF is on the Y axes.), (b) change of in-band noise (P_{inc}/P_{org} , where P_{org} is the noise power with ideal value) vs % change in coefficient b_1 , (c) vs coefficient b_2 , (d) vs coefficient B .

inband noise. These coefficients control the pole positions which also determines the stability of the system. Stability therefore determines the upper limit on these coefficients.

5.3 A Note on Implementation

Traditionally, $\Sigma\Delta$ ADC are implemented in VLSI using switched capacitors of different values (areas). If the same technology is to be used for noise tunable bandpass $\Sigma\Delta$ ADCs, then at least two of the coefficients must be adjusted. One of the coefficients, B , is very sensitive and requires non-linear adjustments. A new value of B will be required for each channel selected (63 channels needed for the GSM system). To do this by switching in different on-chip capacitor banks would be difficult, because, the non-linear adjustment range, combined with the minimum feature size requirement of the process, would result in large capacitor areas and slow the speed of the system [Norsworthy *et al.* 1989]. Therefore, the traditional approach to implementation is unlikely to work.

Possible solutions to this problem need further investigations. This may require the use of external (higher precision) components, the inclusion of a high speed bipolar process (e.g. BiCOMS processes) and perhaps the inclusion of an adaptive adjustment scheme for B (the adaption would seek to minimize the inband noise after channel selection by the decimation filters).

5.4 Conclusion

The above discussion has shown that the design of noise tunable bandpass $\Sigma\Delta$ ADC is more complicated than that of lowpass $\Sigma\Delta$ ADCs, because the accuracy requirements in the tuning coefficients B and b_1 . Small variations in coefficient, B , changes (offsets) the noise null frequency, leading to a rapid increase in inband noise (a 1% variation causes approximately 3dB more noise). In the lowpass case there is no tuning, therefore, inaccuracy in the coefficients has only minor effect on NTF_{2b} . The advantages that the lowpass $\Sigma\Delta$ system has, such as 'high tolerance to circuit imperfection', is only partially correct for the noise tunable $\Sigma\Delta$ ADC.

The problems associated with coefficient sensitivity are likely to rule out traditional $\Sigma\Delta$ CMOS implementation techniques. Alternative techniques will need to be found.

The next chapter considers problems that are related to the radio application, namely the effect of large out-of-band signals on the conversion performance of the desired channel.

Chapter 6

Intermodulation and Adjacent Channel Interference

In this chapter, the effect of the expected multichannel input signal on the performance of the noise tunable bandpass $\Sigma\Delta$ ADC is discussed. The $\Sigma\Delta$ ADC converts the whole input band (many channels), although, only the desired channel has a low quantization noise. The unwanted channels can effect the desired channel if intermodulation distortion is present in the system. In this chapter the intermodulation and blocking performance of a $\Sigma\Delta$ ADC is evaluated in the presence of strong interference signals located in adjacent channels.

6.1 Adjacent Channel Interference (ACI)

A 2nd order noise tunable $\Sigma\Delta$ ADC working in an ideal environment, does not experience intermodulation distortion until the output signal level exceeds 1 unit when saturation occurs. The output bit-stream, which has the value ± 1 , can not track the output signal above 1 unit.

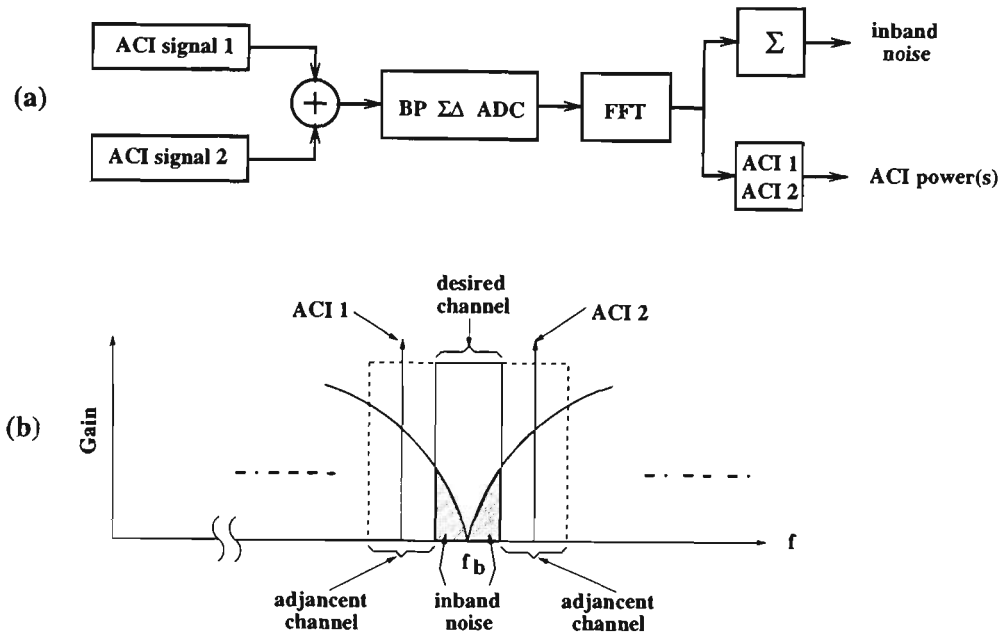


Figure 6.1: (a) Model for simulating adjacent channel interference on desired channel; (b) The frequency domain illustration shows the calculation for inband noise.

Output saturation can be caused by the desired signal (Fig. 4.15) or by any of the other input signals that are large enough. Fig.6.1(a) shows the necessary procedures for simulating the adjacent channel interferences on the desired channel and Fig.6.1(b) shows the frequency domain. When an out-of-band input signal causes saturation, the noise shaping of the $\Sigma\Delta$ ceases to work, and the desired channel inband noise rises. This is shown by the solid line in Fig. 6.2. The figure plots the noise level of the desired channel against the input level of a signal in the adjacent channel. The noise performance is unaffected by the adjacent channel (the system is linear) until output saturation is reached. The noise then rises rapidly. In a multichannel radio environment, this increase of inband noise can totally swamp a weak desired signal, leading to receiver blocking.

In a practical implementation, saturation is not limited to the output. Saturation of intermediate stages, such as the integrator amplifiers can occur. The next section discusses this effect.

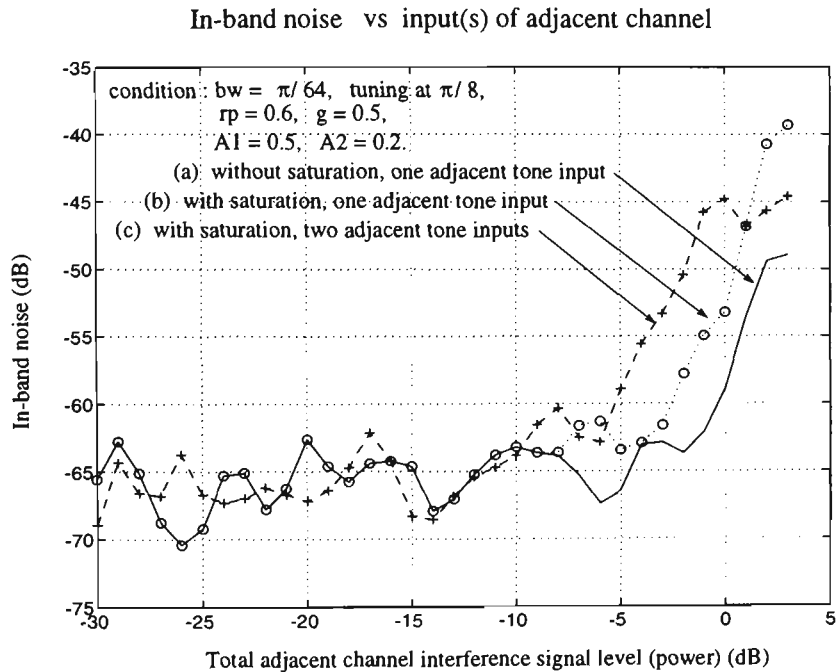


Figure 6.2: Dynamic range of 2nd order tunable bandpass $\Sigma\Delta$ ADC, (a) with one adjacent channel input, working with no saturation unit, (b) with saturation unit (setting limitation from 1 to -1) and (c) with saturation unit and two adjacent inputs. 0dB corresponds to the power of input signal with amplitude of 1 volt. [MATLAB simulation]

6.2 Intermodulation

In the mobile communication environment, the $\Sigma\Delta$ ADC responds to a whole range of multichannel signals. The overload of the system at the input side (input signals adding up at a certain point in time) can drive the input stages (prior to the comparator) of the system into saturation causing intermodulation noise in the desired channel. The increased noise affects the dynamic range and degrades the system performance. Sometimes, it is possible to attenuate many of the out-band signals by prefiltering (prior to the ADC). But in this application, too much prefiltering self defeats the object of the project since selectivity is to be provided in the DSP unit. Adjacent channel interference is therefore still a problem, particularly, if it is much stronger than the desired signal.

To simulate the effect of intermediate stage saturation, the structure shown in Fig.6.3 is chosen. The limiter (drawn in dotted-line) is used to represent the saturation. The maximum amplitude for the limitation is governed by the manufacture of the IC circuit but in this case set to 1 unit, the same as the output quantizer. The simulation process used in this chapter,

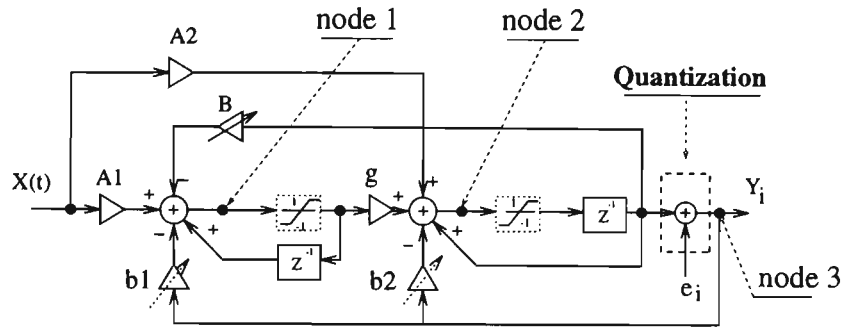


Figure 6.3: The noise tunable 2nd order bandpass $\Sigma\Delta$ A/D converter system with saturation units(dotted-line box) used to investigate the effects of inter-modulation noise on in-band signals.

as shown in Fig.6.1, calculates the noise in the desired channel while gradually increasing the amplitude of an interfering signal in the adjacent channel. The variation of in-band noise level is plotted against the level of the adjacent interference signal. In Fig.6.2 the solid-line (a) represents the simulation result without the intermediate stage limiters (ideal case), the dotted line (b) represents that with the intermediate stage limiters (practical case) and the dashed line (c) shows the effect of two adjacent channel inputs with intermediate stage limiters.

Intermodulation effects, produced by saturation of the output, cause the steep increase in noise level of the desired channel when the input signal exceeds 0dBV. Saturation of the intermediate stages causes a reduction of 2.5dB in the onset of intermodulation noise. This reduction gets larger as the number of interfering signals increase. There is about 3dB (power) degradation in the dynamic range for each out-of-band signal added to system. The interference strength also varies according to the setting of the saturation level. The higher the limit, the weaker the interference.

6.3 Intermediate Stage Transfer Function

Traditional methods used minimize the effects of inter-modulation noise are the scaling of the signal levels to avoid saturation after the summing nodes. Fig.6.4 shows that the magnitudes of the partial signal transfer functions from the input of the system to each internal node (node 1 and node 2) are always less than or equal to the output signal transfer function (at node 3) for frequencies below 1.3 (normalized frequency, $f_s = 2\pi$). Signals

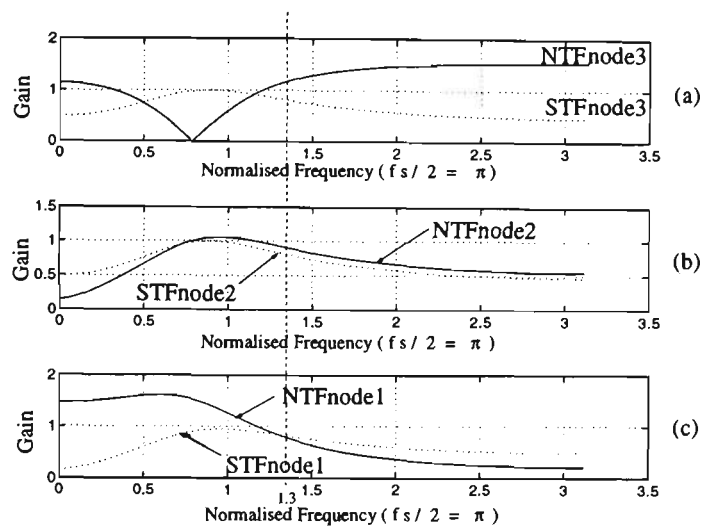


Figure 6.4: The comparison of signal transfer functions(STF) and noise transfer functions(NTF) (tuning at $\pi / 4$) at each node which indicates the cause of intermediate stage saturation.

below this frequency should not cause interstage saturation. That is to say, if there is any overshoot, it should happen at the point just before the comparator, not at nodes 1 and 2. The reason for the apparent contradiction is that the nodes also have to carry a large noise signal caused by the very coarse quantization (1 bit) of the output in a $\Sigma\Delta$ system. So the noise power at each node is therefore also as important as the signal when considering the saturation at internal nodes. Fig. 6.4 (b) and (c) also show the noise transfer functions (gains vs frequency responses) at node 1 and node 2. The average noise gain over the band at these intermediate nodes is smaller than at the output node by approximately 0.5. The noise amplitude will therefore be less at these nodes, but not by a huge amount. The dynamic range headroom at the intermediate nodes will still be reduced by this noise, leading to the early onset of saturation.

Scaling of the transfer function (the traditional way) to avoid large signals at the saturation nodes is only partially successful because of the additional quantization noise component. Thermal noise and device noise also limit the level of scaling that can be applied. The large quantization noise signal in the feedback loop is a unique feature of $\Sigma\Delta$ modulation.

6.4 Conclsion

Scaling of the transfer function to avoid large signals at the saturation nodes is only likely to be partially successful because of the additional quantization noise and other noise components. $\Sigma\Delta$ ADCs operating in a multi-channel environment are likely to have a lower intermodulation and blocking performance than traditional ADCs (i.e flash and successive approximation) with equivalent resolution. $\Sigma\Delta$ ADCs which are to be used in a multichannel environment should be overdesigned to account for the additional loss in dynamic range caused by intermediate stage saturation.

Chapter 7

Conclusion

This research investigated the feasibility of using ADCs in multichannel (whole of band) radio terminals. These terminals receive the whole of transmission band and select the required channel using DSP filtering. The use of DSP processing removes the requirement for expensive crystal filters, accurately controlled synthesizers and VCOs. The number of components are reduced and the performance of the filtering can be improved (linear phase and steeper filter cut-offs).

7.1 The Performance Summary

Traditional $\Sigma\Delta$ ADCs have low power consumption, low cost and small size. Their high sampling frequency makes them suitable for converting wideband signals, but they generate a considerable amount of quantization noise. Noise shaping is used to remove this quantization noise. Lowpass $\Sigma\Delta$ ADCs null the noise at DC and bandpass $\Sigma\Delta$ ADCs null the noise at a certain frequency. It is possible to use bandpass $\Sigma\Delta$ ADCs in multichannel receivers if the frequency of the quantization noise null can be tuned to the desired channel for reception. The feasibility of doing this was the aim of this research.

The new receiver design was presented in chapter 2. It was shown to be an extension to the well know SSB direct conversion receiver. The difference being that now the whole of the band is received rather than just one channel. Filtering is performed in the DSP unit as part of the decimation process prior to demodulation. The requirements of $\Sigma\Delta$ ADC were defined based on the requirements of the current GSM system. The chapter concluded with a brief overview of some major A/D specifications.

Chapter 3 introduced and reviewed the lowpass $\Sigma\Delta$ converter. The mathematics of noise shaping was developed. Zeros located at $(1 + j0)$ in the *NTF* cause null of the noise at DC. The *NTF* pole positions are shown to vary the shape of the *NTF*. Equations for calculating the SNR were presented and shown to give good agreement with Matlab simulations. Both first and second order $\Sigma\Delta$ converters were discussed. A graph relating signal to quantization noise ratio versus oversampling rate and order was given. A second order $\Sigma\Delta$ converter with 64 times oversampling gave a SNR equivalent to a normal 12bit ADC.

In chapter 4, modifications were developed to change a 2nd order lowpass $\Sigma\Delta$ ADC into a second order bandpass $\Sigma\Delta$ ADC . It was shown that noise tuning can be performed by altering two of the coefficients, B and b_1 . B effected the position of the zeros on the unit circle and b_1 the position of the pole frequency. The optimum position of the poles was found to be a compromise between stability requirements and noise performance. A pole position with a radius of 0.6 and a angle, the same as the zero angle gave near optimum performance over the bandwidth considered. The signal to noise ratio was equivalent to 8 bit with an oversampling ratio of 130. A practical radio receiver would require greater resolution and this could be provided by using a higher order, $N > 2$, $\Sigma\Delta$ ADC.

The values of the coefficients were analyzed in Chapter 5. It was shown that changes, as small as 0.12% for B , were required to change the null frequency by one channel. Further analysis showed that the B coefficient was sensitive to adjustment error and a 1% variation could produce up to 3dB increase in the noise power. Sensitivity of this coefficient could be a major implementation limitation if traditional switched capacitor CMOS techniques are used.

Chapter 6 looked at signal overload and intermodulation effects which are important because of the wideband multichannel input signal. It was shown that saturation of the intermediate stages contributed to a reduction in dynamic range (approximately 3dB) in the

presence of a large adjacent channel signal. It was suggested that this problem could be overcome by allowing a safety margin in the original system design.

7.2 Novelty

Novel features of this work include

- Proposing a receiver design in which channel tuning and filtering are done in the DSP unit.
- The proposed use of a $\Sigma\Delta$ ADC in the multichannel (whole-of-band) receiver.
- An analysis of the requirements on the coefficients for tunable operation.
- An investigation into the intermodulation performance of $\Sigma\Delta$ ADC in the presence of out of channel signals.

7.3 Further Work

- Investigation of performance of higher order systems ($N > 2$). Preliminary work on 6th order structure indicates about 92 dB dynamic is achievable at oversampling ratio of 75.
- Implementation alternatives to traditional switched capacitor CMOS technology are required to overcome the coefficient sensitivity requirements.
- The DSP channel selection filtering and decimation process have not been considered. This is a major research project in itself.

Bibliography

- ADAMS R.W., P. F. FERGUSON, A. GANESAN, S. VINCELETLE, A. VOLOPE AND R. LOPERT (1991). Theory and practical implementation of a fifth-order sigma-delta a/d converter. *Audio Engineering Society* Vol. 39, pp. 515–528.
- AGRAWAL B. P. AND K. SHENOI (1983). Design methodology for sigma-delta modulation. *IEEE Trans. Commun.* Vol. COM-31, pp. 360–370.
- ARDALAN S. H. AND J. PAULOS (1986). Stability analysis of high-order sigma-delta modulators. *Proc. 1986 Int. Symp. Circuits Sys.* pp. 715–719.
- ARDALAN S. H. AND J. PAULOS (1987). An analysis of nonlinear behavior in delta-sigma modulators. *IEEE Trans. Circuits and Sys.* Vol. CAS-34, pp. 593–603.
- BENNETT W. R. (1948). Spectra of quantized signals. *Bell Sys. Tech. J.*, Vol. 27, pp. 446–472.
- BISHOP R. J., J.J. PAULOS, M. B. STEER AND S. H. ARDALAN (1990). Table-based simulation of delta-sigma modulation. *IEEE Trans. Circuits and Sys.* Vol. CAS-37, pp. 447–451.
- BRANDT B. P., D. E. WINGARD AND B. A. WOOLEY (1991). Second-order sigma-delta modulation for digital-audio signal acquisition. *IEEE Journal on Solid-State Circuits* Vol. 26, pp. 618–627.
- CANDY J.C. (1974). A use of limit cycle oscillations to obtain robust analog-to-digital converters. *IEEE Trans. on Communication* Vol. COM-22, pp. 298–305.
- CANDY J. C. (1985). A use of double integration in sigma delta modulation. *IEEE Trans. Communication* Vol. COM-33, pp. 249–258.

- CANDY J. C. (1986). Decimation for sigma delta modulation. *IEEE Trans. Communication* Vol. COM-34, pp. 72–76.
- CANDY J. C. AND G. C. TEMES (1992). *Oversampling Methods for A/D and D/A Conversion*. IEEE Press. 445 Hoes Lane, PO Box 1331, Piscataway, NJ 08855-1331.
- CARLEY L. R. (1989). A noise-shaping coder topology for 15+ bit converters. *IEEE J. Solid-State Circuit* Vol. SC-24, pp. 267–273.
- CARLEY L. RICHARD (1987). An oversampling analog-to-digital converter topology for high-resolution signal acquisition system. *IEEE Trans. Circuits and Sys.* Vol. CAS-34, pp. 83–90.
- CAVERS J. AND M. LIAO (1991). Adaptive compensation for imbalance and offset losses in direct conversion transceivers. *IEEE VTC'91 Proc.* pp. 578–583.
- CHAO K. C. H., S. NADEEM, W. L. LEE AND C. G. SODINI (1990). A high order topology for interpolative modulators for oversampling a/d converters. *IEEE Trans. Circuits and Sys.* Vol. CAS-37, pp. 309–318.
- CHU S. AND C. S. BURRUS (1984). Multirate filter design using comb filter. *IEEE Trans. Circuit Sys.*, Vol. CAS-31, pp. 913–924.
- CLAYTON G. B. (1982). *Data Converters*. The Macmillan Press Ltd.
- CROCHIERE R. E. AND L. R. RABINER (1981). Interpolation and decimation of digital signals - a tutorial review. *Proc. IEEE* Vol. 69, pp. 300–331.
- CURTIS S. (1991). Bitstream conversion. *Electronics World* pp. 205–208.
- DARLING T. F. AND M. O. J. HAWKSFORD (1990). Oversampled data conversion techniques. *Audio Engineering Society* Vol. 38, pp. 924–943.
- DAS J. AND P.K. CHATTERJEE (1967). Optimized delta delta modulation system. *Electronics Letters* Vol. 3, pp. 286–287.
- DIJKSTRA E., L. CARDOLETTI, O. NYS, C. PIGUET AND M. DEGRAUWE (1988). Wave digital decimation filters in oversampled a/d converters. *IEEE Proc. ISCAS'88* Vol. ISCAS'88, pp. 2327–2330.
- FRIEDMAN V. (1989). A dual-channel voice-band pcm coder using sigma-delta modulation technology. *IEEE J. Solid-State Circuit* Vol. SC-24, pp. 274–280.

- GARRETT P. H. (1981). *Analog I/O Design*. Reston Publishing Company. Reston , Virginia.
- GOODMAN D. J. AND M. J. CAREY (1977). Nine digital filters for decimation and interpolation. *IEEE Trans. , Speech , Signal Proc.*, Vol. ASSP-25, pp. 121–126.
- GRAY R. M. (1987). Oversampled sigma-delta modulation. *IEEE Trans. Commun.* Vol. COM-35, pp. 481–489.
- GRAY R. M. (1990a). Quantization noise spectra. *IEEE Trans. in Information Theory* Vol. IT-36, pp. 1220–1244.
- GRAY R. M. (1990b). *Source Coding Theory*. Kluwere Academic Press.
- GRAY R. M., W. CHOU AND P. W. WONG (1989). Quantization noise in single-loop sigma-delta modulation with sinusoidal input. *IEEE Trans. Communication* Vol. COM-37, pp. 956–968.
- HAUSER M. W. (1991). Principles of oversampling a/d conversion. *Audio Eng. Soc.*, Vol. 39, No. 1/2, pp. 3–26.
- HAUSER M. W. AND R. W. BRODERSEN (1986). Circuit and technology considerations for mos delta-sigma a/d converters. *IEEE ISCAS'86* pp. 1310–1315.
- HAYASHI T., Y. INABE, K. UCHIMURA AND T. KIMURA (1986). A multistage delta-sigma modulator without double integration loop. *ISSCC Dig. Tech. Paper* pp. 182–183.
- HOESCHELE D. F. (1986). *Analog-to-Digital / Digital-to Analog Conversion Techniques*. John Wiley and Sons Inc.. New York.
- HURST P. J. AND R. A. LEVINSON (1989). Delta-sigma a/ds with reduced sensitivity to op amp noise and gain. *IEEE Proc. ISCAS'89* pp. 254–257.
- INOSE H. AND Y. YASUDA (1963). A unity bit coding method by negative feedback. *Proc. IEEE* Vol. 51, pp. 1524–1533.
- INOSE H., Y. YASUDA AND J. MURAKAMI (1962). A telemetering system by code modulation–sigma-delta modulation. *IRE Trans. Space Elec Telemetry* Vol. SET-8, pp. 204–209.
- JAYANT N. S. AND P. NOLL (1984). *Digital Coding of Waveforms*. Prentice-Hall. Englewood Cliffs, NJ.

- KAREMA T., T. RITONIEMI AND H. TENHUNN (1990). An oversampling sigma-delta a/d converter circuit using two-stage fourth-order modulator. *IEEE Proc. ISCAS'90* pp. 3279–3282.
- KOCH R., B. HEISE, F. ECKBAUER, E. ENGELHARDT, J. A. FISHER AND F. PARZEFALL (1986). A 12-bit sigma-delta analog-to-digital converter with a 15-mhz clock rate. *IEEE J. Solid-State Circuits* Vol. SC-21, pp. 1003–1010.
- LAINNEY G., R. SAINTLAURENS AND P. SENN (1983). Switched-capacitor second-order noise-shaping coder. *Electronics Letters* Vol. 19, No. 4, pp. 149–150.
- LINDQUIST B. (1993). A direct conversion receiver for tdma system. Master's thesis. Lund University. Lund, Sweden.
- LI PING (1993). A combined successive and sigma-delta a/d conversion scheme. *IEEE IS-CAS'93 Proc.* pp. 1294–1297.
- MATSUYA Y., K. UCHIMURA, A. IWATA, T. KOBAYASHI, M. ISHIKAWA AND T. YOSHITOME (1987). A 16b oversampling a/d conversion technology using triple-integration noise shaping. *IEEE J. Solid-State Circuits* Vol. SC-22, pp. 921–929.
- NORSWORTHY S. R., I. G. POST AND H. S. FETTERMAN (1989). A 14-bit 80-khz sigma-delta a/d converter: Modeling, design, and performance evaluation. *IEEE J. Solid-State Circuits* Vol. SC-24, pp. 256–266.
- OPPENHEIM A. V. AND R. W. SCHAFER (1989). *Discrete-Time Signal Processing*. Prentice-Hall. Englewood Cliffs, NJ>.
- PARK S. (1993). Principles of sigma-delta modulation for analog-to-digital converters. Motorola, Inc.
- P. M. AZIZ H. V. SORENSEN AND J. V. SPIEGEL (1994). Multi band sigma delta analog to digital conversion. *IEEE Proc. ICASSP'94* Vol. 3, pp. 249–252.
- REBESCHINI M., N. BAVEL AND P. RAKERS (1989). A high-resolution cmos sigma-delta a/d converter with 320khz output rate. *IEEE Proc. ISCAS'89* pp. 246–249.
- RITONIEMI T., T. KAREMA AND H. TENHUNEN (1990). Design of stable high order 1-bit sigma-delta modulators. *IEEE Proc. ISCAS'90* pp. 3267–3270.

- ROBERT J. AND P. DEVAL (1988). A second-order high-resolution incremental a/d converter with offset and charge injection compensation. *IEEE J. Solid-State Circuits* Vol. 23, pp. 736–741.
- ROOME S.J. (1989). Analysis of quadrature detectors using complex envelop notation. *IEE Proceedings* Vol. Part F(2), No. 136, pp. 95–100.
- SCHREIER R. AND M. SNELGROVE (1989). Bandpass sigma-delta modulation. *Electronics Letters* Vol. 25, No. 23, pp. 1560–1561.
- SCHREIER R. AND M. SNELGROVE (1991). Stability in a general sigma-delta modulator. *IEEE Proc. Int. Symp on Acoustics, Speech and Signal Processing* pp. 1769–1772.
- SHEINGOLD D. H. (1978). *analog - digital CONVERSION NOTES*. Analog Devices, Inc., Norwood, Massachusetts, 02062 U.S.A.
- S.JANTZI, R. SCHREIER AND M. SNELGROVE (1991). Bandpass sigma-delta analog-to-digital conversion. *IEEE Trans. on Circuits and Syses* Vol. 38, No. 11, pp. 1406–1409.
- S.J.ERST (1984). *Receiving System Design*. Artech House , Inc.. 685 Canton Street, Norwood, MA 02062.
- STEELE R. (1975). *Delta Modulation system*. Wiley. New York.
- WALDEN R. H., T. CATALTEPE AND G. C. TEMES (1990). Architectures for high-order multibit modulators. *IEEE Proc. ISCAS'90* pp. 895–898.
- WELLAND D. R., B. P. SIGNORE, E. J. SWANSON, T. TANAKA, K. HAMASHITA, S. HARA AND K. TAKASUKA (1989). Stereo 16-bit delta-sigma a/d cinverter for digital audio. *Audio Engineering Society* Vol. 37, pp. 476–486.
- WIDROW B. (1956). A study of rough amplitude quantization by means of nyquist sampling theory. *IRE Trans. on Circuits Theory* Vol. CT-3, pp. 266–276.

This paper was presented at :

**The 44th IEEE/VTS Vehicular Technology Conference,
Sweden, June, 1994, pp. 1346-1350.**

The title of the paper :

**A Tunable Bandpass Sigma-Delta A/D Conversion for
Mobile Communication Receivers.**

Authors : Shengping Yang, Michael Faulkner and Roman Malyniak

A Tunable Bandpass Sigma-Delta A/D Conversion for Mobile Communication Receiver

Shengping Yang and Michael Faulkner and Roman Malyniak
 Department of Electrical and Electronic Engineering
 Victoria University of Technology
 Australia

Abstract—A channel selective A/D converter for mobile communication receiver by using the $\Sigma\Delta$ modulation is presented. For input signals with different frequencies and relative small bandwidth, the bandpass $\Sigma\Delta$ converter could serve both the roles of tuning and A/D conversion at the same time. The issues of sensitivity of the parameters to the channel selection and channel error tolerance level in terms of inband noise, which are associated with the implementation of channel selective $\Sigma\Delta$ A/D converter in mobile communication environment, are discussed. All the simulation and calculation are based on the simplified second-order bandpass structure, and their results have given some indication to the trade-off between sensitivity and the overdesign necessary to meet the system sensitivity requirement.

I. INTRODUCTION

Oversampled Sigma-Delta ($\Sigma\Delta$) modulation A/D converters have been attracting much attention recently in the VLSI industry. It has many attractive characteristics which naturally and advantageously lend themselves to VLSI signal processing utilizing high levels of integration. In the design of $\Sigma\Delta$ converter, the benefits include inherent linearity, high tolerance to circuit imperfection, and only a small amount of analog circuitry is needed. The advantages in implementation of $\Sigma\Delta$ converter can be found as the circuits do not require any component trimming to achieve high resolution in the conversion process, reduced anti-aliasing filter requirements, and a system architecture that lend itself to switched-capacitor implementation [1] - [4]. The bandpass variant of $\Sigma\Delta$ conversion retains these advantages and offers promising technique for the use in the developing area of digital radio.

Previous work [5]-[8] has targeted the improvement in resolution, signal to noise ratio and dynamic range for audio applications, such as digital audio tape (DAT), compact disc (CD) player and modems.

In this paper, we extend the implementation of bandpass $\Sigma\Delta$ to mobile communication receivers, and plan a future receiver in which all tuning can be done in the A/D conversion, then discuss an important issue - sensitivity of circuit parameters to channel selection, which may determine the minimum number of order the system should have.

The purpose of the investigation of the tunable $\Sigma\Delta$ converters is to explore the usage of the tunable $\Sigma\Delta$ A/D converter in mobile communication receivers and its sensitivity (in terms of inband noise level) of channel selection against the inaccuracy of parameters. Fig. 1 illustrates a possible receiver

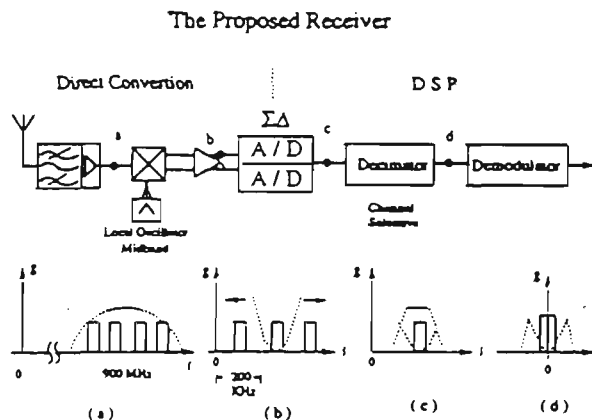


Fig. 1. The proposed receiver with the tunable $\Sigma\Delta$ A/D converter in it. (a) mobile communication channels in receiver band. (b) receiving band down converted to baseband. (c) a interested channel is selected by tunable $\Sigma\Delta$ A/D converter. (d) the interested channel is decimated further down and converted to baseband for demodulation.

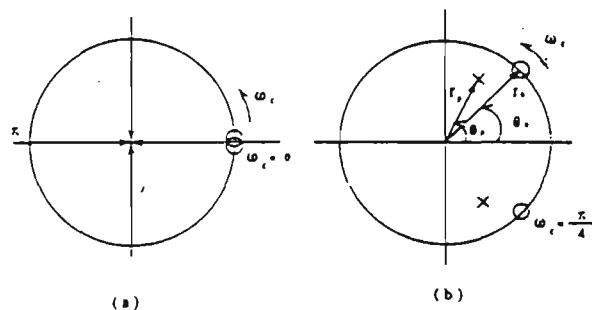


Fig. 2. (a) The pole and zero placements of error transfer function for ordinary second-order lowpass $\Sigma\Delta$ converter and (b) second-order bandpass $\Sigma\Delta$ converter

architecture in which the tunable $\Sigma\Delta$ converter is used.

II. GENERAL DESIGN OF THE SYSTEM DESIGN

A. Channel Location and Tunability

The conventional low-pass band $\Sigma\Delta$ converters place zeros of noise transfer function at $\omega_c = 0$ in order to null quantization noise near dc. If there is a need to null quantization noise at nonzero frequency, say ω_c , then one would obtain a high signal-to-noise ratio in a band around ω_c . This noise shapping concept was extended by R.Schreier[7]. With a narrow-band signal the sampling rate need only be much greater than the bandwidth of the signal (not the carrier frequency as with lowpass $\Sigma\Delta$ converter). The oversampling ratio, R_b , is defined as one-half the sampling rate divided

Spectral Density

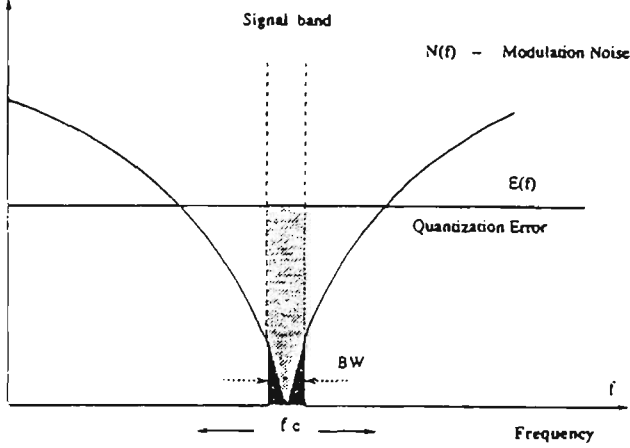


Fig. 3. The comparison of noise spectral density of bandpass $\Sigma\Delta$ converter (shaded dark) with that of normal A/D (shaded grey).

TABLE I

Sampling frequency f_{in}	Channel spacing f_{bw}	Center frequency f_c	Oversampling ratio $R_{lowpass}$	Oversampling ratio $R_{bandpass}$	Normalized value
52 MHz	200 KHz	200 KHz	130	130	$\pi / 130$
		400 KHz	65		$\pi / 65$
		⋮	⋮		⋮
		1000 KHz	26		$\pi / 26$
		1200 KHz	21.67		$\pi / 21.67$
		⋮	⋮		⋮
		2.4 MHz	10.83		$\pi / 10.83$

* This group of data is chosen for GSM system. (Total bandwidth 25 MHz, channel space 200 KHz, and carrier frequency 900 MHz).

Fig. 4. Table I - A comparison of oversampling ratio with same parameters

by the width of the band of interest. Table I illustrates the comparison of lowpass and bandpass in oversampling ratio. The example in [8] shows the advantage the bandpass $\Sigma\Delta$ has compared with the low-pass case. Fig. 2 illustrates the pole and zero placement of the error transfer functions for lowpass and bandpass $\Sigma\Delta$ converters. Fig. 3 shows the noise spectral density for bandpass $\Sigma\Delta$ converter.

Tunability (varying channel location) can be obtained by changing either sampling frequency or the noise-shaping function (changing the value of components in the noise transfer function). Table I illustrates the comparison of lowpass and bandpass in oversampling ratio.

The different value of ω_c represents different ratios of carrier frequency to sampling frequency. Setting the channel near $\omega_c = \pi$ can reduce sampling rate compared to a lowpass $\Sigma\Delta$ converter, but increases the requirement on the anti-aliasing filter.

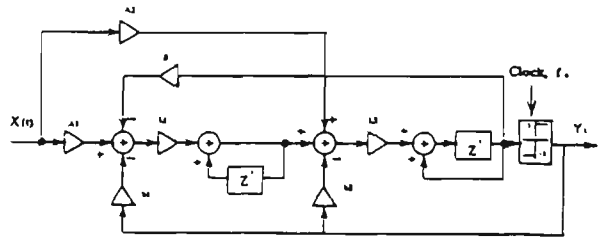


Fig. 5. A original structure of the second-order bandpass $\Sigma\Delta$ quantizer

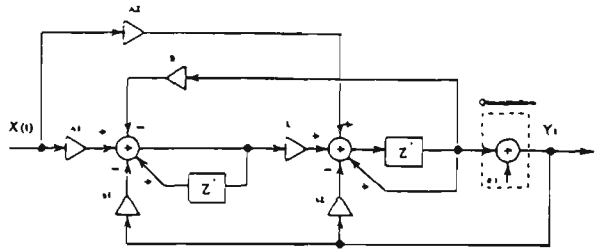


Fig. 6. The simplified structure and sampled-data model of second-order bandpass $\Sigma\Delta$ quantizer

B. System Structure, Modeling and Transfer Function

It is a basic requirement for bandpass $\Sigma\Delta$ modulator to notch the quantization noise at the channel of interest. A easy way to analyze the $\Sigma\Delta$ converter is to model the quantizer as an additive noise source. Fig. 5 shows the structure of the quantizer and Fig. 6 shows the model of simplified structure for analysis. Then input signal and quantization noise have their own transfer function. The mathematical modeling and system transfer function can be obtained based on Fig. 6 and Fig. 2 (in Z domain) as followed:

$$Y(z) = H_s(z) \cdot X(z) + H_n(z) \cdot e(z) \quad (1)$$

where $H_s(z)$ is the signal transfer function (STF):

$$H_s(z) = \frac{\phi_1 z^{-1} - \phi_2 z^{-2}}{1 - \phi_3 z^{-1} + \phi_4 z^{-2}} \quad (2)$$

and $H_n(z)$ is the noise transfer function (NTF):

$$H_n(z) = \frac{1 - \mu z^{-1} + z^{-2}}{1 - \phi_3 z^{-1} + \phi_4 z^{-2}} \quad (3)$$

with

$$\begin{aligned} \phi_1 &= \lambda A_1 + A_2, \\ \phi_2 &= A_2, \\ \phi_3 &= 2 - \lambda(b_1 + B) - b_2, \\ \phi_4 &= 1 - b_2, \\ \mu &= 2 - \lambda B. \end{aligned}$$

It is possible to design and optimize these transfer functions and make the system work better.

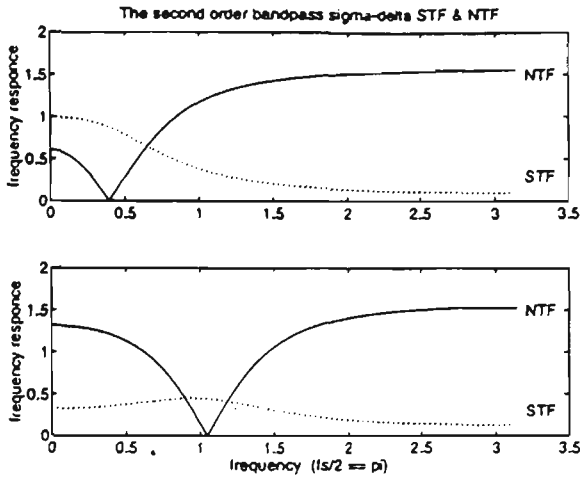


Fig. 7. The 2nd order bandpass $\Sigma\Delta$ converter signal and noise transfer functions at notch points of $\pi/8$ and $\pi/3$ respectively.

C. The Noise Transfer Function

The selection of the noise transfer function is the main consideration of the design. The noise transfer function, $H_n(z)$, is selected to provide maximum in-band attenuation, subject to several constraints [8] as followed:

- i) infinity : $H_n(\infty) = 1$.
- ii) out-of-band : $|H_n(e^{j\omega})| = 1.625, \max_{\omega \in [0, \pi]}$.

In brief, Lee claims that the condition $\max_{\omega \in [0, \pi]} |H_n(e^{j\omega})| < 2$ ensures that the resulting converter is stable, and suggests the use of a NTF with a monotonic magnitude response. By manipulating the parameters in equation (3), a satisfied NTF design can be done.

D. The Signal Transfer Function

In this paper a second-order bandpass $\Sigma\Delta$ converter is chosen for simplicity as shown in Fig. 6. The signal transfer function shares poles with the noise transfer function, but has one less zero. As such its shape can be limited for low-order converters.

The requirement to the signal transfer function is, firstly the nearly constant gain and linear phase in-band, and then high attenuation out-of-band. Fig. 7 shows (calculation result) the signal noise transfer functions tuning at different frequencies. Fig. 8 shows the simulation result of the second-order bandpass $\Sigma\Delta$ converter shown in Fig. 6.

III. SENSITIVITY OF CHANNEL SELECTION

It was mentioned previously that the tuning can be done by changing the circuit parameters. The case is shown in Fig. 8 and the data chosen for calculation is from GMSK, they are 200 KHz channel space, 25 MHz total bandwidth with carrier frequency (e.g 900 MHz) see Fig. 1. Sampling frequency is chosen to be 52 MHz (it is necessary to be, at least, as large as that of the total bandwidth for quadrature sampling). As we know that quantisation noise can not be totally reduced but

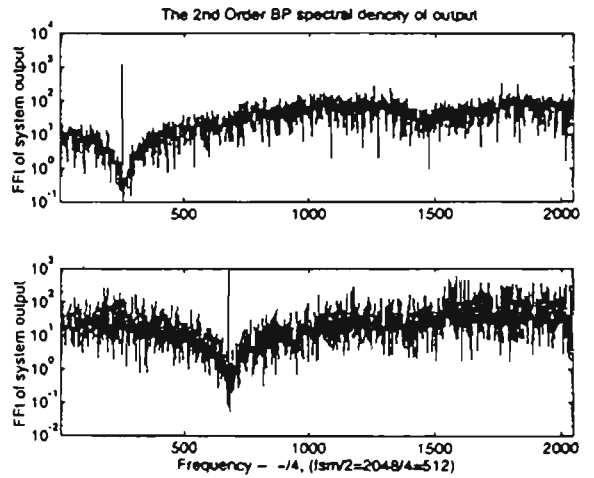


Fig. 8. The simulation result of $\Sigma\Delta$ modulation tuning at $\pi/8$ and $\pi/3$ under an ideal condition.

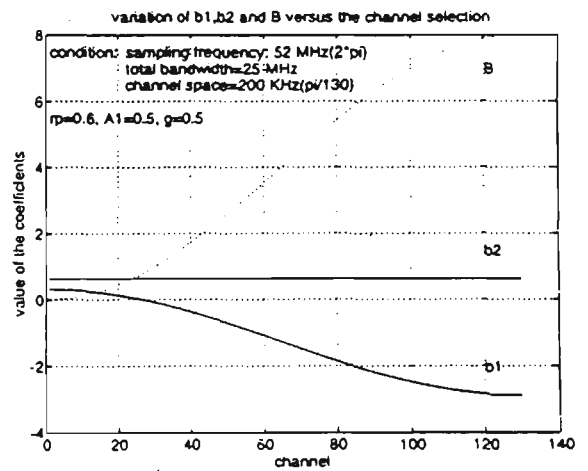


Fig. 9. The coefficients versus channel selection for 2nd order bandpass $\Sigma\Delta$ converter.

can be pushed away from the interested band by manipulating the parameters in the noise transfer function (NTF). Fig. 9 shows the relationship between channel selection and the changing of the coefficients.

Because of the inaccuracy of the coefficients : b_1, b_2 and B (see Fig. 10), tuning can not be done exactly so it is expected, this will cause an increase in inband noise. The question of noise sensitivity to coefficient inaccuracy is important. The increase in noise will give some indication to the amount of overdesign necessary to meet the system sensitivity requirement.

The influence of each individual coefficient on the NTF (tuning point and shape) is shown in Fig.10. It is shown that B affects both the tuning and the shape of the NTF, while b_1 and b_2 only affect the shape of the NTF.

The inband noise can be calculated from the NTF (Eq. 3) as follows :

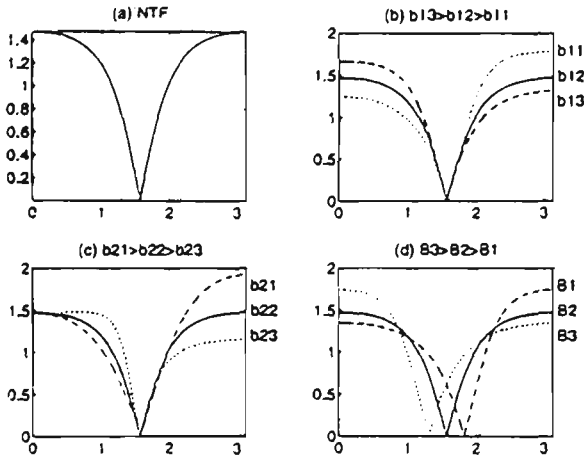


Fig. 10. Normalised frequency on the X axes ($\pi = 26\text{MHz}$), the gain of NTF is on the Y axes. (a) tuning at $\pi/2$, (b) the effect of changing b_1 , (c) b_2 and (d) B .

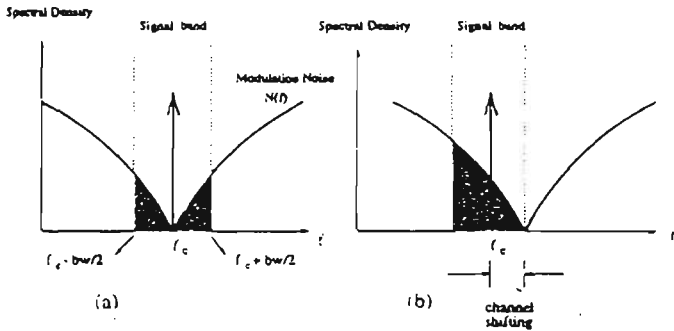


Fig. 11. The shadow areas represent noise power, (a) ideal tuning (tone sitting in the null position), (b) practical tuning, where coefficient errors produce a null offset.

$$P_{n_inband} = \int_{f_c - \frac{bw}{2}}^{f_c + \frac{bw}{2}} |NTF(e^{j\omega})|^2 \cdot Q_n(\omega) \cdot d\omega \quad (4)$$

where $Q_n(\omega)$ is the noise power spectral density. Assuming the quantisation noise from the A/D converter is white [9]-[10] (making $Q_n(\omega)$ a constant), Eq. (5) becomes

$$P_{n_inband} = Q_n \int_{f_c - \frac{bw}{2}}^{f_c + \frac{bw}{2}} |NTF(e^{j\omega})|^2 \cdot d\omega \quad (5)$$

Because of the inaccuracy of the circuit parameters, inband noise will be increased to P_{er_inband} , due to change in the noise shaping function of $NTF'(\omega)$:

$$P_{er_inband} = Q_n \int_{f_c - \frac{bw}{2}}^{f_c + \frac{bw}{2}} |NTF'(e^{j\omega})|^2 \cdot d\omega \quad (6)$$

To investigate the influence of each b_1 , b_2 and B to the inband noise power of the second-order bandpass $\Sigma\Delta$ converter, the following three equations can be used:

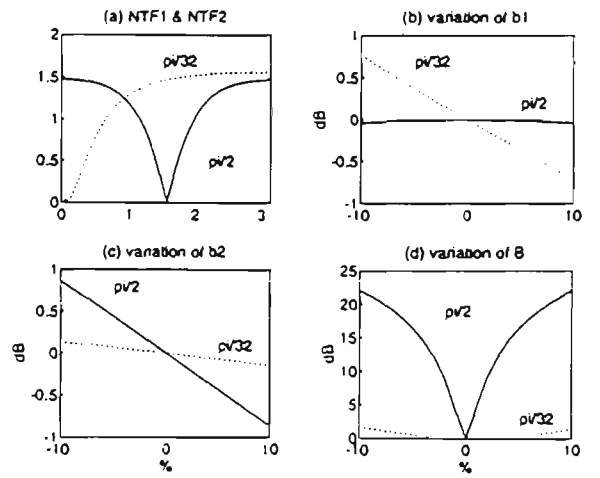


Fig. 12. The inaccuracy of each coefficients, b_1 , b_2 and B , causes tuning off-set and the increase of inband noise, (a) NTF for tuning at $\pi/32$ (dotted line) and $\pi/2$ (solid line) respectively, normalized frequency ($2\pi = 52\text{MHz}$), (b) change of inband noise vs % change in coefficient b_1 , (c) vs coefficient b_2 , (d) vs coefficient B .

$$\frac{\partial P_{n_inband}}{\partial b_1} = Q_n \cdot \int_{f_c - \frac{bw}{2}}^{f_c + \frac{bw}{2}} \frac{\partial(|NTF(e^{j\omega})|^2)}{\partial b_1} \cdot d\omega \quad (7)$$

$$\frac{\partial P_{n_inband}}{\partial b_2} = Q_n \cdot \int_{f_c - \frac{bw}{2}}^{f_c + \frac{bw}{2}} \frac{\partial(|NTF(e^{j\omega})|^2)}{\partial b_2} \cdot d\omega \quad (8)$$

$$\frac{\partial P_{n_inband}}{\partial B} = Q_n \cdot \int_{f_c - \frac{bw}{2}}^{f_c + \frac{bw}{2}} \frac{\partial(|NTF(e^{j\omega})|^2)}{\partial B} \cdot d\omega \quad (9)$$

To simplify the calculation, Fig. (11) can be used. The shadow area in Fig. 11 (a) represents the noise power in an ideal tuning and (b) represents tuning in at a practical situation. The ratio of one over the other may show the sensitivity of channel selection.

Two examples (tuning at $\pi/32$ and $\pi/2$) are shown in Fig. 12. Inband noise is less sensitive to coefficients b_1 and b_2 than to B . The higher the frequency tuned, the more inband noise power is generated for the same amount of error in coefficients B and b_2 . One separate example has shown that with 10% inaccuracy in B , there will be about 22 dB inband noise increase for a channel at $\pi/2$, 10 dB increase for a channel at $\pi/4$ and 2dB increase for a channel at $\pi/32$. The noise increase at higher channel frequencies must be offset by using a more complex (higher order) converter.

IV. CONCLUSION

Tunable $\Sigma\Delta$ bandpass A/D converter provides a new and novel way to implement the A/D converter to the proposed receiver. It does all the tuning and conversion at the same time. The dynamic range of the bandpass $\Sigma\Delta$ converter is

herefore more sensitive to component error than lowpass $\Sigma\Delta$ converter. The careful selection and optimization of system gain and position of poles could improve the sensitivity and the performance of the converter. It is suggested that the higher order bandpass $\Sigma\Delta$ converters are necessary to cover the whole bandwidth of mobile signals.

REFERENCES

- [1] J. C. Candy and G. C. Temes, "Oversampling methods for A/D and D/A conversion," in *oversampling Delta-Sigma Converters*, J.C. Candy and G.C. Temes, Edited. New York: IEEE Press, 1991.
- [2] G.Lainey, R.Saintlaurens and P. Senn, "Switched-Capacity Second-Order Noise-Shaping Coder," in *Electronics Letters*, vol.19, No. 4, pp 149-150, Feb. 1983.
- [3] R.Gray, "Oversampled Sigma-Delta Modulation," in *Trans. IEEE, on communications*, vol. Com-35, No. 5, May 1987.
- [4] B.E.Boser and B.A.Wooley, "The design of Sigma-Delta modulation analog-to-digital converters," *IEEE J. Solid-State Circuit*, vol. 23, pp. 1298-1308, Dec. 1988
- [5] P.Benabes, A. Gauthier and D. Billet, "New Wideband Sigma-Delta converter," in *Electronics Letters*, vol.29, No. 17 Aug. 1993.
- [6] R.Schreier and M.Snelgrove, "Bandpass Sigma-Delta modulation," *Electronics Letters*, vol. 25, No. 23, pp 1560-1561, Nov.1989.
- [7] S.Jantzi, R.Schreier, and M.Snelgrove, "Bandpass Sigma-Delta Analog-to-Digital Conversion," in *Trans. IEEE Circuits and Systems*, vol. 38, No. 11, pp 1406-1409, Nov. 1991.
- [8] W.L. Lee, "A novel higher order interpolative converter topology for high resolution oversampling A/D converters", Master's thesis, Massachusetts Institute of Technology, June 1987, pp. 34-36.
- [9] Max W. Hauser, "Principles of Oversampling A/D Conversion," in *J. Audio Eng. Soc.*, Vol. 39, No. 1/2, 1991 Jan./Feb. pp. 3-26.
- [10] Robert M. Gray, "Quantization Noise Spectra," *Trans. Inform. Theory*, Vol. IT-36, pp. 1220-1244, Nov. 1990.

This paper was presented at :

IEEE International Conference on Universal Wireless Access, Australia, April, 1994, pp. 157-161.

The title of the paper :

The Channel Selective Bandpass Sigma-Delta Analog-to-Digital Conversion for Mobile Communication Terminals.

Authors : Shengping Yang, Michael Faulkner and Roman Malyniak

The Channel Selective Bandpass Sigma-Delta Analog-to-Digital Conversion for Mobile Communication Terminals

Shengping Yang Michael Faulker
 Roman Malyniack

Department of Electrical and Electronic Engineering
 Victoria University of Technology
 Australia

Abstract

A tunable A/D convertor for mobile communication terminal by using the $\Sigma\Delta$ modulation is presented. For input signals with different frequencies and relative small bandwidth, the bandpass $\Sigma\Delta$ convertor could serve both the roles of tuning and A/D conversion at the same time. The channel selection can be done either by changing sampling frequency or changing the parameters of the system. The issue of adjacent channel interference on a second-order tunable $\Sigma\Delta$ modulator is discussed. Simulation provides a promising expectation for higher order tunable $\Sigma\Delta$ modulator

1 Introduction

Oversampled sigma-Delta ($\Sigma\Delta$) modulation A/D converters have been attracting much attention recently in the VLSI industry. It has many attractive characteristics which naturally and advantageously lend themselves to VLSI signal processing utilizing high levels of integration. In the design of $\Sigma\Delta$ the benefits include inherent linearity, high tolerance to circuit imperfection, and only a small amount of analog circuitry is needed. The advantages in implementation of $\Sigma\Delta$ modulator can be found as the circuits do not require any component trimming to achieve high

resolution in the conversion process, reduced anti-aliasing filter requirements, and a system architecture that lend itself to switched-capacitor implementation [1] - [4]. The bandpass variant of $\Sigma\Delta$ conversion retains these advantages and offers promising technique for the use in the developing area of digital radio.

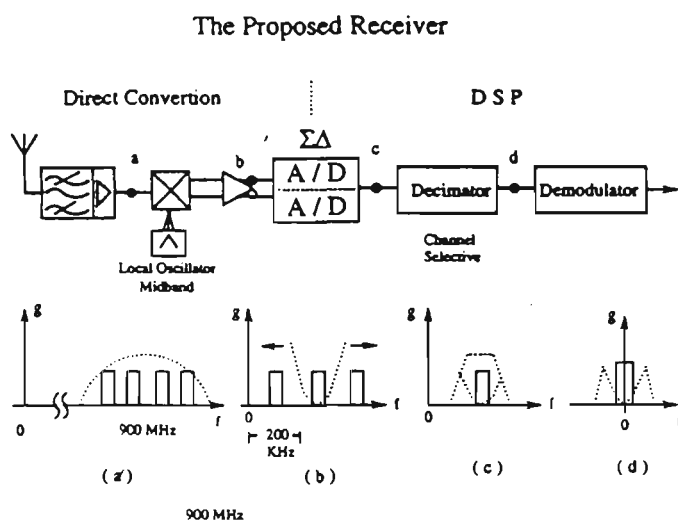


Figure 1: The proposed receiver with the tunable $\Sigma\Delta$ A/D convertor in it. (a) mobile communication channels in receiver band, (b) receiving band down converted to baseband, (c) a interested channel is selected by tunable $\Sigma\Delta$ A/D convertor, (d) the interested channel is decimated further down and converted to baseband for demodulation.

Previous work [5]-[8] has targeted the im-

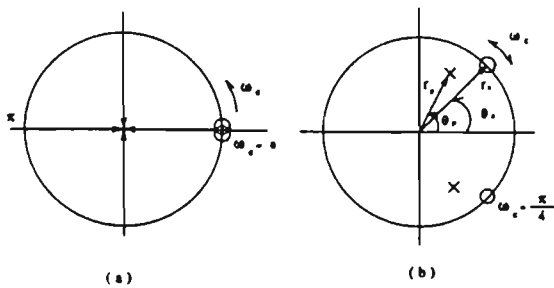


Figure 2: (a) The pole and zero placements of error transfer function for ordinary second-order lowpass $\Sigma\Delta$ modulator and (b) second-order bandpass $\Sigma\Delta$ modulator

provement in resolution, signal to noise ratio and dynamic range for audio applicationin, such as digital audio tape (DAT), compact disc (CD) player and modems. In this paper, we extend the implementation of bandpass $\Sigma\Delta$ to mobile communication terminals, and plan a future receiver in which all tuning can be done in the A/D conversion. We then discuss an important issue – adjacent channel interference, associated with the implementation of mobile communication terminals. The purpose of the investigation of the tunable $\Sigma\Delta$ converters is to explore the usage of the tunable $\Sigma\Delta$ A/D convertor in communication system and its anti-interference ability to adjacent channels. Fig. 1 illustrates a possible receiver archetecture in which the tunable $\Sigma\Delta$ modulator is used.

2 System Design

2.1 Channel Location and Tunability

The conventional low-pass band $\Sigma\Delta$ converters place zeros of noise transfer function at $\omega_c = 0$ in order to null quantization noise near dc. If there is a need to null quantization noise at nonzero frequency, say ω_b , then one would obtain a high signal-to-noise ratio in a band around ω_c . This noise-shapping concept was extended by R.Schreier[6]. With a narrow-band signal the sampling rate need only be much greater than the bandwidth of the signal (not the car-

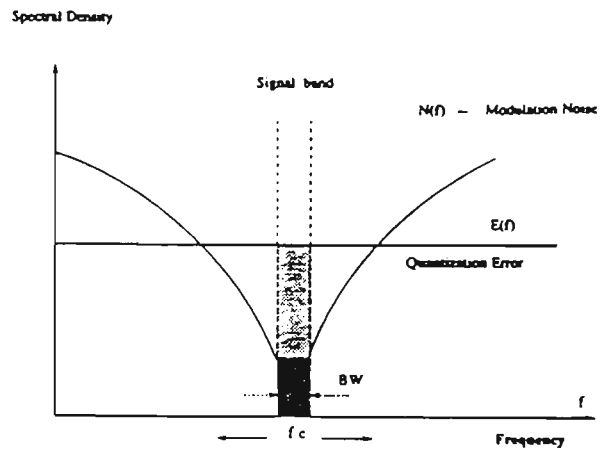


Figure 3: The comparison of noise spectral density of bandpass $\Sigma\Delta$ modulator with that of normal A/D.

rier frequency). The oversampling ratio, R_b , is defined as one-half the sampling rate divided by the width of the band of interest.

The example in [7-8] shows the advantage the bandpass $\Sigma\Delta$ has compared with the low-pass case. Fig. 2 illustrates the pole and zero placement of the error transfer functions for lowpass and bandpass $\Sigma\Delta$ modulators. Fig. 3 shows the noise spectral density for bandpass $\Sigma\Delta$ modulator.

Tunability (varying channel location) can be obtained by changing either sampling frequency or the noise-shapping function (changing the value of components in the noise transfer function). Table I illustrates one situation.

The different value of ω_c represents different ratio of carrier frequency to sampling frequency. The closer the channel is moving to π , the higher requirement is needed on the anti-aliasing filter, vise versus.

2.2 System Structure, Modelling and Transfer Function

It is a basic requirement for bandpass $\Sigma\Delta$ to notch the quantization noise at the channel of interest. A easy way to analyse the $\Sigma\Delta$ modulator is to model the quantizer as an additive noise source. Fig. 5 shows the structure of the quantizer.

Fig. 6 shows the model for analysis. Then input signal and quantization noise have their

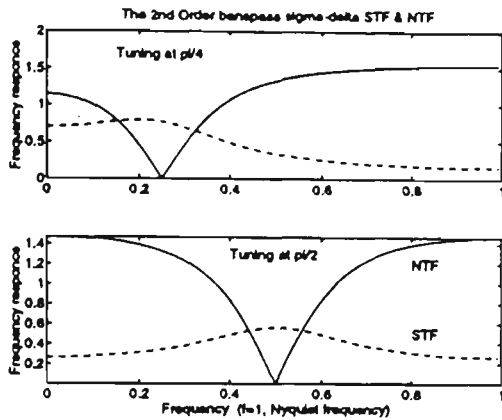


Figure 7: The 2nd order bandpass $\Sigma\Delta$ modulator signal and noise transfer functions at notch points of $\pi/4$ and $\pi/2$ respectively.

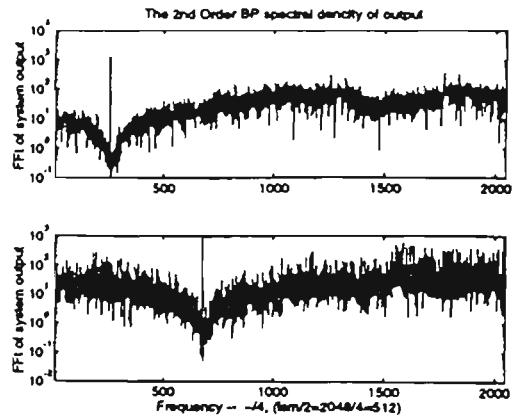


Figure 9: The simulation result of $\Sigma\Delta$ modulation tuning at $\pi/8$ and $\pi/3$ under an ideal conversion.

3 Interference from Adjacent Channels in the Received Band

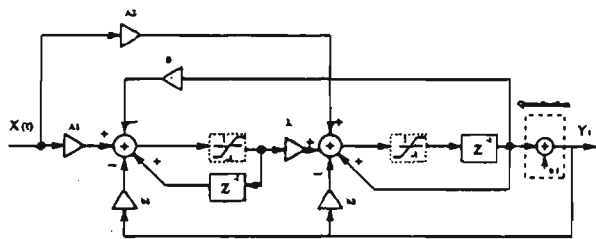


Figure 8: The simplified structure with (a) a saturation unit being set to investigate the intermodulation (included by dot lined block) and (b) no saturation unit omitting dot lined block.

2.5 The simplified structure of the system

In practise of manufacturing a chip, the less component it contains, the more easy it is to be made, and the more accuracy it is. The first step to simplify the structure is to put λ_1 and λ_2 back to A1, b1, B and A2, b2 respectively (see Fig. 5), then take off the addition unit in the integration block and connect feedback side of integration to the previous addition unit. The final structure of the system is shown in Fig. 8. The later simulations is generally based on this model.

Fig. 9 is an example which shows a 2nd order BP $\Sigma\Delta$ modulation working in a clear environment. There will not be any intermodulation if the amplitude at each point after addition (Fig. 8) can be kept below ± 1 . The desired in-band signal covers a much smaller bandwidth than that of the received band. The question of how much interference can be tolerated from adjacent signals in the received band is important. In $\Sigma\Delta$ A/D converter one case of interference from out-band signal to the inband signal is from system saturation (or running out of dynamic range). Inappropriate selections of gain and the position of poles of the signal and noise transfer functions are the causes of system saturation.

In the mobile communication environment, the signal reaching the receiver is a wide-band signal. A typical case for GMSK could be the signals with channel space of 200 kHz and bandwidth of 25 MHz after direct conversion from carrier frequency (e.g 900 MKz) see Fig. 1. All the input signals can add up at a certain point in time, and drive the input stages (prior to the comparator) into saturation. A $\Sigma\Delta$ A/D converter with a saturation unit is set to simulate this design, see Fig. 8. The interference signal is modeled as a signal tone in an adjacent chan-

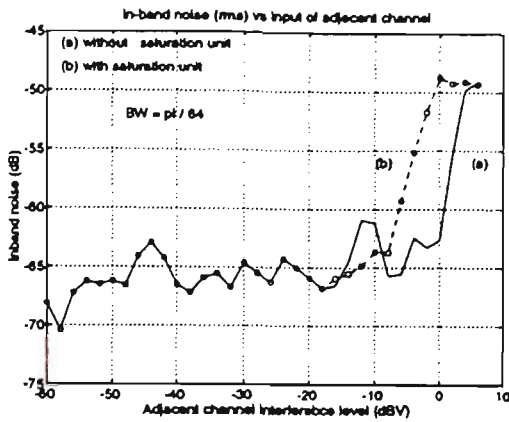


Figure 10: The comparison of dynamic range of 2nd order bandpass $\Sigma\Delta$ A/D converter (a) working with no saturation unit and (b) with saturation unit (setting limitation from 1 to -1), (1 volt = 0dB).

nel. Fig. 10 (a) shows the relative inband noise level versus the input level of a signal in the adjacent channel with no saturation unit, and (b) with a saturation unit. At low interference levels, saturation makes no difference to the modulator performance. When the interference level rises above -10 dBV, saturation of intermediate stages cause the performance of $\Sigma\Delta$ modulator to degrade. The dynamic range of the desired signal is reduced by up to 14 dB. When the adjacent channel interference (ACI) level reaches 0 dBV, the $\Sigma\Delta$ modulator is driven into a limit cycle pattern caused by output saturation (ie. the input signal is larger than the maximum output signal).

4 conclusion

Tunable bandpass A/D converter provides a new and novel way to implement the A/D converter to the proposed receiver. It does all the tuning and conversion at the same time. The careful selection and optimization of system gain and position of poles could save up to 14 dB dynamic range. Higher order $\Sigma\Delta$ A/D converter is expected to give much better performance.

References

- [1] J. C. Candy and G. C. Temes, "Oversampling methods for A/D and D/A conversion," in oversampling Delta-Sigma Converters, J.C. Candy and G.C. Temes, Edited. New York: IEEE Press, 1991.
- [2] G.Lainey, R.Saintlaurens and P. Senn, "Switched-Capacity Second-Order Noise-Shaping Coder," in Electronics Letters, vol.19, No. 4, pp 149-150, Feb. 1983.
- [3] R.Gray, "Oversampled Sigma-Delta Modulation," in Trans. IEEE, on communications, vol. Com-35, No. 5, May 1987.
- [4] B.E.Boser and B.A.Wooley, "The design of sigma-delta modulation analog-to-digital converters," IEEE J. Solid-State Circuit, vol. 23, pp. 1298-1308, Dec. 1988
- [5] P. Benabes, A. Gauthier and D. Billet, "New Wideband Sigma-Delta convertor," in Electronics Letters, vol.29, No. 17 Aug. 1993.
- [6] R.Schreier and M.Snelgrove, "Bandpass sigma-delta modulation," Electronics Letters, vol. 25, No. 23, pp 1560-1561, Nov.1989.
- [7] S.Jantzi, R.Schreier, and M.Snelgrove, "Bandpass Sigma-Delta Analog-to-Digital Conversion," in Trans. IEEE Circuits and Systems, vol. 38, No. 11, pp 1406-1409, Nov. 1991.
- [8] W.L. Lee, "A novel higher order interpolative modulator topology for high resolution oversampling A/D converters", Master's thesis, Massachusetts Institute of Technology, June 1987, pp. 34-36.